International Journal of Digital Earth

ISSN: 1753-8947 (Print) 1753-8955 (Online) Journal homepage: https://www.tandfonline.com/loi/tjde20

Remote sensing of earth's energy budget: synthesis and review

Shunlin Liang, Dongdong Wang, Tao He & Yunyue Yu

To cite this article: Shunlin Liang, Dongdong Wang, Tao He & Yunyue Yu (2019) Remote sensing of earth's energy budget: synthesis and review, International Journal of Digital Earth, 12:7, 737-780, DOI: 10.1080/17538947.2019.1597189

To link to this article: https://doi.org/10.1080/17538947.2019.1597189

INTERNATIONAL JOURNAL OF DIGITAL EARTH
2019, VOL. 12, NO. 7, 737–780
https://doi.org/10.1080/17538947.2019.1597189

Remote sensing of earth's energy budget: synthesis and review

Shunlin Liang[a,b], Dongdong Wang[a], Tao He[b] and Yunyue Yu[c]

[a]Department of Geographical Sciences, University of Maryland, College Park, MD, USA; [b]School of Remote Sensing and Information Engineering, Wuhan University, Wuhan, People's Republic of China; [c]NOAA/NESDIS/Center for Satellite Applications and Research, Riverdale, MD, USA

ABSTRACT

The Earth's climate is largely determined by its energy budget. Since the 1960s, satellite remote sensing has been used in estimating these energy budget components at both the top of the atmosphere (TOA) and the surface. Besides the broadband sensors that have been traditionally used for monitoring Earth's Energy Budget (EEB), data from a variety of narrowband sensors aboard both polar-orbiting and geostationary satellites have also been extensively employed to estimate the EEB components. This paper provides a comprehensive review of the satellite missions, state-of-the art estimation algorithms and the satellite products, and also synthesizes current understanding of the EEB and spatio-temporal variations. The TOA components include total solar irradiance, reflected shortwave radiation/planetary albedo, outgoing longwave radiation, and energy imbalance. The surface components include incident solar radiation, shortwave albedo, shortwave net radiation, longwave downward and upwelling radiation, land and sea surface temperature, surface emissivity, all-wave net radiation, and sensible and latent heat fluxes. Some challenges, and outlook such as virtual constellation of different satellite sensors, temporal homogeneity tests of long time-series products, algorithms ensemble, and products intercomparison are also discussed.

ARTICLE HISTORY
Received 4 December 2018
Accepted 15 March 2019

KEYWORDS
Earth's energy budget; surface radiation budget; satellite; remote sensing; climate change

1. Introduction

Earth's energy budget (EEB) is usually referred to as a balance between the energy coming into the Earth system from the Sun at the top-of-atmosphere (TOA), denoted as incoming shortwave radiative flux – F_0, against energy lost to space that consists of reflected shortwave (F_s) and emitted longwave (F_l) radiative fluxes. EEB at the TOA, often called energy imbalance, can be characterized by net radiation F_n between incoming (F_0) and outgoing radiative fluxes (F_s and F_l) accounting for the remainder on the Earth system – land surfaces, oceans, and atmosphere:

$$F_n = F_0 - F_s - F_l = F_0(1 - \alpha_{\mathrm{TOA}}) - F_l \quad (1)$$

where α_{TOA} is the planetary albedo, or Bond albedo, defining the fraction of incident global mean shortwave radiative flux reflected to space. These four quantities (F_0, $F_s/\alpha_{\mathrm{TOA}}$, F_l and F_n) will be discussed in Section 3.1–3.4, respectively.

CONTACT Shunlin Liang sliang@umd.edu Department of Geographical Sciences, University of Maryland, College Park, MD 20742, USA; School of Remote Sensing and Information Engineering, Wuhan University, Wuhan, Hubei 430079, People's Republic of China

Surface energy balance is central to characterizing surface ecological, hydrological and biogeochemical processes. The surface energy balance equation can be written as

$$R_n = G + H + \lambda ET \tag{2}$$

Where R_n is all-wave net radiation, G is soil heat flux, H is sensible heat flux, and λET is latent heat flux in which λ is the latent heat of evaporation of water and ET is the rate of evaporation of water.

From the perspective of the surface radiation budget (SRB), the net radiation (R_n) represents the balance between incoming radiation from the atmosphere and outgoing radiation from the Earth's surfaces. All-wave net radiation is the sum of shortwave net radiation (R_n^s) and longwave net radiation (R_n^l), and can be expressed by

$$R_n = R_n^s + R_n^l = (1 - \alpha_{sw})F_d^s + F_d^l - F_u^l = (1 - \alpha_{sw})F_d^s + \varepsilon F_d^l - \sigma\varepsilon T_s^4 \tag{3}$$

where α_{sw} is surface shortwave broadband albedo, F_d^s is shortwave downward fluxes incident on the surface, F_d^l and F_u^l are longwave downward and upwelling radiation, ε is the surface longwave broadband emissivity, T_s is the surface skin temperature, and σ is Stefan-Boltzmann's constant.

Surface net radiation and heat fluxes will be discussed in Section 4, including Section 4.1 on incident solar radiation (F_d^s), Section 4.2 on broadband albedo (α_{sw}), Section 4.3 on shortwave net radiation (R_n^s), Section 4.4 on longwave downward radiation (F_d^l), Section 4.5 on longwave upwelling radiation (F_u^l) with subsections on land surface temperature (LST) (Section 4.5.1), land surface emissivity (Section 4.5.2), sea surface temperature (SST) and emissivity (Section 4.5.3), hybrid method (Section 4.5.4) and mean and variations (Section 4.5.5), Section 4.6 on all-wave net radiation (R_n), and Section 4.7 on both sensible and latent heat fluxes (H and λET).

Energy at TOA could be balanced for an equilibrium state without climate change. However, the natural variability of the climate system and anthropogenic intensification of the atmospheric greenhouse effect and land surface changes over recent decades have caused extensive variations in TOA radiative fluxes resulting in TOA energy imbalance (Hansen et al. 2011; Johnson, Lyman, and Loeb 2016; Trenberth et al. 2016; von Schuckmann et al. 2016). Satellite observations can be used to estimate the radiative fluxes at the TOA and the surface (Liang et al. 2010; Loeb, Doelling, et al. 2018), and to further evaluate the changes in atmospheric and surface properties, such as ocean heat transports (Trenberth and Fasullo 2017), cloud amounts and processes, and radiative forcing of aerosols (Satheesh and Ramanathan 2000; Sundström et al. 2015) and sea-ice and snow albedo (Cao et al. 2015; Chen et al. 2015; Flanner et al. 2011; Hartmann and Ceppi 2014; Pistone, Eisenman, and Ramanathan 2014).

Estimation of the radiative fluxes of the Earth system has been traditionally based on broadband sensor observations, such as the Clouds and the Earth's Radiant Energy System (CERES) (Loeb, Doelling, et al. 2018; Loeb et al. 2017). However, considerable progress has been made in estimating these radiative fluxes, particularly at the surface, from narrowband (multispectral) sensor data, such as the Advanced Very High Resolution Radiometer (AVHRR) and the Moderate Resolution Imaging Spectroradiometer (MODIS). With the increased volume of satellite observations from both broadband and multispectral sensors onboard both polar-orbiting and geostationary satellites, numerous EEB products have been generated for various applications. It is, therefore, important to review the development and synthesize recent research results.

To provide quantitative information of these radiation fluxes, we calculated the mean values from four studies (L'Ecuyer et al. 2015; Stephens et al. 2012; Trenberth, Fasullo, and Kiehl 2009; Wild et al. 2015) and displayed them in Figure 1. Since the estimates of sensible and latent heat fluxes from these four studies vary considerable, a range of values with the minimum and maximum values from these four studies is given for each quantity in Figure 1. Although these studies used different approaches and data sources, they continue to be highly regarded. Table 1 shows the major differences in their data sources and methods.

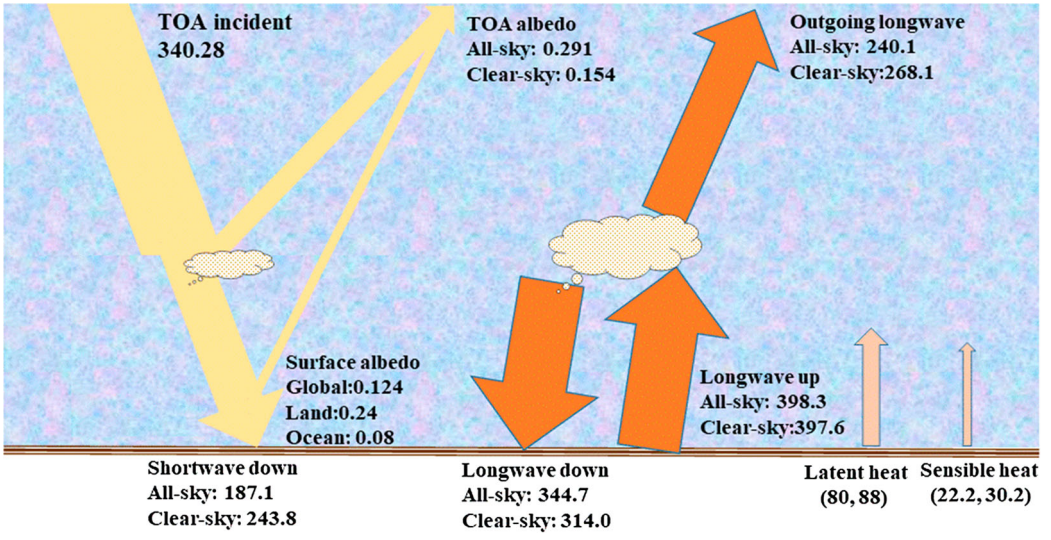

Figure 1. Illustration of the radiative fluxes of the EEB at the TOA and the surface. Their values are estimated from multiple data sources in Wm^{-2} (except albedo) as explained in the text. The surface latent and sensible heat fluxes are given in typical ranges because of their larger estimation uncertainties.

This paper is largely expanded and updated from a recent book chapter (Liang 2017), and provides a comprehensive review of the historical development in monitoring the EEB components. It starts with an overview of the satellite missions and the onboard relevant sensors, then discusses the

Table 1. Selected four studies in this paper: data sources used and some general comments.

Selected studies	Major data sources	Comments
Trenberth, Fasullo, and Kiehl (2009)	CERES and ERBE flux products; reanalyses (NRA, ERA-40, JRA); cloud properties from ISCCP-FD; precipitation data (GPCP and CMAP); surface flux atlases (SOC, WHOI, HOAPS-3)	An update from their earlier study in 1997 Energy balanced at both the TOA and the surface; Two sets of estimates were given for the ERBE period (February 1985 to April 1989) and the CERES periods (March 2000 to May 2004); This paper uses the estimates of only the CERES period
Stephens et al. (2012)	TOA fluxes: TIM, CERES EBAF 2.6r Surface fluxes: GEWEX SRB, ISCCP-FD, CERES ED2 AVG, A Train (Radar + Lidar: L, CCCM), SeaFlux 1.0, precipitation (GPCP), and CMIP5 simulations	Major updates on surface fluxes; The downward longwave radiation at the surface is larger by 10–17 Wm^{-2}; Larger evaporation (latent heat flux) due to more precipitation Mean values from 2000 to 2010 TOA energy imbalance $F_n = 0.6 \pm 0.4$; surface energy imbalance 0.6 ± 17
Wild et al. (2015)	TOA fluxes: CERES EBAF 2.7 products; Land measurements: GEBA and BSRN; Ocean buoy data: IMET, PIRATA, TAO/TRITON; Simulation data of 43 CMIP5 models	Surface observations were used to constrain the model simulations for land and ocean separately; CERES products for the TOA fluxes. The differences between the TOA and the surface for quantifying atmospheric energy budget Uncertainties are also given for each flux The mean energy imbalance at the TOA and at the surface are 1 and 0.6 Wm^{-2}, respectively
L'Ecuyer et al. (2015)	CERES and AVHRR SRB, ISCCP-FD, 2B-FLXHR-lidar, C3M, SeaFlux, Princeton ET, MERRA, GLDAS, GPCP v2.2	A variational data assimilation method was used to integrate various independent data sources by explicitly accounting for their relative accuracies The yielded energy budget estimates simultaneously satisfy all energy and water cycle balance constraints

Note: The full names of various data sources are available in the cited references.

EEB at the TOA and at the surface. Many of these quantities are identified as the essential climate variables (ECV) by the Global Observing System for Climate (GCOS) (GCOS 2016), such as Total Solar Irradiance (TSI), TOA reflected radiation, OLR, surface incident and reflected shortwave radiation, surface downward and upward longwave radiation, SST, LST and surface emissivity. Future challenges and prospects are also discussed.

2. Overview of the satellite missions and sensors

House et al. (1986) reviewed the historical satellite missions and their measurements of the Earth's radiation budget from the beginning of the satellite era until 1984. Since the 1960s, meteorological satellites have dramatically advanced our understanding of the EEB. In contrast to ground-based observations, space-borne observations have the advantage of global coverage. All satellite sensors can be classified as either broadband or narrowband, onboard either polar-orbiting satellites or geostationary satellites.

Space-borne measurements of TSI have been ongoing through a series of temporally-overlapping sensors (Dewitte and Clerbaux 2017; Kopp 2017). The Earth Radiation Budget (ERB) instrument, launched on NASA's NIMBUS 7 spacecraft in November 1978, was the first long-duration spaceflight TSI instrument. Several satellite missions are still operational for making time series measurements, such as the Total Irradiance Monitor (TIM) (Kopp, Lawrence, and Rottman 2005) abroad the SOlar Radiation and Climate Experiment (SORCE) launched in January 2003, the Total Solar Irradiance Monitor (TSIM) (Fang et al. 2014; Wang et al. 2017) instrument abroad Chinese FY3B launched in 2011 and FY3C launched in 2013.

For monitoring TOA reflected radiation and OLR, the typical broadband radiometers are summarized in Figure 2. The broadband sensors on the US polar-orbiting satellites include the ERB aboard Nimbus-7 (Jacobowitz and Tighe 1984), the Earth Radiation Budget Experiment (ERBE) aboard three satellites (Barkstrom and Smith 1986), and CERES (Wielicki et al. 1998). So far, six CERES instruments have been flying on four different spacecraft (Loeb et al. 2016, 2017): one aboard NASA's Tropical Rainfall Measuring Mission (TRMM) spacecraft on 27 November 1997, two aboard NASA's Earth Observing System (EOS) Terra Spacecraft since 18 December 1999 with a 10:30 am. Equatorial crossing time, two onboard NASA's EOS Aqua spacecraft launched on 4 May 2002 with a 1:30 pm. Equatorial crossing time (ECT), one on the Suomi National Polar-orbiting Partnership (S-NPP) spacecraft on 28 October 2011, and one on the first Joint Polar Satellite System (JPSS-1) spacecraft launched on 10 November 2017. The orbit for both S-NPP and JPSS-1 is a 1:30 pm. ECT. CERES has three broadband channels: shortwave (0.3–5 μm), thermal (8–12 μm) and total (0.3–

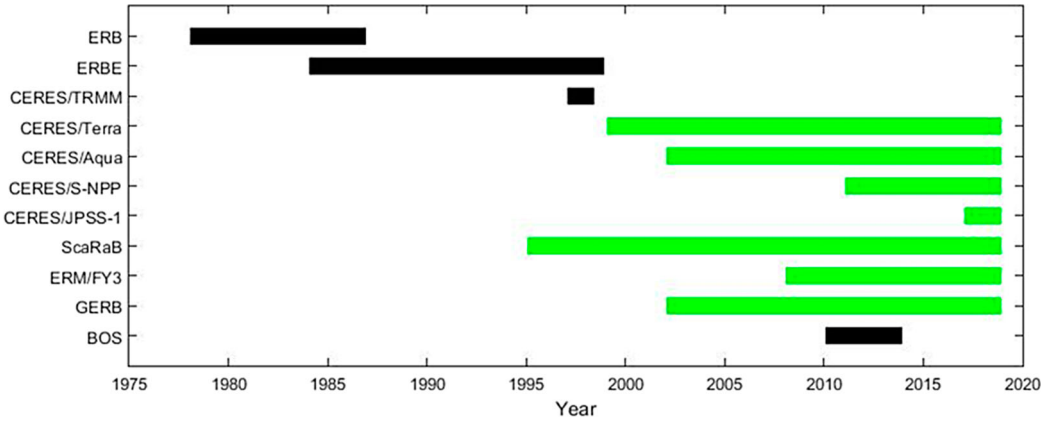

Figure 2. Satellite broadband sensors for measuring TOA reflected shortwave and outgoing longwave radiation abroad polar-orbiting satellites (all except two) and geostationary satellites (GERB and BOS).

>100 μm). Building a CERES follow-on RBI (Radiation Budget Instrument – RBI) instrument that was planned to fly on JPSS-2 was unfortunately cancelled by NASA in January 2018 due to cost overruns for building the RBI.

In addition to the US satellites, there are several other broadband sensors on polar-orbiting platforms. The Scanner for Radiation Budget (ScaRaB) (Kandel et al. 1998; Sathiyamoorthy et al. 2013), jointly developed by France, Russia, Germany and India, is a four-channel scanning radiometer, aboard on Meteor 3–6 launched on 25 January 1994 for 13 months, Resurs-01-4 launched on 10 July 1998 for 7 months and Megha-Tropiques launched on 12 October 2011 for over five years (still operational). It has two broadbands (0.2–4 μm and 0.2–50 μm) for radiation budget and two narrowbands (0.5–0.7 μm, 10.5–12.5 μm) for scene identification. The spatial resolution at nadir is around 50 km. The Chinese meteorological FY3 satellites carry the Earth Radiation Measurement (ERM) instrument with two broadband channels (0.2–4.3 μm and 0.2–50 μm). FY3A was launched 27 May 2008 (Dong et al. 2009).

There are also multiple broadband sensors abroad geostationary satellites such as the Geostationary Earth Radiation Budget (GERB) sensors, carried by Meteosat-8 launched in 2002, and Meteosat-9, launched in 2007 (Brindley and Russell 2017), and the broadband bolometric oscillation sensor (BOS) operated as a part of the payload of PICARD between June 2010 and March 2014 (Zhu et al. 2015). In addition to conventional geostationary satellites, the Deep Space Climate Observatory (DSCOVR) satellite, placed at the neutral gravity point between the Earth and the Sun (Lagrange point 1), has been offering high temporal observations (15–60 min) of the sunlit side of the Earth since 2015. The National Institute of Standards & Technology Advanced Radiometer (NISTAR) and Enhanced Polychromatic Imaging Camera (EPIC) onboard Deep Space Climate Observatory (DSCOVR) provide broadband and multispectral observations, respectively, with a unique perspective into Earth's energy balance since the radiation quantities are retrieved for the entire sunlit globe from sunrise to sunset multiple times per day as the Earth rotates in EPIC's field of view (Herman et al. 2018).

The multispectral sensors aboard both polar-orbiting and geostationary satellites have also been used to estimate EEB radiative fluxes, such as the Medium-Resolution Infrared Radiometer (MRIR) experiment on the Nimbus 2 and 3 spacecraft (Raschke and Bandeen 1970), the Spinning Enhanced Visible and Infrared Imager (SEVIRI) radiometers onboard the METEOSAT Second Generation (MSG) satellites (Schmetz et al. 2002), Geostationary Operational Environmental Satellites (GOES) (Pinker et al. 2007), the Advanced Baseline Imager (ABI) carried by GOES-R that has been renamed to GOES-16 (Laszlo et al. 2008), the Advanced Himawari Imager abroad Himawari-8 (Lee et al. 2018), and MODIS (Wang and Liang 2016).

3. TOA energy budget

This section will present the following four components: total solar irradiance (TSI), planetary albedo, outgoing longwave radiation (OLR) and energy imbalance.

3.1. Total solar irradiance (TSI)

Total solar irradiance (TSI) measurements and their time series are required to support the work of the United Nations Framework Convention on Climate Change (UNFCCC) and the Intergovernmental Panel on Climate Change (IPCC). Many satellite sensors have been used to monitor TSI. Kopp (2017) provided a comprehensive overview of the sensor development and their measurements. The earlier sensors provided larger estimates of solar constant that is integrated from TSI over all wavelengths, but the currently accepted solar constant value is much lower than the earlier estimates. Solar constant $S = 1361\ Wm^{-2}$ was recommended by the International Astronomical Union in 2015, so $F_0 = S/4 = 340.25\ Wm^{-2}$ at the mean distance between the Sun and the Earth. (Coddington et al. 2016; Matthes et al. 2017).

The SOLar SPECtrometer (SOLSPEC) instrument of the SOLAR payload on board the International Space Station (ISS) has performed measurements of solar spectral irradiance from the middle ultraviolet to the infrared (165–3088 nm) ranges. The integral of the SOLAR-ISS solar spectrum yields a solar constant of 1372.3 ± 16.9 Wm^{-2} at 1σ (Meftah, Dame, et al. 2018), which is 11 Wm^{-2} larger than the recommended value but close to the estimated values by earlier sensors. Based on the integrated observations, Gueymard (2018) recently obtained the solar constant of 1361.1 Wm^{-2} with standard uncertainty of 0.5 Wm^{-2}. The good news is that new missions that attempt to provide better TSI estimates are on-going. For example, the Total and Spectral solar Irradiance Sensor (TSIS) (http://lasp.colorado.edu/home/missions-projects/quick-facts-tsis/) was launched to the International Space Station on 15 December 2017 and powered on in March 2018 extending the long record of the solar spectrum measurements.

3.2. Planetary albedo/ reflected shortwave radiation

The fraction of the incoming solar energy reflected by Earth back into space is usually called the planetary albedo. Given F_0, the planetary albedo is equivalent to the reflected shortwave radiation.

The planetary albedo is a fundamental component of the processes that govern the magnitude, distribution, and variability of Earth's climate and climate change (Stephens et al. 2015). In the absence of climate feedbacks, the present-day value is 0.3, which means 30% of the incident solar radiation reaching Earth is reflected back into space and 70% is absorbed by the surface-atmosphere system that is essential to providing the energy necessary to sustain life on Earth. A 5% change in the magnitude of planetary albedo corresponds to a global surface temperature change of approximately 1 K (North, Cahalan, and Coakley 1981). If the average incident solar radiative flux is 340.25 Wm^{-2}, a change in planetary albedo of 0.01 represents a global energy balance change of 3.4 Wm^{-2}, similar in magnitude to the impact of doubling carbon dioxide in the atmosphere (Wielicki et al. 2005).

Based on model simulations, Donohoe and Battisti (2011) found out that the majority of observed global average planetary albedo (88%) is due to atmospheric reflection. Surface reflection makes a relatively small but still significant contribution, particularly the high reflective surfaces such as variability caused by arctic sea ice retreat (Cao et al. 2015; Hartmann and Ceppi 2014; Pistone, Eisenman, and Ramanathan 2014), and land surface snow cover variations (Chen, Liang, and Cao 2016; Chen, Liang, et al. 2016; Chen et al. 2015, 2017; Flanner et al. 2011). Accurate quantification of the radiative forcing due to these surface changes requires further investigations.

Ground measurements of Earthshine by observing the Moon can also be used as proxy to indirectly determine the planetary albedo. It is based on the photometric ratio of the dark (Earthshine) to the bright (Moonshine) sides of the Moon (Palle et al. 2004, 2016). However, satellite remote sensing is the only means to directly monitor the spatial and temporal variations in global planetary albedo. Both broadband and multispectral narrowband satellite data have been used for estimating planetary albedo. For broadband sensor data acquired from both geostationary and polar-orbiting satellites, there are two methods for calculating planetary albedo: empirical angular conversion and radiative transfer computation. The CERES science team uses both methods for estimating planetary albedo/reflected radiative flux (Loeb et al. 2017). Since broadband sensors observe Earth at a specific viewing direction, the first approach develops the angular distribution models (ADM) to convert the observed directional radiances to all-directional flux (Loeb et al. 2005). The second approach calculates the planetary albedo using a radiative transfer model with the inputs of atmospheric and surface properties from other sources (e.g. high-level satellite products, reanalysis data), and is constrained by satellite sensor recorded radiances.

Compared to broadband sensors, data from multispectral radiometers are more profuse and offer higher spatial resolution. Some researchers have attempted to take advantage of such multispectral satellite imagery to retrieve planetary albedo (Lee et al. 2018; Niu and Pinker 2012; Song et al. 2018; Wang and Liang 2016, 2017). Niu and Pinker (2012) developed a two-step approach to first convert narrowband radiance measured by Spinning Enhanced Visible Infrared Imager (SEVIRI) to

broadband radiance and then apply ADMs to retrieve TOA albedo. Wang and Liang (2016, 2017) developed a direct estimation method to retrieve TOA albedo over land from multispectral data collected by MODIS, which combines the angular conversion of radiance to irradiance and the spectral conversion of narrowband to broadband through extensive radiative transfer simulations. The direct estimation methods rely only on satellite observations without using any additional ancillary information. This approach can produce the TOA albedo product at the native spatial resolution of the satellite data. Lee et al. (2018) applied a similar method to estimate TOA albedo from Himawari-8 AHI data.

One of the advantages of estimating planetary albedo from narrowband sensors is the ability to produce long-term and high-resolution satellite products. For example, Song et al. (2018) developed a long-term global TOA albedo product over land from AVHRR data (1981–2017) at a very high spatial resolution (0.05°) in conjunction with MODIS and CERES products. Urbain et al. (2017) processed the Satellite Application Facility on Climate Monitoring (CM SAF) TOA Radiation MVIRI/SEVIRI data record to generate the regional high-resolution TOA albedo. There are several other regional long-term and high-resolution products shown in Table 2.

For both broadband and narrowband sensors, a temporal conversion is needed to convert instantaneous fluxes to hourly, daily, and further monthly values. For geostationary satellite data, such as Geostationary Earth Radiation Budget (GERB) (Brindley and Russell 2017), this procedure is straightforward. For polar-orbiting satellite data, different methods have been used, for example, the CERES team uses global geostationary observations to characterize the temporal variations (Doelling et al. 2013). Wang and Liang (2017) directly estimated daily albedo from the combined Terra and Aqua MODIS observations by assuming constant atmospheric conditions between observations.

Availability of satellite products of TOA albedo enables better understanding of its spatial and temporal variations. According to these CERES Energy Balanced and Filled (EBAF) product Ed4.0 (Loeb, Doelling, et al. 2018), annual mean all-sky reflected flux is 99.1 Wm^{-2} (equivalent to a global albedo of 0.291). The clear-sky reflected flux is 53.3 Wm^{-2} (an albedo of 0.154). The difference between these fluxes (45.8 Wm^{-2}) is taken to be a measure of the cloud influence on the reflected radiative flux. There was a general decreasing trend (-0.57 ± 0.19 Wm^{-2}) from March 2000 – September 2016. The large positive anomalies in shortwave TOA flux coincide with positive

Table 2. Major global TOA planetary albedo/OLR satellite products.

Dataset	Resolutions		Temporal coverage	Spatial coverage	Satellite sensor	Websites; references
	Spatial	Temporal				
ERBE	40 km at nadir	Instantaneous	1984–1990	Global	ERBE	Barkstrom and Smith (1986)
	2.5°	Daily, monthly				
CERES	20 km at nadir	Instantaneous	1997–1998; 2000–present	Global	CERES	Loeb, Doelling, et al. (2018), Loeb et al. (2017)
	1°	Hourly, daily, monthly				
GERB	50 km at nadir	Instantaneous	2002–present	European	GERB	Harries et al. (2005)
	50 km	15 min				
ScaRaB	40 km at nadir	Instantaneous	1994–1995; 1998–1999; 2011–present	30°S–30°N	ScaRaB	Duvel et al. (2001), Roca et al. (2015)
	1°	1–7 times per day				
APP	5 km	Polar	1982–present	Twice/daily	AVHRR	Key et al. (2001)
APP-x	25 km	Polar	1982–present	Twice/daily	AVHRR	Wang and Key (2005a, 2005b)
TAL-AVHRR	0.05°	Global	1981–present	Daily, monthly	AVHRR	WWW6 Song et al. (2018)
TAL-MODIS	1 km	Global	2000–present	Instantaneous, daily	MODIS	WWW6 Wang and Liang (2016, 2017)
MISR	35.2 km	Global	2000–present	Daily, monthly	MISR	WWW7 Diner et al. (1999)
CM-SAF	0.05°	70°N–70°S, 70°W–70°E	1983–2015	Daily, monthly	MVIRI/SEVIRI	WWW8 Urbain et al. (2017)

anomalies in the Arctic sea ice coverage during the early 2000s (Hartmann and Ceppi 2014). In another study, Loeb, Thorsen, et al. (2018) assessed the impacts of the climate warming hiatus and found a marked 0.83 ± 0.41 Wm^{-2} reduction in global reflected shortwave TOA flux during 2000–2017 compared to the hiatus reference years from 2000 to 2014 due to changes in low cloud cover.

The seasonal cycles of planetary albedo are largely influenced by surface albedo (Stephens et al. 2015). The annual cycle of all-sky albedo has two main maxima: a boreal spring-time maximum resulting from the reflection off the brighter snow-covered land surfaces between 30°N and 60°N, and a weaker maximum in the boreal fall season influenced by reflection from mid-latitude clouds of the South Hemisphere (SH). Stephens et al. (2015) further found out that the North Hemisphere (NH) and SH reflect the same amount of sunlight within ~ 0.2 Wm^{-2}. This symmetry is achieved by increased reflection from SH clouds offsetting precisely the greater reflection from the NH land masses.

3.3. Outgoing longwave radiation (OLR)

OLR (F_l) is not only an important component of EEB, but is also widely used as a tool in numerous applications, such as climate sensitivity and diagnosis, weather and climate predictions, studies on monsoon variability and equatorial waves. OLR is considered as a proxy for the deep convection and used as a heuristic indicator of cloudiness or for precipitation estimation. OLR anomalies may also be explored to link with earthquakes because these events can generate thermal anomalies in the atmosphere at low latitudes due to the overabundance of ions from the seismogenic zone (Chakraborty et al. 2018; Shah et al. 2018).

The satellite OLR products are usually generated from broadband sensors (e.g. CERES), but multispectral data also have been used for generating the OLR products (see Table 3). Radiance of an atmospheric window band is sensitive to the thermal emission from the climate system. A well-known method is the use of a single infrared (IR) window band centered at 12.0 μm. Schmetz and Liu (1988) included a water vapor band (e.g. 6.7 μm) aboard the geostationary satellite Meteosat 2 to consider the effect of water vapor in the troposphere. Inoue and Ackerman (2002) used AVHRR two adjacent window bands (e.g. 10.8 and 12.0 μm) to achieve better accuracy over regions with low-level clouds or no clouds. Park et al. (2015) used three channels (6.7, 10.8, and 12.0 μm) from the first Korean geostationary satellite – Communication, Ocean and Meteorological Satellite (COMS). Kim et al. (2018) estimated OLR from one window channel (12.4 μm) and two channels (6.2 and 12.4 μm) from Himawari-8 AHI data with good agreement with the CERES OLR product. Zhou et al. developed the direct estimation method to derive the narrowband to broadband regression coefficients at the detailed viewing zenith angle intervals to estimate OLR directly from MODIS (Zhou et al., "Estimating High Spatial Resolution," 2019) and AVHRR (Zhou et al., "Generating 35-Year High-Resolution," 2019) multispectral thermal data.

The CERES OLR product (Loeb, Doelling, et al. 2018) is based on radiative transfer calculation with inputs of ancillary information of atmospheric and surface properties from other high-level satellite products and reanalysis data, constrained by the CERES observations. Loeb, Doelling, et al. (2018) determined from the CERES EBAF Ed4.0 that annual mean all-sky OLR is 240.1 Wm^{-2} and the clear-sky OLR is 268.1 Wm^{-2}. The clouds blocked the OLR by 27.9 Wm^{-2}.

Table 3. Major OLR satellite products.

Data source	Time span	Spatial resolution	References
CERES	2001–present	1°	Loeb, Doelling, et al. (2018)
AVHRR	1981–2016	0.05°	Zhou et al., "Generating 35-Year High-Resolution," (2019)
HIRS	1979–present	2.5°	Lee et al. (2007)
GEWEX SRB	1983–2007	1°	Stackhouse et al. (2011)
AIRS	2002–present	1°	Sun et al. (2010)

In a recent study, Zhou et al., "Evaluation of Six Outgoing," (2019) compared five satellite OLR products (AVHRR, HIRS, GEWEX-SRB, AIRS, CM-SAF) with the CERES OLR products, and found that all the five OLR products have very close climatology values to CERES with both absolute bias and root-mean-square-deviation (RMSD) < 5 Wm^{-2} in winter and summer seasons, while the AVHRR OLR product matches CERES the best (bias = −1.62 Wm^{-2} for winter, −1.05 Wm^{-2} for summer; RMSD = 1.94 Wm^{-2} for winter, 1.60 Wm^{-2} for summer). Biases vary seasonally over land but are relatively stable over oceans.

Susskind et al. (2012) found global and tropical OLR anomaly time series is strongly correlated with El Niño/La Niña variability: positive values in 2002/2003, 2007, and 2010 for El Nino events and negative values during most of 2008 through spring 2009 correspond to La Niña conditions. Su et al. (2017) determined the trends of tropical (30°N – 30°S) mean daytime and nighttime OLRs from both the CERES and the AIRS from 2003 to 2013, and found decreasing trends because of El Nino conditions early in the period and La Nina conditions at the end. However, the daytime OLR decreased much faster than nighttime, and the causes for the different decreasing rates are unclear.

3.4. Energy imbalance

Satellite observations can be used to monitor changes in TSI, reflected solar, emitted thermal, and hence, net radiation at the TOA with spatial scales from regional to global, and temporal scales from daily to annual. A limitation of the satellite data is their inability to provide an absolute measure of the net TOA radiation imbalance to the required accuracy level because the net TOA radiation imbalance is the difference between incoming and outgoing radiation quantities that are well over two orders of magnitude larger than the net TOA imbalance. Relatively small uncertainties of these radiative fluxes may lead to large errors in estimating TOA energy imbalance. For example, the average global net radiation at the TOA directly from CERES SYN shortwave and longwave all-sky TOA fluxes from July 2005–June 2015 was approximately 4.3 Wm^{-2}, much larger than expected (Loeb, Doelling, et al. 2018). Note that as uncertainty stems mostly from biases, changes over time can be tracked.

It is necessary, therefore, to anchor the satellite data to an absolute scale using other data. Since changes in the energy of the atmosphere, land, and cryosphere are much smaller (Hansen et al. 2011; Trenberth, Fasullo, and Balmaseda 2014), with over 90% of Earth's energy imbalance being stored in the oceans, the most accurate way to determine it is to measure increases in ocean temperatures (along with increases in land temperatures, decreases in ice mass, and increases in atmospheric temperature and moisture). Observations of trends in ocean heat content (OHC) enable the satellite estimates to be anchored to obtain an absolute value heat uptake (Johnson, Lyman, and Loeb 2016; Loeb et al. 2012), as well as providing independent estimates of variations in TOA net radiation.

Loeb et al. (2012) adjusted the satellite-based net radiation to be 0.50 ± 0.43 Wm^{-2} over the period July 2005 to June 2010 based on ocean measurements to depths of 1,800 m. Johnson, Lyman, and Loeb (2016) updated the estimation and found a net heat uptake of 0.71 ± 0.10 Wm^{-2} from 2005 to 2015. In their study, they found the correlation between year-to-year rates of 0–1,800 m ocean heat uptake and the latest release of CERES net radiation is a much-improved 0.78. This striking agreement between two completely independent measures bolsters confidence in both of these complementary climate observation systems and provides valuable insights into climate variability. Nevertheless, it is important to point out that no consensus on the magnitude of the TOA energy imbalance has been reached. For example, Trenberth et al. (2016) provided a higher estimate of TOA net radiation with a larger uncertainty: 0.9 ± 0.3 Wm^{-2} for 2005–2014 based on CERES product, modeling and OHC data.

Based on the CMIP5 climate model simulations, Palmer and McNeall (2014) found that the oceans become the dominant energy store in the Earth System on a timescale of about one year and changes in global OHC provide a more reliable indication of TOA variability than global

averaged surface temperature. Trenberth et al. (2015) pointed out that TOA net radiation is strongly related to the ocean temperatures' variability: mainly ENSO, especially the 2008/2009 and 2011/2012 cold La Niña conditions not only radiated less to space but also reduced cloudiness and increased ASR, while the reverse occurred for the 2010 El Niño scenario.

Multiple studies also have provided the estimates of temporal variations in TOA net radiation. Allan et al. (2014) estimated the TOA net radiation since 1985 by integrating both the CERES product since 2000 and the ERBE product from 1985 to 1999. These two data sets were homogenized and gaps filled using the ERA Interim reanalysis and high-resolution atmosphere model simulations driven by observed sea surface temperatures and sea ice concentrations. Smith et al. (2015) further extended this analysis to as early as 1960 also by incorporating IPCC AR5 simulations and OHC data. They found that the energy imbalance is increasing, and much of the multiyear variability in Earth's energy imbalance from 1960 to 2000 was externally forced by the volcanic eruptions of Agung (1963), El Chichon (1982), and Pinatubo (1991).

There are other methods that can also estimate the TOA energy imbalance. For example, Resplandy et al. (2018) quantified the ocean heat uptake and consequently the TOA energy imbalance by measuring atmospheric oxygen (O_2) and carbon dioxide (CO_2). When the ocean warms, the soluble concentrations of O_2 and CO_2 decrease, and the amount of gas lost by the ocean can be quantified with the complementary change observed in the atmosphere. They estimated that the ocean gained $1.33 \pm 0.20 \times 1022$ joules of heat per year, equivalent to a TOA energy imbalance of 0.83 ± 0.11 Wm^{-2} from 1991 to 2016. Hakuba et al. (2019) recently proposed a satellite mission concept based on accelerometry that measures the radiation pressure acting on earth-orbiting satellites. This methodology of deriving the TOA energy imbalance from the net radiation pressure force acting on Earth-orbiting spacecrafts has been actually demonstrated a long time ago (Bernard 1978; Boudon 1986). This may provide an independent approach for quantifying global and zonal mean TOA energy imbalance on annual and potentially monthly timescales.

4. Surface energy budget

Estimating the surface radiative fluxes makes use of diverse methods, which will be discussed in more details in the following sections. We can roughly group them into two types (see Figure 3). The first type relies on atmospheric and surface properties (e.g. cloud and aerosol optical depth, water vapor, surface reflectance) retrieved from the current satellite data or input from other sources. The surface radiative fluxes can be estimated from radiative transfer calculations or parametric formulae that are usually fitted from extensive radiative transfer simulations. This type of method is based on a solid physical foundation by taking advantage of rigorous radiative transfer models, and can be used to calculate the radiative fluxes accurately if the input parameters of the atmosphere-surface system are accurate. Since the input parameters most likely come from the multiple sources that may have different spatial and temporal resolutions, however, the estimated surface radiative fluxes usually have coarser spatial resolutions. The uncertainties and inconsistency of the inputs from multiple sources may affect the accuracy and quality of the final products (Jia et al. 2018). Besides, this approach also suffers from the issue of data gaps because missing values in any input parameters will lead to data gaps in the retrieved results.

The second type estimates surface radiative fluxes directly from satellite observations, which are usually called the direct estimation methods. They link TOA observations with the surface radiative fluxes using regression/machine learning methods, look-up tables, or other algorithms based on extensive radiative transfer simulations. They are often called hybrid methods because they combine extensive radiative transfer simulations with comprehensive atmospheric and surface properties (physical) with statistical analysis that link the simulated TOA observations and surface fluxes. These types of methods do not need explicit inputs of atmospheric and surface properties, so can be extremely useful when the atmospheric and surface properties are not reliably available or still

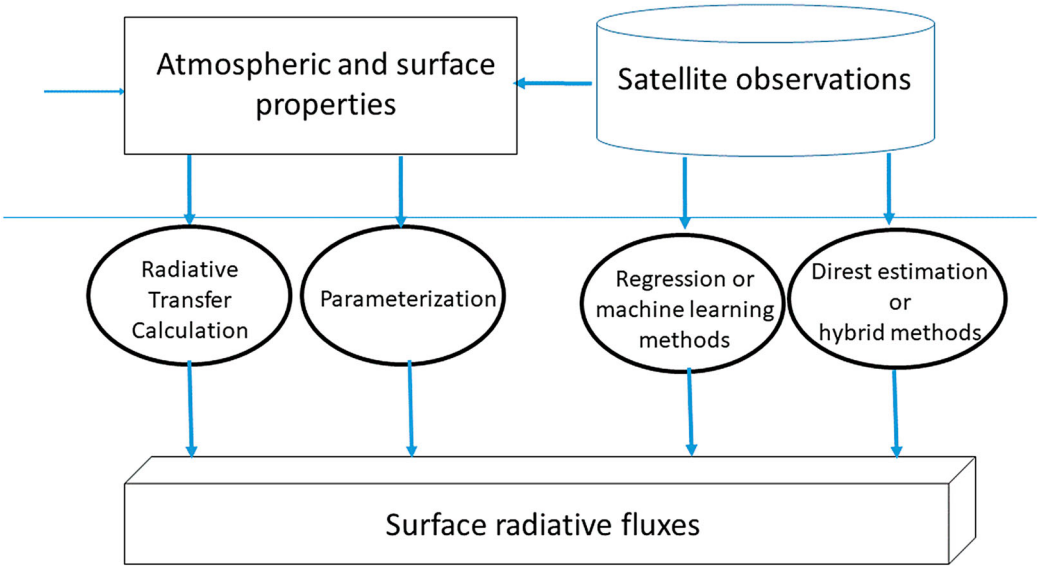

Figure 3. The typical methods for estimating surface radiative fluxes from satellite observations.

have large uncertainties. It is also easy to implement. Besides, they can generate the products at the native spatial resolution of the satellite data.

These two types of methods, along with some others, will be presented in detail in a later discussion of the estimation of a specific surface quantity.

4.1. Incident solar radiation

The incident solar radiation at surface F_d^s is required by almost all land surface models and also for generating other high-level land surface products such as ET and vegetation productivity. It can be either directly measured or estimated from surface meteorological observations using various empirical methods based on the relationship between ground-measured radiation and some meteorological parameters such as sunshine duration and temperature (Yang, Koike, and Ye 2006; Yang et al. 2010). Despite continuous improvements, many regions are still insufficiently covered by direct surface radiation observations, such as vast areas of Africa and South America, as well as ocean areas in general, which prevents a true global assessment.

Spaceborne estimates of incident solar radiation have been reviewed by several studies (Liang et al. 2010; Pinker, Frouin, and Li 1995; Zhang, Liang, and Wang 2017). Besides the broadband radiometers (e.g. CERES), satellite data from multispectral sensors on both polar-orbiting or geostationary satellites also have been used to produce incident surface radiation products, such as the MSG/SEVIRI (Schmetz et al. 2002), GOES (Pinker et al. 2007; Zheng, Liang, and Wang 2008), Geostationary Meteorological Satellite (GMS) 5 (Lu et al. 2010), the Multifunctional Transport Satellite (MTSAT) (Huang et al. 2011), the ABI (Laszlo et al. 2008), MODIS (Liang et al. 2006; Zhang et al. 2014; Zhang, He, et al. 2018) and AVHRR (Liang et al. 2007; Yang, Zhang, et al. 2018). Table 4 lists some major global incident solar radiation satellite products.

Many estimation methods have been proposed (Zhang, Liang, and Wang 2017), and two types of algorithms can be grouped for estimating incident solar radiation from satellite observations (Liang et al. 2010). The first approach uses the retrieved cloud and atmosphere parameters from other sources (e.g. high-level products from other satellite data or reanalysis data) input into radiative transfer (RT) models that have different levels of complexity from simple analytical formulae to sophisticated rigorous models (Oreopoulos et al. 2012). Many parametrization schemes have been

Table 4. Major downward solar radiation (DSR) and net radiation satellite products.

Data set	Radiative fluxes	Spatial resolution	Temporal resolution	Temporal range
GEWEX-SRB V3.0	DSR, net radiation	1°	3 hourly, daily, monthly	1983.7–2007.12
ISCCP-FD	DSR	~280 km	3 hourly	1983.7–2009.12
CERES-EBAF Ed4.0	DSR, net radiation	1°	Monthly	2000.3–present
CM-SAF CLARA-A2	DSR	0.25°	Monthly	1982.1–2015.12
GLASS	DSR, net radiation	5 km	Daily	2000–present
MODIS (MCD18)	DSR	1 km	3 hourly	2000–present

developed as substitutes of complex radiative transfer models (Huang et al. 2018; Qin et al. 2015; Tang et al. 2016, 2017; Wang and Pinker 2009). More sophisticated RT model based methods have also been used for estimating incident solar radiation from the CERES (Kato et al. 2018), the International Satellite Cloud Climatology Project (ISCCP) (Zhang et al. 2004), GEWEX (Pinker et al. 2003) and SEVIRI (Deneke, Feijt, and Roebeling 2008). This approach has clear physical basis, but uses multiple atmospheric and surface products, such as atmospheric water vapor abundance, aerosol and cloud optical depths, and surface reflectance. It may accumulate the uncertainties from estimating these individual products.

The second approach uses the relationship between the TOA observations and incident surface radiation based on collocated surface measurements or extensive RT simulations. The regression methods correlating surface insolation measurements with satellite TOA data are simple and easily implemented (Fritz, Rao, and Weinstein 1964; Tarpley 1979), but a drawback is that the regression coefficients may be geographically dependent. Liang et al. (2006; Liu et al. 2008) generated the photosynthetically active radiation (PAR) and shortwave radiation products from MODIS data directly by searching the LUTs created by the extensive RT simulations. Wang et al. (2010) expanded this approach to retrieve daily PAR from MODIS data onboard two spacecrafts. Zhang et al. (2014) applied this algorithm to generate the first version of the Global LAnd Surface Satellite (GLASS) radiation products (Liang, Zhang, et al. 2013; Liang, Zhao, et al. 2013) by combining multiple geostationary and MODIS satellite data. The LUT method has been used to generate the incident solar radiation product operationally from MODIS data (MCD18) (Zhang et al. 2014), from AVHRR data (CM-SAF CLARA-A2) (Karlsson et al. 2017) and from MSG/SEVIRI data since 2017 (Romano et al. 2018).

There are also some other estimation methods, such as the optimization method (Zhang, He, et al. 2018) and the machine learning methods (Qin et al. 2011; Wang, Yan, and Chen 2012; Yang, Zhang, et al. 2018). Instead of relying on ancillary datasets of atmospheric properties, the optimization method (Zhang, He, et al. 2018) can retrieve aerosol and cloud optical depths and surface reflectance parameters and then further calculate incident solar radiation. Wang, Yan, and Chen (2012) and Ryu et al. (2018) explored the artificial neural network (ANN) to estimate incident solar radiation from MODIS data. Yang, Zhang, et al. (2018) applied the gradient boosting regression tree (GBRT) machine learning method to estimate incident solar radiation over China using the ground observation data collected from the China Meteorological Administration (CMA) Meteorological Information Center and the AVHRR observations at a spatial resolution of 5 km.

Some studies have attempted to evaluate different algorithms and products. Qin et al. (2018) compared the performances of four algorithms for estimating surface incident solar radiation using MODIS atmospheric and surface products over China. Based on extensive ground measurements, Zhang et al. (2015) evaluated four commonly used satellite products, including the GEWEX SRB3.0, ISCCP-FD, University of Maryland SRB V3.3.3 and the CERES EBAF. They found that those products agree much better with surface measurements on a monthly scale with the biases from 5.0 to 18.3 Wm^{-2} and the RMSEs from 18.8 to 34.6 Wm^{-2}, than on a daily time scale. Zhang, Liang, et al. (2016) also applied the similar method to validate six monthly reanalysis datasets (NCEP-NCAR, NCEP-DOE, CFSR, ERA-Interim, MERRA, and JRA-55), and found that reanalysis data have larger biases from 11.3 to 49.8 Wm^{-2}, and the RMSEs from 27.7 to 60.0 Wm^{-2}. Almost all

the reanalysis products showed better accuracies in winter than summer. It was further found out that the biases of cloud fraction (CF) in the reanalyses caused the overestimation (Zhang, Liang, et al. 2016). Wild et al. (2015) evaluated 43 CMIP5 models and found that the mean value varies in a range of more than 40 Wm^{-2} among the CMIP5 models, from 169 to 210 Wm^{-2}, with a standard deviation of almost 10 Wm^{-2}. Incident solar radiation is the component with the largest spread within the CMIP5 models among all land and ocean mean energy balance components.

The global average of incident surface solar radiation estimated from satellite products is 188.6 ± 15 Wm^{-2} (GEWEX), 188.9 ± 20 Wm^{-2} (ISCCP), 188.9 Wm^{-2} (CERES), 192 Wm^{-2} (A-train – L), 189 Wm^{-2} (A-train – CCCM), respectively (Stephens et al. 2012). Note that the estimated values from various EEB studies are different: 184 (Trenberth and Fasullo 2009), 188 ± 6 (Stephens et al. 2012), 185 (179–189) (Wild et al. 2015) and 186 ± 5 (L'Ecuyer et al. 2015) Wm^{-2}, respectively.

Zhang, Liang, et al. (2016) used extensive ground observations at the 1,677 global energy balance archive (GEBA) sites and other four long-term observation ground measurement datasets to estimate the biases of the CERES EBAF and four reanalysis datasets. After removing the averaged bias weighted by the area of the latitudinal band, the global annual mean estimates of incident solar radiation from CERES EBAF was 182.9 Wm^{-2} over the nine-year period from 2001 to 2009, which is much smaller than the previous estimates. Kato et al. (2018) provided the latest CERES estimate (CERES EBAF 4.0) of 187.1 Wm^{-2} averaged from 2005 to 2015. It is clear that existing knowledge on incident solar radiation still has large uncertainties.

The incident surface solar radiation undergoes significant decadal variations (Wild 2009, 2012). The attributing factors of the long-term variations include clouds, aerosols, and radiatively active gases (Wang, Dickinson, et al. 2012; Wild 2012, 2016). In situ measurements of incident solar radiation at weather stations since the 1950s, such as those from the Global Energy Balance Archive (GEBA), are a good data source for determining the long-term trends (Wild et al. 2017). However, instrument replacement (Wang 2014) or different measuring methods (Wang, Dickinson, et al. 2013) can cause uncertainties. He, Wang, et al. (2018) determined the global brightening and dimming trends in China, Europe, and the United States since 1901 using sunshine duration data. Satellite products have also been demonstrated to reveal the long-term variations (Zhang, Liang, and Wang 2017). For example, Hinkelman et al. (2009) using GEWEX/SRB product, version 2.8, estimated a 2.51 Wm^{-2} $decade^{-1}$ dimming between 1983 and 1991, followed by 3.17 Wm^{-2} $decade^{-1}$ brightening from 1991 to 1999, returning to 5.26 Wm^{-2} $decade^{-1}$ dimming over 1999–2004, and a −0.53 Wm^{-2} $year^{-1}$ global dimming over 1999–2004, with similar features in both hemispheres and significant differences between land and ocean. Hatzianastassiou et al. (2012) calculated incident surface radiation using a RT model with different parameters retrieved from satellite data and showed an overall global dimming on the Earth for all-sky conditions, from 2001 to 2006, arising from a stronger solar dimming in the Southeern Hemisphere (−0.48 Wm^{-2} $year^{-1}$) and a slight brightening in Northern Hemisphere (0.028 Wm^{-2} $year^{-1}$).

4.2. Broadband albedo

Surface shortwave broadband albedo (α_{sw}), represents the surface hemispheric reflectivity integrated over the solar spectrum (0.2–5.0 μm). Accurate knowledge of land surface albedo can significantly improve weather and climate model simulations (Boussetta et al. 2015; Knorr, Schnitzler, and Govaerts 2001; Kumar et al. 2014; Viterbo and Betts 1999). Two recent book chapters (He, Wang, and Qu 2017; Qu 2017) have comprehensively discussed land and ocean surface albedos.

Many methods have been developed to generate the global land surface albedo products from both polar-orbiting and geostationary satellite data (Qu et al. 2015). The conventional method shown in Figure 4 consists of three basic steps: atmospheric correction (Liang, Fang, and Chen 2001; Vermote, El Saleous, and Justice 2002) to convert TOA observations to surface directional reflectance; anisotropical reflectance modeling (Roujean, Leroy, and Deschamps 1992; Roujean et al. 1997; Wanner, Li, and Strahler 1995; Wanner et al. 1997) by fitting a bidirectional reflectance

distribution function (BRDF) or bidirectional reflectance factor (BRF) model from accumulated multiangular surface directional reflectance to calculate spectral albedo; and converting the spectral (narrowband) albedo values to broadband albedo (Liang 2001; Liang et al. 2003). This method has been widely used for generating the MODIS land albedo (Schaaf et al. 2002) and others.

The alternative 'direct estimation algorithm', shown in Figure 5, is used to estimate surface albedo directly from TOA observations, which combines all these three steps into a single step through regression analysis to create a best-estimate broadband albedo (Liang 2003; Liang, Strahler, and Walthall 1999; Liang, Stroeve, and Box 2005). The direct estimation method does not require surface reflectance that results from atmospheric correction. Moreover, it also does not need an accumulation of observations during a certain period of time that cannot capture the rapid surface changes. This algorithm has been applied to produce the GLASS albedo product (Liang, Zhao, et al. 2013; Qu et al. 2014) with the MODIS and AVHRR data, and the Visible/Infrared Imager/Radiometer Suite (VIIRS) albedo product (Wang, Liang, et al. 2013; Zhou, Wang, et al. 2016). It has also demonstrated that this method can accurately estimate land surface albedo from different Landsat data (He, Liang, et al. 2018), Chinese HJ data (He et al., "Land Surface Albedo Estimation," 2015), MISR data (He, Liang, and Wang 2017), and the airborne AVIRIS data (He et al., "Estimation of High-Resolution Land Surface," 2014).

The optimization approach has been demonstrated to retrieve atmospheric aerosol optical depth, surface directional reflectance and albedo simultaneously from SEVIRI data (Govaerts et al. 2010; Wagner, Govaerts, and Lattanzio 2010) and MODIS data (He et al. 2012). This type of method can estimate a suite of parameters besides broadband albedo, but is computationally expensive because it usually requires numerous iterations. So far, none of these algorithms have been used for producing global satellite products. New techniques, such as emulation, need to be developed for improving the computational efficiency of this method.

The major long-term global land surface albedo products are listed in Table 5. There are many regional albedo products or short-term products are also available to the public (He, Wang, and Qu 2017).

Two global land surface albedo products (MODIS and GLASS), which are probably the most accurate global land surface albedo products, show that global annual mean values are 0.2417 (GLASS) and 0.2319 (MODIS). We also calculated the annual mean albedo values simulated by the CMIP5 models to be 0.2542 ± 0.0188. The differences in the monthly mean values are much larger.

In contrast to the land surface albedo products, there are few ocean surface albedo products from satellite data. The most complete product is the clouds, albedo and radiation (CLARA) product (Karlsson et al. 2017; Riihela et al. 2013). The GEWEX and CERES products can be used to calculate ocean albedo. The GLASS ocean albedo product from MODIS and AVHRR data is still under development (Feng, Liu, et al. 2016; Qu et al. 2016).

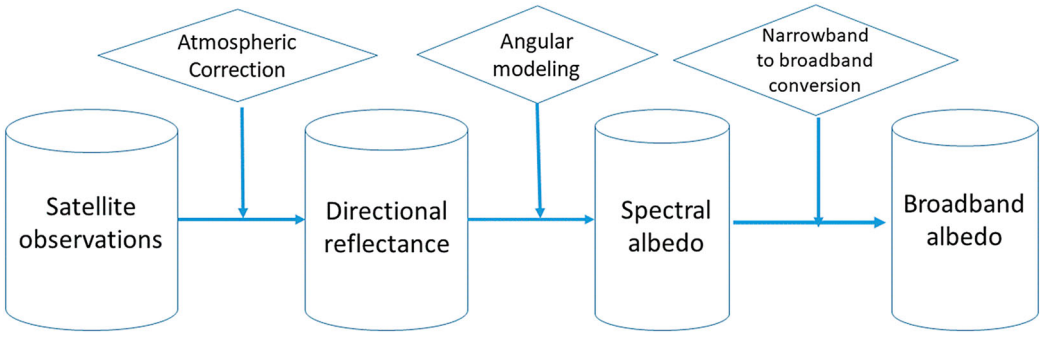

Figure 4. The traditional approach for estimating land surface albedo from satellite data.

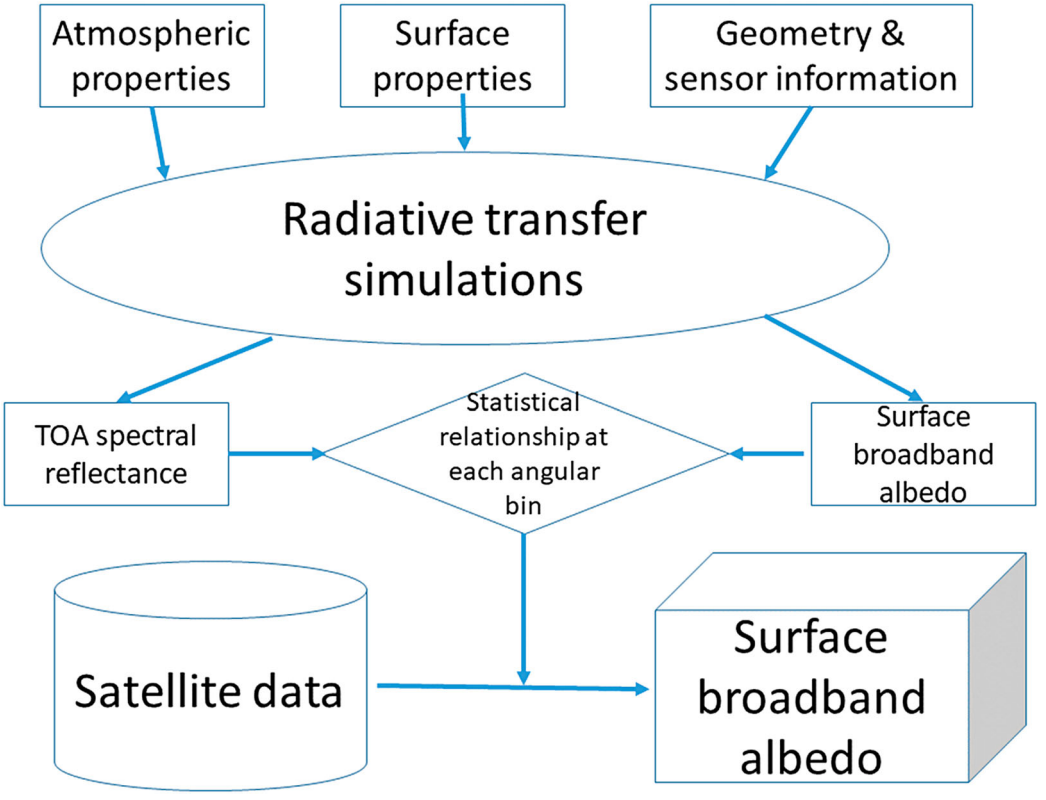

Figure 5. The direct estimation method for estimating land surface albedo from satellite data.

The average ocean albedo is 0.081 ± 0.007 from the CLARA-A2, GEREX, ISCCP, and CERES products, 0.080 from CMIP5 model simulations (He, Liang, and Zhang 2018), and 0.0814 (reanalysis), respectively, which are highly consistent. However, if their monthly averages are examined, there exist considerable differences among those data. The differences are even more significant in the Arctic.

Globally, the mean albedo from CERES is 0.1245 (Kato et al. 2018), and the average albedo is 0.124 ± 0.006 from CLARA-A2, GEWEX, ISCCP and CERES products. The mean albedo from CMIP5 model simulation is 0.130 ± 0.010 (He, Liang, and Zhang 2018), while the average global albedo from reanalysis datasets is 0.1353 ± 0.0085. Independent studies with various data sources typically reported different values of the global average albedo, for example, 0.125 (Trenberth, Fasullo, and Kiehl 2009), 0.122 (Stephens et al. 2012), 0.130 (Wild et al. 2015) and 0.118 (L'Ecuyer et al. 2015), respectively.

Again, the monthly averaged albedo values are significantly different. It is very important to monitor Earth's albedo in sufficiently high spatial and temporal resolutions. Land surface albedo

Table 5. Major global land surface albedo satellite products.

Product name	Satellite data	Spatial resolution	Temporal resolution	Temporal coverage	References
MODIS	MODIS	daily	500 m	2000–present	Schaaf et al. (2002)
VIIRS	VIIRS	daily	750 m	2012–present	Wang, Liang, et al. (2013)
CLARA-A2	AVHRR	5 days	0.25°	1982–2015	Karlsson et al. (2017), Riihela et al. (2013)
GLASS	AVHRR, MODIS	Daily, 8 days	1 km &0.05°	1981–present	Liu et al. (2013), Qu et al. (2014)
GEOLAND2	VEGETATION	10 days	1/112°	1999–present	Hagolle et al. (2005)

is highly variable, depending on many factors, such as land cover types, snow/ice cover, soil moisture. Drought or forest fires can lead to changes in surface albedo (O'Halloran et al. 2012; Zhang and Liang 2014). Fires in Siberian larch forests increased surface albedo during snow-on periods and resulted in strong cooling (Chen et al. 2018). Human activities, such as deforestation (Houspanossian et al. 2017; Loarie et al. 2011; Zhang and Liang 2014), irrigation (Zhu et al. 2011), pollution (Lee and Liou 2012), and urbanization (Hu, Jia, et al. 2016) can greatly alter land surface albedo.

The recession of snow cover can amplify warming (Chen, Liang, and Cao 2016; Chen, Liang, et al. 2016; Chen et al. 2015; Flanner et al. 2011; He et al. 2013; Shi and Liang 2013). On the continental scale, He, Liang, and Song (2014) found from the satellite land albedo products that surface snow cover is a dominating factor that controls the decreasing trend (July) and the increasing trend (January) of land surface albedo. Mortimer and Sharp (2018) calculated the albedo trend of glaciers in Canada's Queen Elizabeth Islands using the MODIS albedo product and found a negative correlation with LST. Li, Ma, et al. (2018) recently found out that the global greening trend also correlates with the decreased trend of albedo during the summer.

Ocean surface albedo largely depends on sea ice, sun glint, whitecaps, and ocean water reflectivity. For example, Arctic Ocean albedo has declined considerably in the past decades (Comiso and Hall 2014; Riihelä, Manninen, and Laine 2013) mainly due to sea ice retreat (Perovich and Polashenski 2012), earlier melt onset (Stroeve et al. 2014) and sea ice thinning (Kwok and Rothrock 2009), which leads the Arctic Ocean to absorb more solar radiation and amplify the Arctic warming (Cao et al. 2015; Flanner et al. 2011; Pistone, Eisenman, and Ramanathan 2014). Cao et al. (2016) recently evaluated the ocean albedo from four reanalysis datasets over the Arctic Ocean, and found that three of them are unable to effectively track the interannual variation of ocean albedo and significantly underestimate the decreasing trend compared to a satellite albedo product.

4.3. Shortwave net radiation

Shortwave net radiation is the shortwave portion of the surface radiation budget. It dominates the energy balance in the daytime since the daytime longwave net radiation is strongly correlated with the daytime shortwave net radiation (Kjaersgaard, Plauborg, and Hansen 2007). One approach to estimate all-wave net radiation is to utilize this relationship between shortwave and all-wave net radiation (Jiang et al. 2015; Wang and Liang 2009a). To understand the climate system, Cess et al. (1991; Li et al. 1993) argued that surface shortwave absorption (net radiation) is a more meaningful quantity than surface incident solar radiation.

Given incident solar radiation F_d^s and surface shortwave albedo α_{sw}, shortwave net radiation can be easily calculated as $F_d^s(1-\alpha_{sw})$. However, the shortcoming of this approach is that the uncertainties of these two quantities may accumulate (He et al., "Estimation of High-Resolution Land Surface Net Shortwave Radiation," 2015). Since each of the two products contains uncertainties and to avoid possible error propagation from the two products, an alternative is to estimate shortwave net radiation directly.

Ramanathan (1986) first found a simple proportionality between surface shortwave net radiation with TOA shortwave net radiation. Cess and Vulis (1989) later found out this relationship is linear based on more accurate atmospheric radiative transfer simulations, which was later verified by using ground measurements and ERBE data under clear-sky conditions (Cess et al. 1991). Li et al. (1993) improved the linear relationship that is independent of cloud-optical depth and surface albedo and so can be applied to estimate surface shortwave net radiation under overcast skies. Masuda, Leighton, and Li (1995) further improved the parametrization model developed by (Li et al. 1993) using a newer version of the radiative transfer package (LOWTRAN) for better treatment of water vapor absorption in the detailed radiative transfer calculations and correcting the impacts of the surface elevation (surface pressure), ozone amount, aerosol type and amount, as well as cloud height and cloud type. These simple models were applied to satellite data acquired by broadband sensors, such as ERBE, which have coarse spatial resolutions. Tang, Li, and Zhang (2006) applied this type

of parametrization method to narrowband MODIS data by developing the TOA narrowband to broadband albedo conversion for different solar zenith angle, viewing zenith angle and relative azimuth angle.

The TOA narrowband to broadband albedo conversion may introduce additional uncertainties to the parametrization method. Kim and Liang (2010; Zhu et al. 2016) proposed the hybrid method to estimate shortwave net radiation directly from MODIS TOA and surface reflectance data under both cloudy and clear sky conditions without the narrowband to broadband conversion of TOA albedo. It integrates extensive radiative transfer simulations (physical) and regression analysis (statistical) at each angular bin (the solar zenith angle, viewing zenith angle and the relative azimuth angle are divided into multiple intervals, and a cell of these three angular dimensions is called an angular bin). This method is also called direct estimation method with the similar framework very similar to that in Figure 5. It does not require ancillary data that typically have different spatial and spectral resolutions. They demonstrated that the shortwave net radiation estimated by this hybrid (direct estimation) method is more accurate than the TOA albedo based method. The further development of this hybrid method has removed the requirement of surface reflectance. He et al., "Estimation of High-Resolution Land Surface Net Shortwave Radiation," (2015) refined the hybrid method and applied to the hyperspectral Airborne Visible/Infrared Imaging Spectrometer (AVIRIS) data. They executed the topographical and water vapor correction, and demonstrated that this hybrid method is more accurate than that calculated from the surface albedo and insolation. They also showed that hyperspectral data can generate more accurate estimates of surface shortwave net radiation than the multispectral data. These studies focused on estimating instantaneous surface shortwave net radiation. Wang, Liang, and Tao (2014) extended this method by incorporating water vapor as one additional dimension of the LUT and then applied to Landsat data for calculating both instantaneous and daily average surface shortwave net radiation. Wang et al., "Estimation of Daily Surface Shortwave Net Radiation," (2015) further estimated daily shortwave net radiation by combing MODIS data from both Terra and Aqua satellites. Wang et al., "Surface Shortwave Net Radiation Estimation," (2015) continued to apply this method to the Medium-Resolution Spectral Imager (MERSI) data of the Chinese Feng-Yun 3 (FY-3) satellite and explored the possible improvement of accuracy by combining MERSI and MODIS data. Zhang and Li (2016) applied this method to estimate surface shortwave net radiation from Chinese geostationary FY-2D satellite data by first converting TOA spectral reflectance to TOA broadband albedo.

The hybrid (direct estimation) methods based on the TOA multispectral reflectance usually perform better than the parametrization methods based on TOA broadband-albedo. One of the major reasons is that TOA spectral reflectance contains information of both the atmosphere and the surface, which are important for accurate determination of surface shortwave net radiation.

4.4. Longwave downward radiation

The downward longwave radiation at the surface (F_d^l), the direct measure of radiative heating of atmosphere to surface, plays an important role in numerous applications. The concentrations and the associated vertical distributions of water vapor, carbon dioxide and trace gases including ozone, methane, nitrous dioxide, and aerosols, affect the downward longwave radiation.

The difficulty in estimating F_d^l from satellite observations is because only atmospheric window radiances at the TOA can convey information on the near-surface radiation field, and the atmosphere below 500 m from the surface accounts for 80% of the total surface downward longwave radiation. Under cloudy sky conditions, satellite data in the thermal IR region usually cannot be used for estimating downward longwave radiation at surface directly because the radiation fields at the surface and at the TOA are usually decoupled.

Cheng, Liang, and Wang (2017) reviewed various estimation methods for generating the products from satellite remote sensing, including radiative transfer calculation with atmospheric profiles and parameterization. If the atmospheric profiles are known from surface radiosonde, a radiosonde

balloon, or derived from satellite sounding data, a radiative transfer model can be used to calculate the downward longwave radiation (Darnell, Gupta, and Staylor 1986; Frouin, Gautier, and Morcrette 1988). The radiative transfer model needs to be computationally efficient and the generated products largely depend largely on the accuracy of atmospheric temperature and moisture profiles. The satellite products from remote sensing data include the ISCCP-FD, GEWEX, and CERES products that have temporal and similar spatial resolutions to other EEB components discussed earlier. In addition, the EUMETSAT CM-SAF also produces the monthly longwave downward radiation product by merging AVHRR and SEVERI data (Schulz et al. 2009) with a spatial resolution of 15 km.

Another approach is to develop parametric formulae. Various parameterization methods have been summarized (Cheng, Liang, and Wang 2017; Wang and Dickinson 2013). The idea is to develop simplified mathematical formula to calculate the downward longwave radiation based on some surface meteorological variables, such as water vapor pressure, air temperature, and the precipitable water. The most common form for calculating F_d^l is $\varepsilon_a \sigma T_a^4$ where ε_a and T_a is the effective atmospheric emissivity and air temperature, σ is Stefan–Boltzmann's constant. Many parametric formulae calculate ε_a. Parameterization methods are usually site specific, and they are affected by geographical locations and local atmospheric conditions. The accuracy of meteorological parameter-based models is typically 5–30 Wm^{-2} (Cheng, Liang et al. 2017), depending on the suitability of the model to the local atmospheric conditions and the data used for model calibration. Obtaining all meteorological parameters over large areas is also challenging.

A hybrid (direct estimation) method that combines physical radiative transfer simulation and statistical analysis has also been developed to estimate clear-sky F_d^l (Cheng, Liang et al. 2017; Wang and Liang 2009c, 2010; Wang, Liang, and Augustine 2009) from satellite thermal IR observations, such as MODIS and GOES. The framework is very similar to that in Figure 5, consisting of two steps. The first step is to undertake extensive radiative transfer simulations. Surface downward and TOA radiance for a particular satellite instrument are simulated using a radiative transfer model and a large number of clear-sky atmospheric profiles in combination of surface temperature and emissivity. The physics that govern the surface longwave radiation budget are embedded in the radiative transfer simulation processes. The second step is to conduct a statistical analysis of the simulated databases to derive models. Cheng, Liang et al. (2017) applied this method to MODIS data and found based on in-situ measurements that the estimated F_d^l has high accuracy with the bias and RMSE of 0.0597 and 21.008 Wm^{-2}, respectively.

Under cloudy-sky conditions, many empirical formulae have been developed to link F_d^l with the following parameters (Wang, Shi, et al. 2018): precipitable water, cloud fraction, liquid water path and/or ice water path, etc. For example, Duarte, Dias, and Maggiotto (2006) evaluated several empirical formulae using cloud fraction that can be calculated from incident shortwave radiation to correct clear-sky F_d^l. Guo and Cheng (2018) developed a linear model and a multivariate adaptive regression spline (MARS) model to estimate the cloudy-sky longwave net radiation from a satellite-derived surface shortwave net radiation product. Gupta, Darnell, and Wilber (1992) derived F_d^l by parameterizing cloud-base temperature and the water vapor content below the cloud base. Forman and Margulis (2009) estimated cloud-coupled F_d^l using reference- level air temperature and vapor pressure, cloud-base temperature and liquid water path. Bisht and Bras (2010) calculated cloudy F_d^l utilizing the MODIS cloud data product (MOD06_L2) for cloud top temperature, cloud fraction, cloud emissivity, cloud optical thickness and land surface temperature. Yu et al. (2018) compared three types of algorithms: (i) four empirical algorithms determining cloudy F_d^l by simple cloud correction using the cloud fraction, (ii) three parameterized algorithms determining the cloud contribution by cloud temperature, and (iii) a semiempirical algorithm parameterized by the cloud water path developed by Zhou and Cess (2001). They found out based on actual satellite data products that the cloud-temperature-based algorithms were greatly influenced by the uncertainty in cloud base temperature and cloud fraction and showed acceptable results when cloud fractions were accurate. The Zhou-Cess algorithm revealed the best results at most sites and was less impacted by cloud parameter uncertainties; Wang, Shi, et al. (2018) used a parametric formula to calculate the

cloudy F_d^l by integrating MODIS and AIRS/AMSU measurements to generate the atmospheric profiles.

After comparing two satellite and three reanalysis datasets with observations collected at 169 global land sites from 1992 to 2010, and 24 buoy sites from 2002 to 2011, Wang and Dickinson (2013) found that these datasets have significant differences, and the CERES product over the deserts has much larger uncertainties. They provided the best estimate of global means from 2003 to 2010: 342 ± 3 Wm^{-2} (global), 307 ± 3 Wm^{-2} (land), and 356 ± 3 Wm^{-2} (ocean). Wild et al. (2015) found that the 43 CMIP models simulate substantially different estimates of downward longwave radiation. In comparison, four EEB studies gave substantially different estimates of F_d^l: 333 (Trenberth and Fasullo 2009), 345.6 (Stephens et al. 2012), 342 (Wild et al. 2015), and 341 (L'Ecuyer et al. 2015) Wm^{-2}, respectively.

Consistent with global warming, most datasets show substantial increases in longwave downward radiation temporally, with the derived linear trends of global mean up to 1.9 Wm^{-2} per decade. Based on the longest records of downward thermal radiation currently available from BSRN, Wild (2016) obtained an overall mean increase in downward thermal radiation of + 2.0 Wm^{-2} per decade since the early 1990s. This corresponds to the rate of energy increase at the Earth's surface due to the enhanced greenhouse effect that is causing global warming. Zhou, Chen, et al. (2016) claimed that desert amplification between 50°S and 50°N is likely attributable primarily to enhanced longwave radiative forcing associated with a stronger water vapor feedback over drier ecoregions in response to the positive global-scale greenhouse gas forcing. Cao et al. (2017) also reported strong observational evidence, for the first time from long-term (1984–2014) spatially complete satellite records, that increased cloudiness and atmospheric water vapor in winter and spring have caused an extraordinary downward longwave radiative flux to the ice surface, which may then amplify the Arctic wintertime ice-surface warming. In addition, they also provided observed evidence that it is quite likely the enhancement of the wintertime greenhouse effect caused by water vapor and cloudiness that has advanced the time of onset of ice melting in mid-May through inhibiting sea-ice refreezing in the winter and accelerating the pre-melting process in the spring, and in turn triggered the positive sea-ice albedo feedback process and accelerated the sea ice melting in the summer.

4.5. Longwave upwelling radiation

We can calculate upwelling longwave radiation F_u^l given downward longwave radiation (F_d^l), surface temperature (T_s), and surface emissivity (ε). This is the conventional method for calculating F_u^l since both T_s and ε can be estimated directly from satellite observations. The disadvantage of this approach is that the uncertainties of the T_s and ε products (Cheng and Liang 2017; Li and Duan 2017) make us impossible to estimate F_u^l accurately (Wang and Liang 2009b). If the surface temperature and emissivity products are not accurate, the accuracy of the upwelling longwave radiation will be affected. The alternative solution is to estimate surface longwave upwelling radiation from TOA longwave observations directly. In the following subsections, we will discuss these related variables and approaches separately.

4.5.1. Land surface temperature

Land surface temperature (LST), T_s, can be estimated mainly from thermal-IR remote sensing, but also from passive microwave remote sensing (Aires et al. 2001; Njoku and Li 1999). LST detected by infrared thermal sensors provides finer spatial resolution only under clear-sky conditions. Because clouds and aerosols are essentially transparent to microwave radiation at frequencies below about 12 GHz, microwave remote sensing has the potential to eliminate the atmospheric contamination. However, passive microwave sensors have coarser spatial resolution and the estimated LST may have lower accuracy. Integration of estimated LST from both thermal and microwave satellite data will produce all-weather high-resolution LST satellite products (Duan, Li, and Leng 2017).

The progress in LST estimation from thermal remote sensing has been recently reviewed (Li et al. 2013; Li and Duan 2017; Yu, Liu, and Yu 2017). Besides the traditional split-window algorithms, Li and Duan (2017) also reviewed other estimation methods, such as single channel methods, multi-channel methods, multi-angular methods, and multi-temporal methods.

Validation of the satellite LST products is very important (Hulley and Hook 2009; Wang and Liang 2009b). The MODIS global LST product (Wan and Li 1997) is probably the most reliable LST product so far, with the accuracy of 1 K verified for homogenous surfaces, such as water bodies and sandy land (Wan 2008). Wang, Liang, and Meyer (2008) also compared night-time LST data using eight ground thermal infrared (TIR) temperature observation stations and verified that the error or deviation rate (bias) was around −3.23°C to 0.72°C. The JPSS satellite series mission provides similar quality of the LST product from the VIIRS instrument (Liu et al. 2015; Yu, Privette, and Pinheiro 2005). Validation results proved that the anticipated accuracy of ASTER LST product of + 1.5 K has been met (Sabol et al. 2009), under unusual atmospheric conditions of anomalously high humidity or spatial variability, atmospheric compensation can be incomplete and errors in temperature and emissivity images can be larger than anticipated. The standard deviation of LST from the Infrared Atmospheric Sounder Interferometer (IASI) over the tropics is about 1.3 K (Capelle et al. 2012). The RMSE of the MSG–SEVIRI LST product compared with ground measurements is up to 2 K (Freitas et al. 2010). Duan et al. (2018) validated the latest MODIS LST product (C6) using measurements from 38 validation sites worldwide over eight land cover type. They found the C6 MODIS LST products are in good agreement, with bias and RMSE values of less than 1 K although overestimation in the C6 MODIS LST products can be found over two bare soil sites. The retrieval accuracy for microwave sensors is far worse, probably larger than 2.5 K (Prigent, Jimenez, and Aires 2016). Other validation studies for AATSR (Coll et al. 2012) and VIIRS (Li, Sun, et al. 2014; Niclos et al. 2018) LST products.

The satellite derived LST data sets have been used for multiple applications including large-scale ecosystem disturbance detection (Mildrexler, Zhao, and Running 2009), drought monitoring (Rhee, Im, and Carbone 2010), land cover monitoring (Julien and Sobrino 2009; Karnieli et al. 2010), biodiversity studies (Albright et al. 2011), and urban heat island effects (Jin 2012). LST products have been widely assimilated into land surface models to estimate turbulent fluxes (Bateni and Liang 2012; Crow, Wood, and Pan 2003; Qin et al. 2007; Xu, Liang, and Liu 2011; Xu, Liu, et al. 2011), soil moisture and other quantities.

Some numerical models have simulated unrealistic LST, for example, Moncet et al. (2011) compared MODIS LST with the ISCCP LST. For July 2003 monthly averages over all clear-sky locations, the ISCCP-MODIS differences were + 5.0 K and + 2.5 K for day and night, respectively, and there were areas with differences as large as 25 K.

Some efforts have inter-compared LST satellite products. For example, Duan, Li et al. (2017) compared two versions of MODIS LST products (C5 and C6) and ASTER LST product over bare soils. They found that the accuracy of the C6 MODIS LST product is superior to that of the C5 MODIS LST product, and the absolute biases of the differences between the C6 MODIS LST and ASTER LST over bare soil surfaces are from 0.2 to 1.5 K. Ouyang, Chen, and Lei (2018) compared the LST from the AATSR and numerical simulations. Soliman et al. (2012) found MODIS and AATSR monthly LST products match very well with a mean-difference (MD) of −1.1 K. Ermida et al. (2017) compared the LST derived from the Advanced Microwave Scanning Radiometer-Earth Observing System (AMSR-E) with LST estimated from thermal data such as MODIS and SEVIRI. They found the higher discrepancies between AMSR-E and MODIS over deserts and snow-covered areas, and the differences between AMSR-E and MODIS are significantly reduced after masking out snow and deserts, with a bias change from 2.6/4.6 K to 3.0/1.4 K for daytime/nighttime and a standard deviation (STD) decrease from 7.3/7.9 K to 5.1/3.9 K.

The MODIS LST product has been used to determine the long-term trends. Sobrino and Julien (2013) determined the global LST trends from MODIS LST monthly product from 2000 to 2011 and found an increasing trend in morning LST from 0.12 to 0.14 K/year. Zhou and Wang (2016) found

that the MODIS LST over global deserts increased by 0.25°C/decade from 2002 to 2015, whereas the reanalyses estimated a trend varying from −0.14 to 0.10°C/decade.

Note that land surface air temperature (T_{air}) is often needed for various applications. LST is not equal to surface air temperature numerically (Good et al. 2017; Lian et al. 2017). For example, LST is generally higher than Tair over arid and sparsely vegetated regions in the middle-low latitudes, but LST is lower than Tair in tropical rainforests due to strong evaporative cooling, and in the high-latitude regions due to snow-induced radiative cooling. The commonly used global air temperature datasets are usually created from interpolation of scattered meteorological measurements, which may have large uncertainties (Rao, Liang, and Yu 2018). Air temperature at the surface cannot be accurately estimated from satellite data. Although the sounding channels enable us to determine the atmospheric profiles of temperature and water vapor, the air temperature near surface is not accurate for land applications. The alternative is to estimate near surface air temperature from LST using one of these three types of methods: statistical approaches (Chen, Quan, et al. 2016; Li, Zhou, et al. 2018; Oyler et al. 2016; Xu, Knudby, and Ho 2014; Zakšek and Schroedter-Homscheidt 2009), the temperature-vegetation index (TVX) approach (Czajkowski et al. 2000; Prihodko and Goward 1997) and machine learning methods (Xu et al. 2018). The similar parametrization formula has been developed to assess the climate effects of the recent changes in global forest cover (Alkama and Cescatti 2016). Since the LST products from thermal-IR observations have many gaps due to cloud contamination, thus, the generated air temperature is not continuous. Rao et al. (2019) recently developed a machine learning method to estimate spatiotemporally continuous air temperature using not only LST but also incident solar radiation and TOA albedo/OLR.

4.5.2. Land surface emissivity

For dense vegetation and water surfaces, surface emissivity ε equals almost one. For non-vegetated surfaces, ε is significantly less than one. Unfortunately, due to the lack of reliable observations, a constant emissivity value or very simple parameterizations are adopted in most land surface models and general circulation models.

There are few broadband emissivity satellite products available, although several spectral emissivity products exist. In theory, all spectral emissivity products can be converted into broadband emissivity using various conversion formulae (Cheng et al. 2013; Jin and Liang 2006; Ogawa and Schmugge 2004; Tang et al. 2011), but creating a long-term broadband emissivity product from multiple satellite data is not an easy task since it requires a series of consistent processing steps. The GLASS emissivity product is the only thermal-IR broadband emissivity ready to be used by the community. The details on land surface emissivity are described by Cheng and Liang (2017).

4.5.3. Sea surface temperature (SST) and emissivity

In-situ SST measurements are mainly from ships and from drifting/moored buoys, generally precise and fundamentally unaffected by variations in weather conditions. Therefore, in-situ data are used as reference for 'sea truth'.

Satellite SST products can be generated from both thermal-IR observations (Walton 2016) and microwave data (Hosoda 2010). Compared to LST estimation, SST estimation from thermal-IR observations is much simpler because the sea surface emissivity is less variable. The traditional split-window approaches for estimating SST from brightness temperatures of two channels (T_i, T_j) in the atmospheric window (11–13 μm) have been widely used. To improve estimation accuracy, the simplest formula above has been further developed into more complex forms, such as MCSST (multi-channel sea surface temperature), non-linear SST (NLSST) algorithm, and the generalized non-linear SST (GNLSST) algorithm (Walton 2016).

Microwave observations can be also useful to estimate SST under almost all weather conditions since microwave measurements can penetrate clouds. However, the spatial resolution of microwave measurements is relatively low compared with infrared measurements. Microwave SST retrieval was first attempted using the Scanning Multichannel Microwave Radiometer (SMMR) onboard Seasat

and Nimbus-7 satellites that were launched in 1978. High-quality microwave SST product was first retrieved from the Tropical Rainfall Measuring Mission Microwave Imager (TMI) data in 1997 within 38°N–38°S. RMSD between TMI and buoy SST ranges from 0.5°C to 0.7°C (Wentz et al. 2000). The first global SST product from the polar-orbiting satellite was generated from the Advanced Microwave Scanning Radiometer-Earth Observing System (AMSR-E) operated during 4 May 2002 to 4 October 2011. The AMSR-E version 7 SST products provided by remote sensing systems showed a small bias of −0.05°C and a standard deviation of 0.48°C, respectively, when compared with in situ SST observations (Gentemann 2014).

The microwave SST products are currently available from WindSat from January 2003, Advanced Microwave Scanning Radiometer-2 (AMSR2) from May 2012, the Global Precipitation Measurement (GPM) Microwave Radiometer (GMI) from February 2014, and the Chinese Haiyang-2 (HY-2) from August 2011 (Liu et al. 2017).

To achieve higher spatial and temporal resolution of the SST products, efforts have been made to integrate the products from both thermal-IR and microwave data (Banzon et al. 2016; Hosoda, Kawamura, and Sakaida 2015; Reynolds et al. 2007).

Global mean SST time series of monthly anomalies from several datasets exhibit a clear warming tendency in addition to consistent interannual variability in all analyses. The magnitude of SST anomaly trends ranges from 0.09°C to 0.14°C decade-1 (Huang et al. 2016). Despite of the warming slowdown, Karl et al. (2015) reported that global SST since 2000 has continued to exhibit a significant warming trend.

Emissivity is a required quantity for calculating surface longwave radiation budget, but also important in retrieving surface temperature from thermal observations. Satellite-retrieved SSTs with an absolute accuracy of 0.3 K is highly desired for applications in climate monitoring and operational oceanography (Barton 1992), which requires the emissivity to be determined with an accuracy of 0.5% (Hanafin and Minnett 2005).

A number of studies have been devoted to modeling the thermal infrared emissivity of wind-roughened sea surfaces (Hanafin and Minnett 2005; Henderson, Theiler, and Villeneuve 2003; Masuda, Takashima, and Takayama 1988; Nalli, Minnett, and Van Delst 2008; Wu and Smith 1997), but the discrepancies between model calculated emissivity values and in situ measurements are only partially resolved at greater observation angles and high wind speeds. None of these models were used for calculating hemispheric sea surface emissivity.

Cheng, Cheng et al. (2017) developed a lookup table approach for calculating hemispherical broadband emissivity values as a function of wind speed. After incorporating the foam effect, hemispherical broadband emissivity was expressed as a linear function of the hemispherical broadband emissivity values of sea water and foam, weighted by the fraction of foam coverage. With this method, they produced an hourly sea surface hemispherical broadband emissivity product with a resolution of 10 km and global coverage that covers the period from 2003 to 2005, using wind speed data from Modern-Era Retrospective analysis for Research and Applications (MERRA)-2.

4.5.4. Hybrid methods

The hybrid methods, or direct estimation methods, have also been used for estimating F_u^l. Wang, Liang, and Augustine (2009) developed the hybrid method to estimate upwelling radiation from MODIS using both artificial neural network (ANN) and linear regression, and also compared with the temperature-emissivity based method. They found that the biases and RMSEs of the ANN model method are ~5 Wm^{-2} smaller than the temperature-emissivity method and ~2.5 Wm^{-2} smaller than the linear regression method. Wang and Liang (2010) later applied to geostationary GOES sounding data and the ABI of the GOES-R data. Jiao et al. (2015) applied this method to generate two-year F_u^l from MODIS data over Tibetan Plateau. Cheng and Liang (2016) further improved the linear model suitable for global product generation by incorporating more representative atmospheric profiles. This approach can produce the products at the native spatial resolution of satellite data (~1 km), but only under clear-sky conditions. Efforts have been made to

refine this method by incorporating the anisotropy of LST and/or emissivity (Hu, Du, et al. 2016; Hu et al. 2017).

4.5.5. Mean and variation

The longwave upwelling radiation products from remote sensing data include ISCCP-FD, GEWEX, CERES, and EUMETSAT CM-SAF. The accuracy of these three data sets varies from 21 Wm^{-2} to 33.6 Wm^{-2} at the monthly timescale and at a spatial resolution of 100–280 km. The meteorological, hydrological and agricultural research communities require an accuracy of 5–10 Wm^{-2} for longwave upwelling radiation retrieved from satellite data at a 25–100 km spatial resolution and 3-h daily temporal resolution.

Upwelling longwave radiation simulations from different GCM models have very large differences. Zhang, Rossow, and Stackhouse (2007) found that the difference of skin temperature among four reanalysis data sets is around 2–4 K that can easily cause 10–15 Wm^{-2} uncertainty in calculated surface upwelling longwave fluxes. Most models have simplified surface emissivity, which is another major source of uncertainty (Jin and Liang 2006).

From CERES EBAF, Wild et al. (2015) determined the mean values of F_u^l: 374.4 (land), 408.3 (ocean), and 398.8 (global) Wm^{-2}, and the corresponding thermal net radiation are: −62.9 (land), −49.3 (ocean), and −53.5 (global). Since upwelling is smaller than downward thermal radiation, the net thermal radiation is negative. The largest negative values occur over dry lands, particularly over deserts.

4.6. Surface all-wave net radiation

All-wave net radiation is the sum of shortwave and longwave net radiation. The spatial and temporal variation of the surface net radiation is responsible for the redistribution of the available energy, for example, controlling the inputs of latent and sensible heat fluxes into the atmosphere, and the oceanic heating over the ocean. Zhang, Li, et al. (2018) recently found that surface net radiation rather than soil moisture limits actual evapotranspiration over an alpine Kobresia meadow on the northeastern Qinghai-Tibetan Plateau. Surface all-wave net radiation is dominated by the shortwave net radiation except at the poles. It is generally greatest in the summer tropical and subtropical oceans with maxima near the Tropic of Cancer during July and the Tropic of Capricorn during January. The seasonal variability of all-wave net radiation is very similar to that of shortwave net radiation.

After calculating shortwave and longwave net radiation, all-wave net radiation can be calculated by adding them together (Bisht and Bras 2011; Verma et al. 2016; Wang et al., "Estimating Clear-Sky All-Wave Net Radiation," 2015). Under cloudy-sky conditions, longwave net radiation cannot be accurately estimated unless reliable cloud information can be provided (Flerchinger et al. 2009; Wang and Liang 2009c). Bisht et al. (2005) proposed the scheme for deriving the components of surface energy budget over large heterogeneous areas under clear-sky using only the MODIS products and calculated instantaneous net radiation for the first time. They also proposed the sinusoidal model that can estimate the diurnal cycle of net radiation with a single instantaneous net radiation estimated from the satellite. Bisht and Bras (2010) extended their method to cloudy sky conditions, and applied to estimate instantaneous and daily net radiation over the South Great Plains for a time period covering all seasons of 2006. The RMSE of instantaneous and daily average net radiation estimated under cloudy condition were 37 and 38 Wm^{-2}, compared to ground measurements. Ryu et al. (2008) evaluated the land surface radiation balance derived from MODIS over a heterogeneous farmland area and a rugged deciduous forest in the Korea Flux Network. Their study suggested that the scale mismatch among the radiometer footprint, heterogeneity of the land surface properties, and MODIS extent should be considered in both the algorithm development and validation processes. The AVHRR data was also widely used to estimate the components of land surface radiation balance, including all-wave net radiation. Ma and Pinker (2012) derived surface shortwave albedo, land

surface temperature, and emissivity from AVHRR data, land-surface and other observation data, computed the downward shortwave and longwave radiation at surface, and determined the net radiation over the Tibetan Plateau by summing all the components. The validation results indicated that the derived surface shortwave albedo and land surface temperature for the Tibetan Plateau area were comparable to the land-surface status, and the absolute percentage difference between derived net radiation and the field observation was less than 10%. Combined AVHRR data and meteorological data, Zhang and Li (2016) calculated surface net radiation at 1 km from 2008 to 2010 over Tibetan Plateau based on a group of MODIS land and atmosphere high-level products and surface elevation data (DEM).

Direct estimation for estimating all-wave net radiation from TOA satellite observations have also been explored (Pinker and Corio 1984; Pinker and Tarpley 1988). Pinker, Ewing, and Tarpley (1985) linearly regressed the surface daily average net radiation at selected sites over Canada with collocated TOA shortwave net radiation and OLR from GOES-E data for a period of two years. They also demonstrated that the average 7-day net radiation can be more accurately estimated than the daily average. Wang et al., "Estimating Clear-Sky All-Wave Net Radiation," (2015) estimated all-wave net radiation as one integral variable from the combined visible and shortwave infrared and thermal infrared data measured by MODIS and MODIS/ASTER Airborne Simulator (MASTER). They demonstrated the direct estimation approach generated more accurate results than the component-based approach that first estimates shortwave and longwave net radiation respectively and then adds them together.

Another method is to establish the empirical relationship between all-wave net radiation and shortwave net radiation and other meteorological parameters empirically (Jiang and Liang 2017). These methods can estimate only daytime net radiation since there is no shortwave radiation in the evening. Jiang et al. (2015) evaluated seven such empirical models and also developed a new model based on an extensive ground measurement dataset collected worldwide. They also replaced simple statistical models with a neural network (Jiang et al. 2014). A preliminary global product has been developed using this method (Jiang et al. 2016).

There are multiple surface net radiation products generated from satellite data (see Table 4). The CERES product has been shown to have a high accuracy over land surfaces with RMSE of 33.56 and 25.57 Wm^{-2}, for the daily and monthly products (Jia et al. 2016). The GLASS day-time net radiation product over land surfaces has a much finer spatial resolution (5 km) and a comparable accuracy (RMSE of 31.61 Wm^{-2}) (Jiang et al. 2016).

Jia et al. (2018) calculated the mean and annual trends of the Rn across the land surface using monthly CERES product, GLASS net radiation product and three reanalysis products, and found a general decreasing trend. However, they also found that the misleading increasing trend during 2000–2008 from the CERES EBAF2.8 product was mainly caused by version inconsistency in input data such as aerosol optical thickness and atmospheric profiles (in 2006 and 2008) and cloud properties (in 2002). This wrong trend was not revealed when the CERES product was validated using ground measurements, which demonstrates that temporal analysis provides powerful quality control for global time series satellite products when the validation using ground measurements fails to capture potential issues. Of course, another ways is to compare the trends of satellite products and surface observations instead of climatological means.

4.7. Surface heat fluxes

The energy that is required for evapotranspiration (ET) is called latent heat, the largest component from the available net radiation. The remaining net radiation is mainly used for heating the near surface temperature and is referred to as sensible heat since the ground heat flux is relatively small. The division of/separation of the surface net radiation into sensible and latent heat flux has important implications for regional and global warming and water cycles.

Numerous review papers (Glenn et al. 2007; Kalma, McVicar, and McCabe 2008; Katul et al. 2012; Li et al. 2009; Shuttleworth 2007; Wang and Dickinson 2012) have examined the development of measurement, estimation and simulation of ET. Remote sensing methods for estimating ET can be grouped as either empirical, physically based, or simulations. Empirical methods link satellite observations with ET through various statistical models or machine learning algorithms. Carter and Liang (2018) recently evaluated twelve different empirical regression algorithms for estimating daily ET using surface measurements from 181 Ameriflux and Fluxnet sites and MODIS high-level data products. These algorithms have variable performances with median RMSE of about 25 Wm^{-2} and median bias within 10 Wm^{-2}. The physically based approaches estimate ET from the Penman-Monteith (Li, Liang, et al. 2014; Mu et al. 2007; Mu, Zhao, and Running 2011) or Priestley–Taylor (Yao, Liang, Yu, et al. 2017; Yao et al. 2013) equation. Various land surface models driven by different satellite products, such as surface skin temperature, vegetation indices, net radiation, and so on, have been used for simulating surface ET.

Many regional and global ET products have been generated. Mueller et al. (2013) evaluated 40 ET datasets and produced monthly synthesis products by merging individual products. Peng et al. (2016) compared six different ET products over the Tibetan Plateau. More validation and intercomparisons under different conditions is needed to better characterize performance of various products and provide basis for product integration. Baik, Liaqat, and Choi (2018) evaluated uncertainties among four widely available ET (GLDAS, GLEAM, MOD16, and MERRA) products.

Efforts have also been made to integrate multiple algorithms or products for producing better ET estimation using various methods, such as Kalman filter (Pipunic, Walker, and Western 2008), Bayesian model averaging (BMA) (Vinukollu et al. 2011; Yao et al. 2014), supporting vector machine (Yao et al., "Improving Global Terrestrial Evapotranspiration Estimation," 2017), empirical orthogonal functions (EOF) (Feng, Li et al. 2016), simple Taylor skill's score (STS) (Baik, Liaqat, and Choi 2018; Yao et al., "Estimation of High-Resolution Terrestrial Evapotranspiration," 2017), triple collocation (Khan et al. 2018), and maximizing temporal correlation (Baik, Liaqat, and Choi 2018).

Based on simple satellite algorithms, land surface model (LSM) simulations driven with observation-based forcing, reanalysis data, and IPCC AR4 simulations from 11 GCMs from 1986 to 1995, Wang and Dickinson (2012) estimated globally averaged terrestrial ET to vary from 24.1 Wm^{-2} (0.83 mm/d) to 42.0 Wm^{-2} (1.45 mm/d). Yao et al. (2016) integrated the IPCC AR5 model simulation results based on the calibration process using surface eddy covariance observations, and estimated the global average ET over land is 39.7 Wm^{-2}. Based on reanalysis, IPCC AR5 simulations and other datasets, Wild et al. (2015) estimated the latent heat flux to be 38 Wm^{-2} over land and 100 Wm^{-2} over ocean, their weighted global average of land (0.292) and ocean (0.708) is 82 Wm^{-2}. The global averaged latent heat flux estimated from other studies are also variable, for example 80 (Trenberth and Fasullo 2009), 88 ± 10 (Stephens et al. 2012), 82 (70–85) (Wild et al. 2015), and 81 ± 4 (L'Ecuyer et al. 2015), respectively.

Several studies have focused on ET trends in recent decades and have revealed large discrepancies in the direction and cause of these changes. Based on a data driven ET dataset, Jung et al. (2010) found an increased trend from 1982 to 1997 consistent with the expected acceleration of the hydrological cycle caused by an increased evaporative demand associated with rising radiative forcing and temperatures. They also found a decreased trend from 1998 to 2008, which was attributed to a concurrent reduction in soil water availability in the Southern Hemisphere. Miralles et al. (2014) revealed that ET estimated from satellite observations has increased in northern latitudes at rates consistent with expectations derived from temperature trends from 1980 to 2011, but the dynamics of the El Niño/Southern Oscillation (ENSO) have dominated the multi-decadal variability of ET at the global scale. Some studies (Jasechko et al. 2013; Zhang, Pena-Arancibia, et al. 2016) suggested that the increased ET was dominated by transpiration that is attributed to the greening of land surfaces due to increased CO2 (Zhu et al. 2016). For example, Zeng et al. (2018) simulated that the global satellite observed LAI enhancement of 8% between 1981 and 2011 has caused an increases of 12.06 ± 2.4 mm yr^{-1} in evapotranspiration, about $55\% \pm 25\%$ of the observed increases in land

evapotranspiration. Mao et al. (2015) revealed a significant increasing trend of ET in each hemisphere from 1982 to 2010 using multiple estimates from remote sensing-based datasets and process-oriented land surface models. They also concluded that climate, and in particular, changes in precipitation, was the dominant control of multi-year ET trends and variability. The overall CO2 physiological and structural effect led to decreasing plants transpiration and the total ET, especially in areas where vegetation was dense, and nitrogen deposition and land use change on ET were less important and acted locally. Duethmann and Blöschl (2018) analyzed the ET trends over 156 catchments in Austria from 1977 to 2014 and found 60% of the catchments ($p \leq 0.05$) with an average increase of 29 ± 14 mm y^{-1} $decade^{-1}$ (± standard deviation) or $4.9 \pm 2.3\%$ $decade^{-1}$. They attributed $38 \pm 13\%$ of the observed increase in catchment evapotranspiration to increased atmospheric demand and available energy, $30 \pm 12\%$ to increased vegetation activity, and $32 \pm 5\%$ to increased soil moisture due to increases in precipitation. Li, He, et al. (2018) determined an increased trend of ET in China with a rate of 10.7 mm yr^{-1} per decade from 1982 to 2015 ($p < 0.05$) although about 22% of the area showed a decreasing trend in ET likely due to decreasing precipitation and/or vegetation browning.

Bentamy et al. (2017) found out that RMSD among three satellite remote sensing products (IFREMER, SEAFLUX and J-OFURO) products are about 30 and 7 Wm^{-2} for latent heat flux and sensible heat flux, respectively.

Remote sensing cannot accurately estimate sensible heat flux. Given net radiation and latent heat flux, the global climatological value of sensible heat flux can be inferred. Wild et al. (2015) calibrated the CMIP5 model simulations using surface measurements and estimated the sensible heat flux of land, ocean and globe to be 32, 16, and 20.7 Wm^{-2}. This value differs considerably from the global averaged sensible heat flux from other studies: 17 Wm^{-2} (Trenberth and Fasullo 2009), 24 ± 7,21 (15–25) Wm^{-2} (Stephens et al. 2012), and 25 ± 4 Wm^{-2} (L'Ecuyer et al. 2015) Wm^{-2}.

5. Challenges and outlook

Remote sensing of Earth's energy budget (EEB) by monitoring their mean and variability in both space and time provides insight into the overall behavior of the climate system and also helps us understand the climate consequences of anthropogenic activities. This paper has reviewed the historical development in satellite observing capabilities of EEB and synthesized our recent understanding of the spatio-temporal variations in all relevant EEB components at both the top-of-atmosphere (TOA) and the surface.

Significant progress in estimating EEB from satellite observations has been made in the past half century, but satellite estimation of EEB still has large uncertainties. For example, most recent studies expect the TOA energy imbalance to be within 0.5–1 Wm^{-2}. Satellite estimation of EEB is based on three individual radiative fluxes (incident solar, reflected shortwave and emitted longwave radiation). As these fluxes are of the order of hundreds of Wm^{-2}, their difference, characterizing the energy imbalance, is too small to be estimated accurately so that the accuracy of 0.1 Wm^{-2} required by the GCOS (GCOS 2016) would be difficult to meet. The radiometric calibration errors of the satellite sensors also make it impossible to estimate the residual accurately. The ocean heat content (OHC) data have been used to anchor the satellite estimates. More efforts are needed to improve the accuracy of estimating EEB components as well as the overall energy imbalance. Other independent approaches should be continuously pursued, including measurements of radiation pressure or atmospheric oxygen (O_2) and carbon dioxide (CO_2).

Various satellite sensors have been used to estimate EEB. Traditionally, broadband sensors (e.g. CERES) have been used to serve this purpose. However, enormous efforts have been undertaken to estimate the individual EEB components from multispectral satellite sensors, which can help reduce the estimation uncertainty and also possibly extend the data record back to the early 1980s. Unfortunately, the current observing satellite systems with multispectral sensors were not planned in a comprehensive, focused manner required to adequately monitor the long-term EEB variability.

NASA cancelled the Radiation Budget Instrument (RBI) sensor,a scanning radiometer capable of measuring Earth's reflected sunlight and emitted thermal radiation scheduled to be on NOAA's JPSS-2 mission in 2021, because of the cost overruns. Therefore, it is still uncertain if the US will maintain the long-term global continuous broadband data records although the effort is being made to develop a lower cost alternative through the new Earth Venture-Continuity (EV-C) program (NASA 2018).

There are multiple broadband sensors aboard the geostationary satellites and also numerous narrowband sensors in both geostationary and polar-orbiting satellites, but these satellites are operated by different agencies and countries. Better planning and coordination through improved international cooperation will be essential for monitoring global EEB to ensure improved accuracy and consistency. Constellation of satellites may be a way to improve the estimation accuracy. Based on idealized simulations, Gristey et al. (2017) determined that a baseline constellation of 36 satellites is needed to estimate the global daily mean reflected solar radiation and OLR with the error of 0.16 Wm^{-2} and -0.13 Wm^{-2}. In fact, the constellation of small satellites for the EEB has been recently proposed (Meftah, Keckhut, et al. 2018), but more urgent studies are needed on virtual constellation, 'a coordinated set of space and/or ground segment capabilities from different partners that focuses on observing a particular parameter or set of parameters of the Earth system' as defined by the Committee of Earth Observation Satellite (CEOS) (https://agupubs.onlinelibrary.wiley.com/doi/full/10.1002/2017EF000627). Virtual constellations of planned and existing satellite sensors may help avoid any data gaps, improve the estimation accuracy, and ultimately overcome the underlying limitations of data availability and tradeoffs that govern the design and implementation of any single satellite sensor. While integrating observations from multiple satellite sensors is not new, the integration and harmonization of multi-sensor data is still challenging (Wulder et al. 2015).

Well-calibrated satellite data are a prerequisite for reliable quantification of EEB, but some earlier missions did not have onboard calibration devices and complicated calibration procedures were executed to address the degradation of onboard optical devices over time. For TOA radiation budget, Ohring et al. (2005) recommend a long-term stability of 0.3 Wm^{-2} per decade for shortwave and 0.2 Wm^{-2} per decade for longwave at the 95% confidence level. Loeb et al. (2016) demonstrated that the TOA fluxes from CERES fall within these stability requirements. The Climate Absolute Radiance and Refractivity Observatory (CLARREO) (Wielicki et al. 2013) aims to provide an in-orbit reference calibration standard for other satellite sensors. It is hoped that CLARREO will have enhanced absolute accuracy and stability compared to existing satellite instruments. Note that CLARREO will only provide shortwave irradiance and the similar system may be needed for longwave irradiance although most on-board blackbody calibrators can provide accurate radiometric calibration. Inter-calibration of multiple narrowband sensors is even more required because many sensors do not have in-flight calibration devices and are not even regularly calibrated using post-flight vicarious calibration techniques.

For the time series of radiative fluxes estimated from satellite observations, changes in sensors and/or retrieval algorithms can also affect their consistency and stability besides satellite drifts and sensor radiometric calibration. Various methods have been developed to detect any artificial changes (Reeves et al. 2007). Brinckmann, Trentmann, and Ahrens (2014) applied three of the statistical tests to detect any break-like inhomogeneities of the CM-SAF incident solar radiation product from geostationary satellite observations, and found heterogeneities between 1988 and 1990 when the problematic Metersat-3 was used by comparing with reanalysis data. Sanchez-Lorenzo, Wild, and Trentmann (2013) conduced a comprehensive test on the same satellite product using the GEBA surface measurements as reference and found the inhomogeneous problem in the product before 1994. Krähenmann et al. (2013) detected the breaking points using these tests and proposed a homogenization methodology to correct the mean shifts between the breaking points based on the statistical relationship between satellite products and ground measurements. The challenge is that any homogenization methods should not remove the actual trends (Sanchez-Lorenzo et al. 2017), such as those dimming and brightening periods as discussed in Section 4.1.

Most of the developed estimation algorithms are intended for the specific satellite data and a specific variable. Various approaches have been developed to estimate the parameter through algorithm ensembles or integration of the estimates from the individual algorithms (Liang et al. 2017). Progress has been made to integrate multiple satellite data (Ma, Liu, et al. 2017) and estimate a group of variables simultaneously through data assimilation approaches (Lewis et al. 2012; Ma, Liang, et al. 2017; Ma et al. 2018; Shi, Xiao, et al. 2016; Shi et al. 2017; Xiao et al. 2015). In light of virtual constellation, research in this direction deserves special attention. Integrating multiple satellite data from both multispectral and broadband sensors needs further exploration.

There are still large differences in estimating the surface radiation budget from various studies. The difference is even greater when redistributing net radiation into sensible and latent heat fluxes. One challenging issue is that most global satellite products have not taken into account the effects of surface topography yet. It has been demonstrated that surface topography can significantly affect the estimation of incident short wave radiation (Wang, Yan, et al. 2018; Wu et al. 2018) and surface albedo (Wen et al. 2018). Another challenging issue is that existing global satellite products have pixel size much larger than the footprints of ground-based flux measurements, making it difficult to assess the accuracy of satellite radiation products over heterogeneous landscapes (Cescatti et al. 2012). With more attentions to developing the high-spatial resolution satellite data products, the effects of surface topography and heterogeneity have to be properly addressed. Schwarz et al. (2018) conducted a comprehensive analysis on the representativeness of point observations of incident solar radiation on the monthly mean time scale. Lohmann (2018) provided a comprehensive review on the recent advances in the characterization of incident solar radiation variability mainly on small spatial and temporal scales. Upscaling surface 'point' measurements to the coarse resolution pixel using high-resolution satellite estimates (Liang et al. 2002), as illustrated in Figure 6, is probably the only feasible approach now for addressing the heterogeneity issue. Besides characterizing the uncertainties of satellite products using ground measurements, intercomparison of different products of the same radiative flux is also extremely important.

As more and more algorithms have been proposed and multiple products of the same variable are generated, it is important to assess their quality and accuracy using surface measurements. There are different measurement networks at the land surface, but additional networks and instrumentation are still needed in complex terrain or those areas currently insufficiently sampled. Different measurement methods for the same quantity need to be cross calibrated. Wang, Dickinson, et al. (2013) found out the method measuring the total incident solar radiation at surface produces a different trend from measuring direct and diffuse components separately. Instrument changes may also cause changes in measurements at long-term observation sites (Yang, Wang, and Wild 2018).

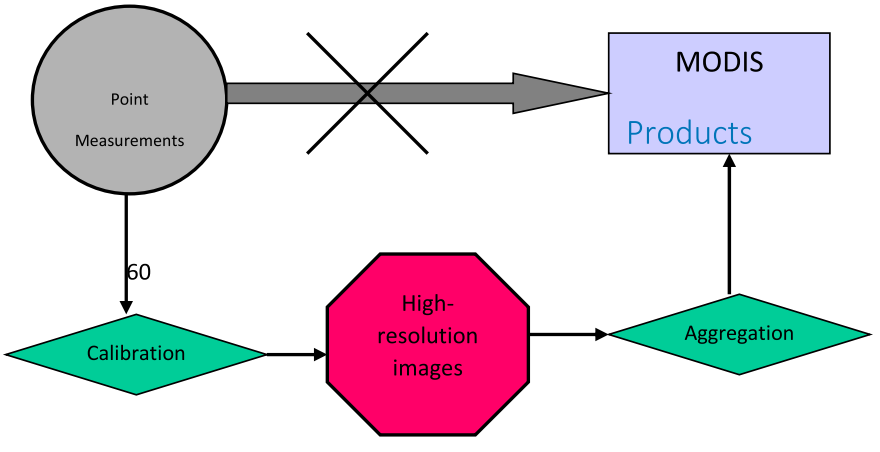

Figure 6 . Illustration of validating MODIS land surface albedo using high-resolution imagery (Liang et al. 2002).

There are usually multiple satellite products for each EEB component. All products have uncertainties, and some contain data gaps in both space and time. An important research area is the integration of multiple satellite products of the same variable. This has several advantages: (1) improving accuracy, since the integrated product is highly likely to be more accurate than the individual products that are first 'calibrated' by the surface measurements; (2) enhancing data quality, since many data gaps can be effectively filled; and (3) producing more complete spatial and temporal coverage if high-spatial-resolution and low-temporal-resolution products are integrated with low-spatial-resolution and high-temporal-resolution products. Many methods for integrating the multiple high-level products have been explored (Liang et al. 2017), such as Empirical orthogonal functions (EOF) for integrating the evapotranspiration products (Feng, Li et al. 2016), the Multi-resolution Tree (MRT) method for integrating multiple products of land surface broadband albedo (He et al., "Fusion of Satellite Land Surface," 2014) and land surface emissivity (Shi, Liang, et al. 2016), and Bayesian model averaging (BMA) method for integrating longwave downward radiation at surface and surface latent heat flux products (Wu et al. 2012; Yao et al. 2014).

Large differences/ between satellite products and model simulations continue to exist. Because satellite products are more accurate while the model simulated data cover much longer temporal range, calibrating the models using satellite products may produce long time series EEB datasets (Feng and Wang 2018).

In short, current estimates of the energy fluxes at the TOA and the surface directly from satellite observations have not been able to meet the accuracy requirements. However, with both broadband and numerous multispectral narrowband sensors acquiring a huge amount of observations and many innovative inversion methods consistently proposed, we will improve the estimation of energy fluxes significantly. It has been widely thought that the energy budget, particularly the heat fluxes (latent and sensible), at the surface has larger uncertainties, which requires us to improve many aspects of surface measurements, satellite data retrieval and integration with model simulations. Our current estimates of the TOA energy imbalance largely rely on the CERES products anchored by the ocean heat content measurements. Multispectral narrowband data and other approaches may provide the potential of independent estimates.

Acknowledgments

We are very grateful for the anonymous reviewers for their constructive comments and suggestions that have greatly improved the presentation of this paper.

Disclosure statement

No potential conflict of interest was reported by the authors.

Funding

This work was supported by National Key Research and Development Program of China [grant number 2016YFA0600101] and National Aeronautics and Space Administration [grant number 80NSSC18K0620].

References

Aires, F., C. Prigent, W. B. Rossow, and M. Rothstein. 2001. "A New Neural Network Approach Including First Guess for Retrieval of Atmospheric Water Vapor, Cloud Liquid Water Path, Surface Temperature, and Emissivities Over Land from Satellite Microwave Observations." *Journal of Geophysical Research: Atmospheres* 106: 14887–14907.

Albright, T. P., A. M. Pidgeon, C. D. Rittenhouse, M. K. Clayton, C. H. Flather, P. D. Culbert, and V. C. Radeloff. 2011. "Heat Waves Measured with MODIS Land Surface Temperature Data Predict Changes in Avian Community Structure." *Remote Sensing of Environment* 115: 245–254.

Alkama, R., and A. Cescatti. 2016. "Biophysical Climate Impacts of Recent Changes in Global Forest Cover." *Science* 351: 600–604.

Allan, R. P., C. Liu, N. G. Loeb, M. D. Palmer, M. Roberts, D. Smith, and P.-L. Vidale. 2014. "Changes in Global Net Radiative Imbalance 1985–2012." *Geophysical Research Letters* 41: 5588–5597.

Baik, J., U. W. Liaqat, and M. Choi. 2018. "Assessment of Satellite- and Reanalysis-Based Evapotranspiration Products with Two Blending Approaches Over the Complex Landscapes and Climates of Australia." *Agricultural and Forest Meteorology* 263: 388–398.

Banzon, V., T. M. Smith, T. M. Chin, C. Y. Liu, and W. Hankins. 2016. "A Long-Term Record of Blended Satellite and in Situ Sea-Surface Temperature for Climate Monitoring, Modeling and Environmental Studies." *Earth System Science Data* 8: 165–176.

Barkstrom, B. R., and G. L. Smith. 1986. "The Earth Radiation Budget Experiment: Science and Implementation." *Reviews of Geophysics* 24: 379–390.

Barton, I. J. 1992. "Satellite-Derived Sea Surface Temperatures-A Comparison Between Operational, Theoretical, and Experimental Algorithms." *Journal of Applied Meteorology* 31: 433–442.

Bateni, S., and S. Liang. 2012. "Estimating Surface Energy Fluxes Using a Dual-Source Data Assimilation Approach Adjoined to the Heat Diffusion Equation." *Journal of Geophysical Research: Atmospheres* 117: D17118.

Bentamy, A., J. F. Piolle, A. Grouazel, R. Danielson, S. Gulev, F. Paul, H. Azelmat, et al. 2017. "Review and Assessment of Latent and Sensible Heat Flux Accuracy Over the Global Oceans." *Remote Sensing of Environment* 201: 196–218.

Bernard, A. 1978. "Radiation Pressures Determination with the Cactus Accelerometer." *Space Research* 18: 163–168.

Bisht, G., and R. L. Bras. 2010. "Estimation of Net Radiation from the MODIS Data Under All Sky Conditions: Southern Great Plains Case Study." *Remote Sensing of Environment* 114: 1522–1534.

Bisht, G., and R. L. Bras. 2011. "Estimation of Net Radiation from the Moderate Resolution Imaging Spectroradiometer Over the Continental United States." *IEEE Transactions on Geoscience and Remote Sensing* 49: 2448–2462.

Bisht, G., V. Venturini, S. Islam, and L. Jiang. 2005. "Estimation of the Net Radiation Using MODIS (Moderate Resolution Imaging Spectroradiometer) Data for Clear Sky Days." *Remote Sensing of Environment* 97: 52–67.

Boudon, Y. 1986. "Measurement of the Radiation Pressures by Accelerometry: A New Way to the Determination of the Earth Radiation Budget. Result Obtained with Castor/Cactus Experiment." In *Current Issues in Climate Research*, 341–352. Dordrecht: Springer.

Boussetta, S., G. Balsamo, E. Dutra, A. Beljaars, and C. Albergel. 2015. "Assimilation of Surface Albedo and Vegetation States from Satellite Observations and Their Impact on Numerical Weather Prediction." *Remote Sensing of Environment* 163: 111–126.

Brinckmann, S., J. Trentmann, and B. Ahrens. 2014. "Homogeneity Analysis of the CM SAF Surface Solar Irradiance Dataset Derived from Geostationary Satellite Observations." *Remote Sensing* 6: 352–378.

Brindley, H. E., and J. E. Russell. 2017. "Top of Atmosphere Broadband Radiative Fluxes from Geostationary Satellite Observations." In *Comprehensive Remote Sensing: Vol. 5, Earth's Energy Budget*, edited by S. Liang, 85–113. England: Elsevier.

Cao, Y., S. Liang, X. Chen, and T. He. 2015. "Assessment of Sea Ice Albedo Radiative Forcing and Feedback Over the Northern Hemisphere from 1982 to 2009 Using Satellite and Reanalysis Data." *Journal of Climate* 28: 1248–1259.

Cao, Y., S. Liang, X. Chen, T. He, D. Wang, and X. Cheng. 2017. "Enhanced Wintertime Greenhouse Effect Reinforcing Arctic Amplification and Initial Sea-Ice Melting." *Scientific Reports* 7: 8462.

Cao, Y., S. Liang, T. He, and X. Chen. 2016. "Evaluation of Four Reanalysis Surface Albedo Data Sets in Arctic Using a Satellite Product." *IEEE Geoscience and Remote Sensing Letters* 13: 384–388.

Capelle, V., A. Chedin, E. Pequignot, P. Schlussel, S. M. Newman, and N. A. Scott. 2012. "Infrared Continental Surface Emissivity Spectra and Skin Temperature Retrieved from IASI Observations Over the Tropics." *Journal of Applied Meteorology and Climatology* 51: 1164–1179.

Carter, C., and S. Liang. 2018. "Comprehensive Evaluation of Empirical Algorithms for Estimating Land Surface Evapotranspiration." *Agricultural and Forest Meteorology* 256-257: 334–345.

Cescatti, A., B. Marcolla, S. K. S. Vannan, J. Y. Pan, M. O. Román, X. Yang, P. Ciais, R. B. Cook, B. E. Law, and G. Matteucci. 2012. "Intercomparison of MODIS Albedo Retrievals and In Situ Measurements Across the Global FLUXNET Network." *Remote Sensing of Environment* 121: 323–334.

Cess, R., E. G. Dutton, J. J. DeLuisi, and F. Jiang. 1991. "Determining Surface Solar Absorption from Broadband Satellite Measurements for Clear Skies: Comparison with Surface Measurements." *Journal of Climate* 4: 236–247.

Cess, R. D., and I. L. Vulis. 1989. "Inferring Surface Solar Absorption from Broadband Satellite Measurements." *Journal of Climate* 2: 974–985.

Chakraborty, S., S. Sasmal, S. K. Chakrabarti, and A. Bhattacharya. 2018. "Observational Signatures of Unusual Outgoing Longwave Radiation (OLR) and Atmospheric Gravity Waves (AGW) as Precursory Effects of May 2015 Nepal Earthquakes." *Journal of Geodynamics* 113: 43–51.

Chen, X., S. Liang, and Y. Cao. 2016. "Satellite Observed Changes in the Northern Hemisphere Snow Cover Phenology and the Associated Radiative Forcing and Feedback Between 1982 and 2013." *Environmental Research Letters* 11: 084002.

Chen, X., S. Liang, Y. Cao, and T. He. 2016. "Distribution, Attribution, and Radiative Forcing of Snow Cover Changes Over China from 1982 to 2013." *Climatic Change* 137: 363–377.

Chen, X., S. Liang, Y. Cao, T. He, and D. Wang. 2015. "Observed Contrast Changes in Snow Cover Phenology in Northern Middle and High Latitudes from 2001–2014." *Scientific Reports* 5: 16820.
Chen, D., T. V. Loboda, T. He, Y. Zhang, and S. Liang. 2018. "Strong Cooling Induced by Stand-Replacing Fires Through Albedo in Siberian Larch Forests." *Scientific Reports* 8: 4821.
Chen, X., D. Long, Y. Hong, S. Liang, and A. Hou. 2017. "Observed Radiative Cooling Over the Tibetan Plateau for the Past Three Decades Driven by Snow Cover Induced Surface Albedo Anomaly." *Journal of Geophysical Research: Atmospheres* 122: 6170–6185.
Chen, Y. H., J. L. Quan, W. F. Zhan, and Z. Guo. 2016. "Enhanced Statistical Estimation of Air Temperature Incorporating Nighttime Light Data." *Remote Sensing* 8: 23.
Cheng, J., X. Cheng, S. Liang, R. Niclòs, A. Nie, and Q. Liu. 2017. "A Lookup Table-Based Method for Estimating Sea Surface Hemispherical Broadband Emissivity Values (8–13.5 μm)." *Remote Sensing* 9: 245. doi:210.3390/rs9030245.
Cheng, J., and S. Liang. 2016. "Global Estimates for High-Spatial-Resolution Clear-Sky Land Surface Upwelling Longwave Radiation from MODIS Data." *IEEE Transactions on Geoscience and Remote Sensing* 54: 4115–4129.
Cheng, J., and S. Liang. 2017. "Land Surface Emissivity." In *Comprehensive Remote Sensing Vol. 5 Earth's Energy Budget*, edited by S. Liang, 217–263. Oxford: Elsevier.
Cheng, J., S. Liang, and W. Wang. 2017. "Surface Downward Longwave Radiation." In *Comprehensive Remote Sensing Vol. 5 Earth's Energy Budget*, edited by S. Liang, 196–216. Oxford: Elsevier.
Cheng, J., S. Liang, W. Wang, and Y. Guo. 2017. "An Efficient Hybrid Method for Estimating Clear-Sky Surface Downward Longwave Radiation from MODIS Data." *Journal of Geophysical Research: Atmospheres* 122: 2616–2630.
Cheng, J., S. Liang, Y. Yao, and X. Zhang. 2013. "Estimating the Optimal Broadband Emissivity Spectral Range for Calculating Surface Longwave Net Radiation." *IEEE Geoscience and Remote Sensing Letters* 10: 401–405.
Coddington, O., J. L. Lean, P. Pilewskie, M. Snow, and D. Lindholm. 2016. "A Solar Irradiance Climate Data Record." *Bulletin of the American Meteorological Society* 97: 1265–1282.
Coll, C., E. Valor, J. M. Galve, M. Mira, M. Bisquert, V. Garcia-Santos, E. Caselles, and V. Caselles. 2012. "Long-Term Accuracy Assessment of Land Surface Temperatures Derived from the Advanced Along-Track Scanning Radiometer." *Remote Sensing of Environment* 116: 211–225.
Comiso, J. C., and D. K. Hall. 2014. "Climate Trends in the Arctic as Observed from Space." *Wiley Interdisciplinary Reviews: Climate Change* 5: 389–409.
Crow, W. T., E. F. Wood, and M. Pan. 2003. "Multiobjective Calibration of Land Surface Model Evapotranspiration Predictions Using Streamflow Observations and Spaceborne Surface Radiometric Temperature Retrievals." *Journal of Geophysical Research-Atmospheres* 108: 4725. doi:10.1029/2002JD003292.
Czajkowski, K. P., S. N. Goward, S. J. Stadler, and A. Walz. 2000. "Thermal Remote Sensing of Near Surface Environmental Variables: Application Over the Oklahoma Mesonet." *The Professional Geographer* 52: 345–357.
Darnell, W. L., S. K. Gupta, and W. F. Staylor. 1986. "Downward Longwave Surface Radiation from Sun-Synchronous Satellite Data: Validation of Methodology." *Journal of Climate and Applied Meteorology* 25: 1012–1021.
Deneke, H. M., A. J. Feijt, and R. A. Roebeling. 2008. "Estimating Surface Solar Irradiance from METEOSAT SEVIRI-Derived Cloud Properties." *Remote Sensing of Environment* 112: 3131–3141.
Dewitte, S., and N. Clerbaux. 2017. "Measurement of the Earth Radiation Budget at the Top of the Atmosphere—A Review." *Remote Sensing* 9: 1143.
Diner, D., R. Davies, T. Varnai, C. Moroney, C. Borel, S. A. W. Gerstl, and S. L. Nelson. 1999. *MISR Level-2 Top-of-Atmosphere Albedo ATBD (JPL D-13401, Rev. D)*. Pasadena, CA: NASA JPL.
Doelling, D. R., N. G. Loeb, D. F. Keyes, M. L. Nordeen, D. Morstad, C. Nguyen, B. A. Wielicki, D. F. Young, and M. Sun. 2013. "Geostationary Enhanced Temporal Interpolation for CERES Flux Products." *Journal of Atmospheric and Oceanic Technology* 30: 1072–1090.
Dong, C., J. Yang, Z. Yang, N. Lu, J. Shi, P. Zhang, Y. Liu, B. Cai, and W. Zhang. 2009. "An Overview of a New Chinese Weather Satellite FY-3A." *Bulletin of the American Meteorological Society* 90: 1531–1544.
Donohoe, A., and D. S. Battisti. 2011. "Atmospheric and Surface Contributions to Planetary Albedo." *Journal of Climate* 24: 4402–4418.
Duan, S. B., Z. L. Li, J. Cheng, and P. Leng. 2017. "Cross-Satellite Comparison of Operational Land Surface Temperature Products Derived from MODIS and ASTER Data Over Bare Soil Surfaces." *ISPRS Journal of Photogrammetry and Remote Sensing* 126: 1–10.
Duan, S. B., Z. L. Li, and P. Leng. 2017. "A Framework for the Retrieval of All-Weather Land Surface Temperature at a High Spatial Resolution from Polar-Orbiting Thermal Infrared and Passive Microwave Data." *Remote Sensing of Environment* 195: 107–117.
Duan, S. B., Z. L. Li, H. Wu, P. Leng, M. F. Gao, and C. G. Wang. 2018. "Radiance-Based Validation of Land Surface Temperature Products Derived from Collection 6 MODIS Thermal Infrared Data." *International Journal of Applied Earth Observation and Geoinformation* 70: 84–92.
Duarte, H. F., N. L. Dias, and S. R. Maggiotto. 2006. "Assessing Daytime Downward Longwave Radiation Estimates for Clear and Cloudy Skies in Southern Brazil." *Agricultural and Forest Meteorology* 139: 171–181.

Duethmann, D., and G. Blöschl. 2018. "Why Has Catchment Evaporation Increased in the Past 40 Years? A Data-Based Study in Austria." *Hydrology and Earth System Sciences Discussion* 22: 5143–5158.
Duvel, J.-P., M. Viollier, P. Raberanto, R. Kandel, M. Haeffelin, L. Pakhomov, V. Golovko, J. Mueller, R. Stuhlmann, and the International ScaRaB Scientific Working Group. 2001. "The ScaRaB–Resurs Earth Radiation Budget Dataset and First Results." *Bulletin of the American Meteorological Society* 82: 1397–1408.
Ermida, S. L., C. Jimenez, C. Prigent, I. F. Trigo, and C. C. DaCamara. 2017. "Inversion of AMSR-E Observations for Land Surface Temperature Estimation: 2. Global Comparison with Infrared Satellite Temperature." *Journal of Geophysical Research: Atmospheres* 122: 3348–3360.
Fang, W., H. R. Wang, H. D. Li, and Y. P. Wang. 2014. "Total Solar Irradiance Monitor for Chinese FY-3A and FY-3B Satellites – Instrument Design." *Solar Physics* 289: 4711–4726.
Feng, F., X. L. Li, Y. J. Yao, S. Liang, J. Q. Chen, X. Zhao, K. Jia, K. Pinter, and J. H. McCaughey. 2016. "An Empirical Orthogonal Function-Based Algorithm for Estimating Terrestrial Latent Heat Flux from Eddy Covariance, Meteorological and Satellite Observations." *Plos One* 11: 16.
Feng, Y., Q. Liu, Y. Qu, and S. Liang. 2016. "Estimation of the Ocean Water Albedo from Remote Sensing and Meteorological Reanalysis Data." *IEEE Transactions on Geoscience and Remote Sensing* 54: 850–868.
Feng, F., and K. C. Wang. 2018. "Merging Satellite Retrievals and Reanalyses to Produce Global Long-Term and Consistent Surface Incident Solar Radiation Datasets." *Remote Sensing* 10: 20.
Flanner, M., K. Shell, M. Barlage, D. Perovich, and M. Tschudi. 2011. "Radiative Forcing and Albedo Feedback from the Northern Hemisphere Cryosphere Between 1979 and 2008." *Nature Geoscience* 4: 151–155.
Flerchinger, G. N., W. Xaio, D. Marks, T. J. Sauer, and Q. Yu. 2009. "Comparison of Algorithms for Incoming Atmospheric Long-Wave Radiation." *Water Resources Research* 45: 13.
Forman, B. A., and S. A. Margulis. 2009. "High-Resolution Satellite-Based Cloud-Coupled Estimates of Total Downwelling Surface Radiation for Hydrologic Modelling Applications." *Hydrology and Earth System Sciences* 13: 969–986.
Freitas, S. C., I. F. Trigo, J. M. Bioucas-Dias, and F. M. Gottsche. 2010. "Quantifying the Uncertainty of Land Surface Temperature Retrievals from SEVIRI/METEOSAT." *IEEE Transactions on Geoscience and Remote Sensing* 48: 523–534.
Fritz, S., P. K. Rao, and M. Weinstein. 1964. "Satellite Measurements of Reflected Solar Energy and the Energy Received at the Ground." *Journal of the Atmospheric Sciences* 21: 141–151.
Frouin, R., C. Gautier, and J. J. Morcrette. 1988. "Downward Longwave Irradiance at the Ocean Surface from Satellite Data – Methodology and In Situ Validation." *Journal of Geophysical Research* 93: 597–619.
GCOS. 2016. *The Global Observing System for Climate: Implementation Needs, GCOS-200, GOOS-214*. Geneva: World Meteorological Organization.
Gentemann, C. L. 2014. "Three Way Validation of MODIS and AMSR-E Sea Surface Temperatures." *Journal of Geophysical Research: Oceans* 119: 2583–2598.
Glenn, E. P., A. R. Huete, P. L. Nagler, K. K. Hirschboeck, and P. Brown. 2007. "Integrating Remote Sensing and Ground Methods to Estimate Evapotranspiration." *Critical Reviews in Plant Sciences* 26: 139–168.
Good, E. J., D. J. Ghent, C. E. Bulgin, and J. J. Remedios. 2017. "A Spatiotemporal Analysis of the Relationship Between Near-Surface Air Temperature and Satellite Land Surface Temperatures Using 17 Years of Data from the ATSR Series." *Journal of Geophysical Research: Atmospheres* 122: 9185–9210.
Govaerts, Y. M., S. Wagner, A. Lattanzio, and P. Watts. 2010. "Joint Retrieval of Surface Reflectance and Aerosol Optical Depth from MSG/SEVIRI Observations with an Optimal Estimation Approach: 1." *Theory. Journal of Geophysical Research-Atmospheres* 115: 16.
Gristey, J. J., J. C. Chiu, R. J. Gurney, S. C. Han, and C. J. Morcrette. 2017. "Determination of Global Earth Outgoing Radiation at High Temporal Resolution Using a Theoretical Constellation of Satellites." *Journal of Geophysical Research: Atmospheres* 122: 1114–1131.
Gueymard, C. A. 2018. "A Reevaluation of the Solar Constant Based on a 42-Year Total Solar Irradiance Time Series and a Reconciliation of Spaceborne Observations." *Solar Energy* 168: 2–9.
Guo, Y. M., and J. Cheng. 2018. "Feasibility of Estimating Cloudy-Sky Surface Longwave Net Radiation Using Satellite-Derived Surface Shortwave Net Radiation." *Remote Sensing* 10: 14.
Gupta, S. K., W. L. Darnell, and A. C. Wilber. 1992. "A Parameterization for Longwave Surface Radiation from Satellite Data: Recent Improvements." *Journal of Applied Meteorology* 31: 1361–1367.
Hagolle, O., A. Lobo, P. Maisongrande, F. Cabot, B. Duchemin, and A. De Pereyra. 2005. "Quality Assessment and Improvement of Temporally Composited Products of Remotely Sensed Imagery by Combination of Vegetation 1 and 2 Images." *Remote Sensing of Environment* 94: 172–186.
Hakuba, M. Z., G. L. Stephens, B. Christophe, A. E. Nash, B. Foulon, S. V. Bettadpur, B. D. Tapley, and F. H. Webb. 2019. "Earth's Energy Imbalance Measured from Space." *IEEE Transactions on Geoscience and Remote Sensing* 57: 32–45.
Hanafin, J. A., and P. J. Minnett. 2005. "Measurements of the Infrared Emissivity of a Wind-Roughened Sea Surface." *Applied Optics* 44: 398–411.

Hansen, J., M. Sato, P. Kharecha, and K. von Schuckmann. 2011. "Earth's Energy Imbalance and Implications." *Atmospheric Chemistry and Physics* 11: 13421–13449.
Harries, J. E., J. E. Russell, J. A. Hanafin, H. Brindley, J. Futyan, J. Rufus, S. Kellock, et al. 2005. "The Geostationary Earth Radiation Budget Project." *Bulletin of the American Meteorological Society* 86: 945–960.
Hartmann, D. L., and P. Ceppi. 2014. "Trends in the CERES Dataset, 2000-13: The Effects of Sea Ice and Jet Shifts and Comparison to Climate Models." *Journal of Climate* 27: 2444–2456.
Hatzianastassiou, N., C. D. Papadimas, C. Matsoukas, K. Pavlakis, A. Fotiadi, M. Wild, and I. Vardavas. 2012. "Recent Regional Surface Solar Radiation Dimming and Brightening Patterns: Inter-Hemispherical Asymmetry and a Dimming in the Southern Hemisphere." *Atmospheric Science Letters* 13: 43–48.
He, T., S. Liang, and D.-X. Song. 2014. "Analysis of Global Land Surface Albedo Climatology and Spatial-Temporal Variation During 1981–2010 from Multiple Satellite Products." *Journal of Geophysical Research: Atmospheres* 119: 10,281–10,298.
He, T., S. Liang, and D. Wang. 2017. "Direct Estimation of Land Surface Albedo from Simultaneous MISR Data." *IEEE Transactions on Geoscience and Remote Sensing* 55: 2605–2617.
He, T., S. Liang, D. Wang, Y. Cao, F. Gao, Y. Yu, and M. Feng. 2018. "Evaluating Land Surface Albedo Estimation from Landsat MSS, TM, ETM +, and OLI Data Based on the Unified Direct Estimation Approach." *Remote Sensing of Environment* 204: 181–196.
He, T., S. Liang, D. Wang, X. Chen, D.-X. Song, and B. Jiang. 2015. "Land Surface Albedo Estimation from Chinese HJ Satellite Data Based on the Direct Estimation Approach." *Remote Sensing* 7: 5495–5510.
He, T., S. Liang, D. Wang, Q. Shi, and M. L. Goulden. 2015. "Estimation of High-Resolution Land Surface Net Shortwave Radiation from AVIRIS Data: Algorithm Development and Preliminary Results." *Remote Sensing of Environment* 167: 20–30.
He, T., S. Liang, D. Wang, Q. Shi, and X. Tao. 2014. "Estimation of High-Resolution Land Surface Shortwave Albedo from AVIRIS Data." *IEEE Journal of Selected Topics in Applied Earth Observations and Remote Sensing* 7: 4919–4928.
He, T., S. Liang, D. D. Wang, Y. M. Shuai, and Y. Y. Yu. 2014. "Fusion of Satellite Land Surface Albedo Products Across Scales Using a Multiresolution Tree Method in the North Central United States." *IEEE Transactions on Geoscience and Remote Sensing* 52: 3428–3439.
He, T., S. Liang, D. Wang, H. Wu, Y. Yu, and J. Wang. 2012. "Estimation of Surface Albedo and Directional Reflectance from Moderate Resolution Imaging Spectroradiometer (MODIS) Observations." *Remote Sensing of Environment* 119: 286–300.
He, T., S. Liang, Y. Yu, Q. Liu, and F. Gao. 2013. "Greenland Surface Albedo Changes in July 1981–2012 from Satellite Observations." *Environmental Research Letters* 8: 044043. doi:044010.041088/041748-049326/044048/044044/044043.
He, T., S. Liang, and X. Zhang. 2018. "Comparison of Global, Ocean and Land Surface Albedos from Satellite Datasets and CMIP5 Models." *Climate Dynamics*, Revised.
He, T., D. Wang, and Y. Qu. 2017. "Land Surface Albedo." In *Comprehensive Remote Sensing, Vol. 5 Earth's Energy Budget*, edited by S. Liang, 140–162. Oxford: Elsevier.
He, Y. Y., K. C. Wang, C. Zhou, and M. Wild. 2018. "A Revisit of Global Dimming and Brightening Based on the Sunshine Duration." *Geophysical Research Letters* 45: 4281–4289.
Henderson, B. G., J. Theiler, and P. Villeneuve. 2003. "The Polarized Emissivity of a Wind-Roughened Sea Surface: A Monte Carlo Model." *Remote Sensing of Environment* 88: 453–467.
Herman, J., L. Huang, R. McPeters, J. Ziemke, A. Cede, and K. Blank. 2018. "Synoptic Ozone, Cloud Reflectivity, and Erythemal Irradiance from Sunrise to Sunset for the Whole Earth as Viewed by the DSCOVR Spacecraft from the Earth–Sun Lagrange 1 Orbit." *Atmospheric Measurement Techniques* 11: 177–194.
Hinkelman, L. M., P. W. Stackhouse, B. A. Wielicki, T. P. Zhang, and S. R. Wilson. 2009. "Surface Insolation Trends from Satellite and Ground Measurements: Comparisons and Challenges." *Journal of Geophysical Research* 114: D00D20. doi:10.1029/2008JD011004.
Hosoda, K. 2010. "A Review of Satellite-Based Microwave Observations of Sea Surface Temperatures." *Journal of Oceanography* 66: 439–473.
Hosoda, K., H. Kawamura, and F. Sakaida. 2015. "Improvement of New Generation Sea Surface Temperature for Open Ocean (NGSST-O): A New Sub-Sampling Method of Blending Microwave Observations." *Journal of Oceanography* 71: 205–220.
House, F. B., A. Gruber, G. E. Hunt, and A. T. Mecherikunnel. 1986. "History of Satellite Missions and Measurements of the Earth Radiation Budget (1957–1984)." *Reviews of Geophysics* 24: 357–377.
Houspanossian, J., R. Gimenez, E. Jobbagy, and M. Nosetto. 2017. "Surface Albedo Raise in the South American Chaco: Combined Effects of Deforestation and Agricultural Changes." *Agricultural and Forest Meteorology* 232: 118–127.
Hu, T., B. Cao, Y. M. Du, H. Li, C. Wang, Z. J. Bian, D. L. Sun, and Q. H. Liu. 2017. "Estimation of Surface Upward Longwave Radiation Using a Direct Physical Algorithm." *IEEE Transactions on Geoscience and Remote Sensing* 55: 4412–4426.

Hu, T., Y. M. Du, B. Cao, H. Li, Z. J. Bian, D. L. Sun, and Q. H. Liu. 2016. "Estimation of Upward Longwave Radiation from Vegetated Surfaces Considering Thermal Directionality." *IEEE Transactions on Geoscience and Remote Sensing* 54: 6644–6658.

Hu, Y. H., G. S. Jia, C. Pohl, X. X. Zhang, and J. van Genderen. 2016. "Assessing Surface Albedo Change and Its Induced Radiation Budget Under Rapid Urbanization With Landsat and GLASS Data." *Theoretical and Applied Climatology* 123: 711–722.

Huang, G., S. Liang, N. Lu, M. Ma, and D. Wang. 2018. "Toward a Broadband Parameterization Scheme for Estimating Surface Solar Irradiance: Development and Preliminary Results on MODIS Products." *Journal of Geophysical Research: Atmospheres* 123: 12,180–12,193.

Huang, B. Y., C. Y. Liu, V. F. Banzon, H. M. Zhang, T. R. Karl, J. H. Lawrimore, and R. S. Vose. 2016. "Assessing the Impact of Satellite-Based Observations in Sea Surface Temperature Trends." *Geophysical Research Letters* 43: 3431–3437.

Huang, G., M. Ma, S. Liang, S. Liu, and X. Li. 2011. "A LUT-Based Approach to Estimate Surface Solar Irradiance by Combining MODIS and MTSAT Data." *Journal of Geophysical Research* 116: D22201.

Hulley, G. C., and S. J. Hook. 2009. "Intercomparison of Versions 4, 4.1 and 5 of the MODIS Land Surface Temperature and Emissivity Products and Validation with Laboratory Measurements of Sand Samples from the Namib Desert, Namibia." *Remote Sensing of Environment* 113: 1313–1318.

Inoue, T., and S. A. Ackerman. 2002. "Radiative Effects of Various Cloud Types as Classified by the Split Window Technique Over the Eastern Sub-Tropical Pacific Derived from Collocated ERBE and AVHRR Data." *Journal of the Meteorological Society of Japan* 80: 1383–1394.

Jacobowitz, H., and R. J. Tighe. 1984. "The Earth Radiation Budget Derived from the NIMBUS 7 ERB Experiment." *Journal of Geophysical Research: Atmospheres* 89: 4997–5010.

Jasechko, S., Z. D. Sharp, J. J. Gibson, S. J. Birks, Y. Yi, and P. J. Fawcett. 2013. "Terrestrial Water Fluxes Dominated by Transpiration." *Nature* 496: 347–350.

Jia, A., B. Jiang, S. Liang, X. Zhang, and H. Ma. 2016. "Validation and Spatiotemporal Analysis of CERES Surface Net Radiation Product." *Remote Sensing* 8: 90.

Jia, A., S. Liang, B. Jiang, X. Zhang, and G. Wang. 2018. "Comprehensive Assessment of Global Surface Net Radiation Products and Uncertainty Analysis." *Journal of Geophysical Research: Atmospheres* 123: 1970–1989.

Jiang, B., and S. Liang. 2017. "Land Surface Net Radiation." In *Comprehensive Remote Sensing Vol. 5: Earth's Energy Budget*, edited by S. Liang, 304–331. Oxford: Elsevier.

Jiang, B., S. Liang, H. Ma, X. Zhang, Z. Xiao, X. Zhao, K. Jia, Y. Yao, and A. Jia. 2016. "GLASS Daytime All-Wave Net Radiation Product: Algorithm Development and Preliminary Validation." *Remote Sensing* 8: 222.

Jiang, B., Y. Zhang, S. Liang, G. Wohlfahrt, A. Arain, A. Cescatti, T. Georgiadis, et al. 2015. "Empirical Estimation of Daytime Net Radiation from Shortwave Radiation and Ancillary Information." *Agricultural and Forest Meteorology* 211-212: 23–36.

Jiang, B., Y. Zhang, S. Liang, X. Zhang, and Z. Xiao. 2014. "Surface Daytime Net Radiation Estimation Using Artificial Neural Networks." *Remote Sensing* 6: 11031–11050.

Jiao, Z. H., G. J. Yan, J. Zhao, T. X. Wang, and L. Chen. 2015. "Estimation of Surface Upward Longwave Radiation from MODIS and VIIRS Clear-Sky Data in the Tibetan Plateau." *Remote Sensing of Environment* 162: 221–237.

Jin, M. S. 2012. "Developing an Index to Measure Urban Heat Island Effect Using Satellite Land Skin Temperature and Land Cover Observations." *Journal of Climate* 25: 6193–6201.

Jin, M., and S. Liang. 2006. "An Improved Land Surface Emissivity Parameter for Land Surface Models Using Global Remote Sensing Observations." *Journal of Climate* 19: 2867–2881.

Johnson, G. C., J. M. Lyman, and N. G. Loeb. 2016. "Improving Estimates of Earth's Energy Imbalance." *Nature Climate Change* 6: 639–640.

Julien, Y., and J. A. Sobrino. 2009. "The Yearly Land Cover Dynamics (YLCD) Method: An Analysis of Global Vegetation from NDVI and LST Parameters." *Remote Sensing of Environment* 113: 329–334.

Jung, M., M. Reichstein, P. Ciais, S. I. Seneviratne, J. Sheffield, M. L. Goulden, G. Bonan, et al. 2010. "Recent Decline in the Global Land Evapotranspiration Trend Due to Limited Moisture Supply." *Nature* 467: 951–954.

Kalma, J. D., T. R. McVicar, and M. F. McCabe. 2008. "Estimating Land Surface Evaporation: A Review of Methods Using Remotely Sensed Surface Temperature Data." *Surveys in Geophysics* 29: 421–469.

Kandel, R., M. Viollier, P. Raberanto, J. P. Duvel, L. A. Pakhomov, V. A. Golovko, A. P. Trishchenko, J. Mueller, E. Rashke, and R. Stuhlmann. 1998. "The ScaRaB Earth Radiation Budget Dataset." *Bulletin of the American Meteorological Society* 79: 765–783.

Karl, T. R., A. Arguez, B. Huang, J. H. Lawrimore, J. R. McMahon, M. J. Menne, T. C. Peterson, R. S. Vose, and H.-M. Zhang. 2015. "Possible Artifacts of Data Biases in the Recent Global Surface Warming Hiatus." *Science* 348: 1469–1472.

Karlsson, K.-G., K. Anttila, J. Trentmann, M. Stengel, J. F. Meirink, A. Devasthale, T. Hanschmann, S. Kothe, E. Jaaskelainen, and J. Sedlar. 2017. "CLARA-A2: The Second Edition of the CM SAF Cloud and Radiation Data Record from 34 Years of Global AVHRR Data." *Atmospheric Chemistry and Physics* 17: 5809–5828.

Karnieli, A., N. Agam, R. T. Pinker, M. Anderson, M. L. Imhoff, G. G. Gutman, N. Panov, and A. Goldberg. 2010. "Use of NDVI and Land Surface Temperature for Drought Assessment: Merits and Limitations." *Journal of Climate* 23: 618–633.

Kato, S., F. G. Rose, D. A. Rutan, T. J. Thorsen, N. G. Loeb, D. R. Doelling, X. Huang, W. L. Smith, W. Su, and S. H. Ham. 2018. "Surface Irradiances of Edition 4.0 Clouds and the Earth's Radiant Energy System (CERES) Energy Balanced and Filled (EBAF) Data Product." *Journal of Climate*.

Katul, G. G., R. Oren, S. Manzoni, C. Higgins, and M. B. Parlange. 2012. "Evapotranspiration: A Process Driving Mass Transport and Energy Exchange in the Soil-Plant-Atmosphere-Climate System." *Reviews of Geophysics* 50: RG3002.

Key, J., X. Wang, J. Stroeve, and C. Fowler. 2001. "Estimating the Cloudy Sky Albedo of Sea Ice and Snow from Space." *Journal of Geophysical Research: Atmospheres* 106: 12489–12497.

Khan, M. S., U. W. Liaqat, J. Baik, and M. Choi. 2018. "Stand-Alone Uncertainty Characterization of GLEAM, GLDAS and MOD16 Evapotranspiration Products Using an Extended Triple Collocation Approach." *Agricultural and Forest Meteorology* 252: 256–268.

Kim, B.-Y., K.-T. Lee, J.-B. Jee, and I.-S. Zo. 2018. "Retrieval of Outgoing Longwave Radiation at Top-Of-Atmosphere Using Himawari-8 AHI Data." *Remote Sensing of Environment* 204: 498–508.

Kim, H., and S. Liang. 2010. "Development of a New Hybrid Method for Estimating Land Surface Shortwave Net Radiation from MODIS Data." *Remote Sensing of Environment* 114: 2393–2402.

Kjaersgaard, J. H., F. L. Plauborg, and S. Hansen. 2007. "Comparison of Models for Calculating Daytime Long-Wave Irradiance Using Long Term Data Set." *Agricultural and Forest Meteorology* 143: 49–63.

Knorr, W., K. G. Schnitzler, and Y. Govaerts. 2001. "The Role of Bright Desert Regions in Shaping North African Climate." *Geophysical Research Letters* 28: 3489–3492.

Kopp, G. 2017. "Earth's Incoming Energy: The Total Solar Irradiance." In *Comprehensive Remote Sensing, Vol. 5: Earht's Energy Budget*, edited by S. Liang, 32–66. London: Elsevier.

Kopp, G., G. Lawrence, and G. Rottman. 2005. "The Total Irradiance Monitor (TIM): Science Results." *Solar Physics* 230: 129–139.

Krähenmann, S., A. Obregon, R. Müller, J. Trentmann, and B. Ahrens. 2013. "A Satellite-Based Surface Radiation Climatology Derived by Combining Climate Data Records and Near-Real-Time Data." *Remote Sensing* 5: 4693–4718.

Kumar, P., B. K. Bhattacharya, R. Nigam, C. M. Kishtawal, and P. K. Pal. 2014. "Impact of Kalpana-1 Derived Land Surface Albedo on Short-Range Weather Forecasting Over the Indian Subcontinent." *Journal of Geophysical Research: Atmospheres* 119: 2764–2780.

Kwok, R., and D. Rothrock. 2009. "Decline in Arctic Sea Ice Thickness from Submarine and ICESat Records: 1958–2008." *Geophysical Research Letters* 36: L15501. doi:10.1029/2009GL039035.

Laszlo, I., P. Ciren, H. Q. Liu, S. Kondragunta, J. D. Tarpley, and M. D. Goldberg. 2008. "Remote Sensing of Aerosol and Radiation from Geostationary Satellites." *Advances in Space Research* 41: 1882–1893.

L'Ecuyer, T. S., H. K. Beaudoing, M. Rodell, W. Olson, B. Lin, S. Kato, C. A. Clayson, et al. 2015. "The Observed State of the Energy Budget in the Early Twenty-First Century." *Journal of Climate* 28: 8319–8346.

Lee, H. T., A. Gruber, R. G. Ellingson, and I. Laszlo. 2007. "Development of the HIRS Outgoing Longwave Radiation Climate Dataset." *Journal of Atmospheric and Oceanic Technology* 24: 2029–2047.

Lee, S. H., B. Y. Kim, K. T. Lee, I. S. Zo, H. S. Jung, and S. H. Rim. 2018. "Retrieval of Reflected Shortwave Radiation at the Top of the Atmosphere Using Himawari-8/AHI Data." *Remote Sensing* 10: 25.

Lee, W. L., and K. N. Liou. 2012. "Effect of Absorbing Aerosols on Snow Albedo Reduction in the Sierra Nevada." *Atmospheric Environment* 55: 425–430.

Lewis, P., J. Gomez-Dans, T. Kaminski, J. Settle, T. Quaife, N. Gobron, J. Styles, and M. Berger. 2012. "An Earth Observation Land Data Assimilation System (EO-LDAS)." *Remote Sensing of Environment* 120: 219–235.

Li, Z., and S. Duan. 2017. "Land Surface Temperature." In *Comprehensive Remote Sensing Vol. 5 Earth's Energy Budget*, edited by S. Liang, 264–283. Oxoford: Elsevier.

Li, X. Y., Y. He, Z. Z. Zeng, X. Lian, X. H. Wang, M. Y. Du, G. S. Jia, et al. 2018. "Spatiotemporal Pattern of Terrestrial Evapotranspiration in China During the Past Thirty Years." *Agricultural and Forest Meteorology* 259: 131–140.

Li, Z., H. G. Leighton, K. Masuda, and T. Takashima. 1993. "Estimation of SW Flux Absorbed at the Surface from TOA Reflected Flux." *Journal of Climate* 6: 317–330.

Li, X., S. Liang, W. Yuan, G. Yu, X. Cheng, Y. Chen, T. Zhao, et al. 2014. "Estimation of Evapotranspiration Over the Terrestrial Ecosystems in China." *Ecohydrology* 7: 139–149.

Li, Q. P., M. G. Ma, X. D. Wu, and H. Yang. 2018. "Snow Cover and Vegetation-Induced Decrease in Global Albedo from 2002 to 2016." *Journal of Geophysical Research: Atmospheres* 123: 124–138.

Li, H., D. L. Sun, Y. Y. Yu, H. Y. Wang, Y. L. Liu, Q. H. Liu, Y. M. Du, H. S. Wang, and B. A. Cao. 2014. "Evaluation of the VIIRS and MODIS LST Products in an Arid Area of Northwest China." *Remote Sensing of Environment* 142: 111–121.

Li, Z. L., R. L. Tang, Z. M. Wan, Y. Y. Bi, C. H. Zhou, B. H. Tang, G. J. Yan, and X. Y. Zhang. 2009. "A Review of Current Methodologies for Regional Evapotranspiration Estimation from Remotely Sensed Data." *Sensors* 9: 3801–3853.

Li, Z.-L., B.-H. Tang, H. Wu, H. Ren, G. Yan, Z. Wan, I. F. Trigo, and J. A. Sobrino. 2013. "Satellite-Derived Land Surface Temperature: Current Status and Perspectives." *Remote Sensing of Environment* 131: 14–37.

Li, X. M., Y. Y. Zhou, G. R. Asrar, and Z. Y. Zhu. 2018. "Developing a 1 km Resolution Daily Air Temperature Dataset for Urban and Surrounding Areas in the Conterminous United States." *Remote Sensing of Environment* 215: 74–84.

Lian, X., Z. Z. Zeng, Y. T. Yao, S. S. Peng, K. C. Wang, and S. L. Piao. 2017. "Spatiotemporal Variations in the Difference Between Satellite-Observed Daily Maximum Land Surface Temperature and Station-Based Daily Maximum Near-Surface Air Temperature." *Journal of Geophysical Research: Atmospheres* 122: 2254–2268.

Liang, S. 2001. "Narrowband to Broadband Conversions of Land Surface Albedo I." *Remote Sensing of Environment* 76: 213–238.

Liang, S. 2003. "A Direct Algorithm for Estimating Land Surface Broadband Albedos from MODIS Imagery." *IEEE Transactions on Geoscience and Remote Sensing* 41: 136–145.

Liang, S. 2017. "Remote Sensing of Earth's Energy Budget: An Overview of Recent Progress." In *Comprehensive Remote Sensing Vol. 5: Earth's Energy Budget*, edited by S. Liang, 1–31. Oxford: Elsevier.

Liang, S., H. Fang, and M. Chen. 2001. "Atmospheric Correction of Landsat ETM+ Land Surface Imagery: I. Methods." *IEEE Transactions on Geoscience and Remote Sensing* 39: 2490–2498.

Liang, S., H. Fang, M. Chen, C. Shuey, C. Walthall, C. Daughtry, J. Morisette, C. Schaaf, and A. Strahler. 2002. "Validating MODIS Land Surface Reflectance and Albedo Products: Methods and Preliminary Results." *Remote Sensing of Environment* 83: 149–162.

Liang, S., C. Shuey, H. Fang, A. Russ, M. Chen, C. Walthall, C. Daughtry, and R. Hunt. 2003. "Narrowband to Broadband Conversions of Land Surface Albedo: II. Validation." *Remote Sensing of Environment* 84: 25–41.

Liang, S., A. Strahler, and C. Walthall. 1999. "Retrieval of Land Surface Albedo from Satellite Observations: A Simulation Study." *Journal of Applied Meteorology* 38: 712–725.

Liang, S., J. Stroeve, and J. E. Box. 2005. "Mapping Daily Snow/Ice Shortwave Broadband Albedo from Moderate Resolution Imaging Spectroradiometer (MODIS): The Improved Direct Retrieval Algorithm and Validation with Greenland *in situ* Measurement." *Journal of Geophysical Research-Atmospheres* 110: D10109. doi:10.1029/2004JD005493.

Liang, S., D. Wang, J. Cheng, T. He, X. Tao, Y. Yao, and X. Zhang. 2017. "Methodologies for Integrating Multiple High-Level Remotely Sensed Land Products." In *Comprehensive Remote Sensing Vol. 2 Remote Sensing Data Processing and Analysis Methodology*, edited by M. M. Crawford, 278–317. Oxford: Elsevier.

Liang, S., K. Wang, X. Zhang, and M. Wild. 2010. "Review on Estimation of Land Surface Radiation and Energy Budgets from Ground Measurement, Remote Sensing and Model Simulations." *IEEE Journal of Selected Topics in Applied Earth Observations and Remote Sensing* 3: 225–240.

Liang, S., X. Zhang, Z. Xiao, J. Cheng, Q. Liu, and X. Zhao. 2013. *Global LAnd Surface Satellite (GLASS) Products: Algorithms, Validation and Analysis*. Cham: Springer Science & Business Media.

Liang, S., X. Zhao, W. Yuan, S. Liu, X. Cheng, Z. Xiao, X. Zhang, et al. 2013. "A Long-Term Global LAnd Surface Satellite (GLASS) Dataset for Environmental Studies." *International Journal of Digital Earth* 6: 5–33.

Liang, S., T. Zheng, R. Liu, H. Fang, S. C. Tsay, and S. Running. 2006. "Mapping Incident Photosynthetically Active Radiation (PAR) from MODIS Data." *Journal of Geophysical Research-Atmospheres* 111: D15208. doi:15210.11029/12005JD006730.

Liang, S., T. Zheng, D. D. Wang, K. C. Wang, R. G. Liu, S. C. Tsay, S. Running, and J. Townshend. 2007. "Mapping High-Resolution Incident Photosynthetically Active Radiation Over Land from Polar-Orbiting and Geostationary Satellite Data." *Photogrammetric Engineering and Remote Sensing* 73: 1085–1089.

Liu, M., L. Guan, W. Zhao, and G. Chen. 2017. "Evaluation of Sea Surface Temperature from the HY-2 Scanning Microwave Radiometer." *IEEE Transactions on Geoscience and Remote Sensing* 55: 1372–1380.

Liu, R., S. Liang, H. He, J. Liu, and T. Zheng. 2008. "Mapping Incident Photosynthetically Active Radiation from MODIS Data Over China." *Remote Sensing of Environment* 112: 998–1009.

Liu, Q., L. Wang, Y. Qu, N. Liu, S. Liu, H. Tang, and S. Liang. 2013. "Priminary Evaluation of the Long-Term GLASS Albedo Product." *International Journal of Digital Earth* 6: 69–95. doi:10.1080/17538947.17532013.17804601.

Liu, Y., Y. Yu, P. Yu, F. M. Göttsche, and I. F. Trigo. 2015. "Quality Assessment of S-NPP VIIRS Land Surface Temperature Product." *Remote Sensing* 7: 12215–12241.

Loarie, S. R., D. B. Lobell, G. P. Asner, and C. B. Field. 2011. "Land-Cover and Surface Water Change Drive Large Albedo Increases in South America." *Earth Interactions* 15: 1–16.

Loeb, N. G., D. R. Doelling, H. Wang, W. Su, C. Nguyen, J. G. Corbett, L. Liang, C. Mitrescu, F. G. Rose, and S. Kato. 2018. "Clouds and the Earth's Radiant Energy System (CERES) Energy Balanced and Filled (EBAF) Top-of-Atmosphere (TOA) Edition-4.0 Data Product." *Journal of Climate* 31: 895–918.

Loeb, N. G., S. Kato, K. Loukachine, and N. Manalo-Smith. 2005. "Angular Distribution Models for Top-of-Atmosphere Radiative Flux Estimation from the Clouds and the Earth's Radiant Energy System Instrument on the Terra Satellite. Part I: Methodology." *Journal of Atmospheric and Oceanic Technology* 22: 338–351.

Loeb, N. G., J. M. Lyman, G. C. Johnson, R. P. Allan, D. R. Doelling, T. Wong, B. J. Soden, and G. L. Stephens. 2012. "Observed Changes in Top-of-The-Atmosphere Radiation and Upper-Ocean Heating Consistent Within Uncertainty." *Nature Geoscience* 5. doi:10.1038/NGEO1375.

Loeb, N. G., N. Manalo-Smith, W. Y. Su, M. Shankar, and S. Thomas. 2016. "CERES Top-of-Atmosphere Earth Radiation Budget Climate Data Record: Accounting for In-Orbit Changes in Instrument Calibration." *Remote Sensing* 8: 14.

Loeb, N. G., W. Su, D. R. Doelling, T. Wong, P. Minnis, S. Thomas, and W. F. Miller. 2017. "Earth's Top-of-Atmosphere Radiation Budget." In *Comprehensive Remote Sensing, Vol. 5, Earth's Energy Budget*, edited by S. Liang, 67–84. London: Elsevier.

Loeb, N., T. Thorsen, J. Norris, H. Wang, and W. Su. 2018. "Changes in Earth's Energy Budget During and After the "Pause" in Global Warming: An Observational Perspective." *Climate* 6: 62.

Lohmann, G. 2018. "Irradiance Variability Quantification and Small-Scale Averaging in Space and Time: A Short Review." *Atmosphere* 9: 264.

Lu, N., R. Liu, J. Liu, and S. Liang. 2010. "An Algorithm for Estimating Downward Shortwave Radiation from GMS-5 Visible Imagery and its Evaluation Over China." *Journal of Geophysical Research* 115: D18102. doi:18110.11029/12009JD013457.

Ma, H., S. Liang, Z. Xiao, and H. Shi. 2017. "Simultaneous Inversion of Multiple Land Surface Parameters from MODIS Optical–Thermal Observations." *ISPRS Journal of Photogrammetry and Remote Sensing* 128: 240–254.

Ma, H., S. Liang, Z. Xiao, and D. Wang. 2018. "Simultaneous Estimation of Multiple Land Surface Parameters from VIIRS Optical-Thermal Data." *IEEE Geoscience and Remote Sensing Letters* 15: 151–160.

Ma, H., Q. Liu, S. Liang, and Z. Xiao. 2017. "Simultaneous Estimation of Leaf Area Index, Fraction of Absorbed Photosynthetically Active Radiation and Surface Albedo from Multiple-Satellite Data." *IEEE Transactions on Geoscience and Remote Sensing* 55: 4334–4354. doi:4310.1109/TGRS.2017.2691542.

Ma, Y., and R. T. Pinker. 2012. "Modeling Shortwave Radiative Fluxes from Satellites." *Journal of Geophysical Research-Atmospheres* 117: 19.

Mao, J. F., W. T. Fu, X. Y. Shi, D. M. Ricciuto, J. B. Fisher, R. E. Dickinson, Y. X. Wei, et al. 2015. "Disentangling Climatic and Anthropogenic Controls on Global Terrestrial Evapotranspiration Trends." *Environmental Research Letters* 10: 13.

Masuda, K., H. Leighton, and Z. Li. 1995. "A New Parameterization for the Determination of Solar Flux Absorbed at the Surface from Satellite Measurements." *Journal of Climate* 8: 1615–1629.

Masuda, K., T. Takashima, and Y. Takayama. 1988. "Emissivity of Pure and Sea Waters for the Model Sea Surface in the Infrared Window Regions." *Remote Sensing of Environment* 24: 313–329.

Matthes, K., B. Funke, M. E. Andersson, L. Barnard, J. Beer, P. Charbonneau, M. A. Clilverd, et al. 2017. "Solar Forcing for CMIP6 (v3.2)." *Geoscientific Model Development* 10: 2247–2302.

Meftah, M., L. Dame, D. Bolsee, A. Hauchecorne, N. Pereira, D. Sluse, G. Cessateur, et al. 2018. "SOLAR-ISS: A New Reference Spectrum Based on SOLAR/SOLSPEC Observations." *Astronomy & Astrophysics* 611: A1.

Meftah, M., P. Keckhut, L. Dame, S. Bekki, A. Sarkissian, and A. Hauchecorne. 2018. "Think the Way to Measure the Earth Radiation Budget and the Total Solar Irradiance With a Small Satellites Constellation." In *Sensors and Systems for Space Applications Xi*, edited by K. D. Pham and G. Chen. Bellingham: Spie-Int Soc Optical Engineering. doi:10.1117/12.2303616.

Mildrexler, D. J., M. Zhao, and S. W. Running. 2009. "Testing a MODIS Global Disturbance Index Across North America." *Remote Sensing of Environment* 113: 2103–2117.

Miralles, D. G., M. J. van den Berg, J. H. Gash, R. M. Parinussa, R. A. M. de Jeu, H. E. Beck, T. R. H. Holmes, et al. 2014. "El Niño–La Niña Cycle and Recent Trends in Continental Evaporation." *Nature Climate Change* 4: 122–126.

Moncet, J. L., P. Liang, A. E. Lipton, J. F. Galantowicz, and C. Prigent. 2011. "Discrepancies Between MODIS and ISCCP Land Surface Temperature Products Analyzed With Microwave Measurements." *Journal of Geophysical Research: Atmospheres* 116: D21105. doi:10.1029/2010JD015432.

Mortimer, C. A., and M. Sharp. 2018. "Spatiotemporal Variability of Canadian High Arctic Glacier Surface Albedo from MODIS Data, 2001-2016." *The Cryosphere* 12: 701–720.

Mu, Q., F. A. Heinsch, M. Zhao, and S. W. Running. 2007. "Development of a Global Evapotranspiration Algorithm Based on MODIS and Global Meteorology Data." *Remote Sensing of Environment* 111: 519–536.

Mu, Q., M. Zhao, and S. W. Running. 2011. "Improvements to a MODIS Global Terrestrial Evapotranspiration Algorithm." *Remote Sensing of Environment* 115: 1781–1800.

Mueller, B., M. Hirschi, C. Jimenez, P. Ciais, P. A. Dirmeyer, A. J. Dolman, J. B. Fisher, et al. 2013. "Benchmark Products for Land Evapotranspiration: LandFlux-EVAL Multi-Data Set Synthesis." *Hydrology and Earth System Sciences* 17: 3707–3720.

Nalli, N. R., P. J. Minnett, and P. Van Delst. 2008. "Emissivity and Reflection Model for Calculating Unpolarized Isotropic Water Surface-Leaving Radiance in the Infrared. I: Theoretical Development and Calculations." *Applied Optics* 47: 3701–3721.

NASA. 2018. "Measurement and Instrumen Requirement Recommendations for an Earth Venture Continuity Earth Radiation Budget Instrument." In *NASA Earth Radiation Budget Working Group Report*. Washington, DC: NASA.

Niclos, R., L. Perez-Planells, C. Coll, J. A. Valiente, and E. Valor. 2018. "Evaluation of the S-NPP VIIRS Land Surface Temperature Product Using Ground Data Acquired by an Autonomous System at a Rice Paddy." *ISPRS Journal of Photogrammetry and Remote Sensing* 135: 1–12.

Niu, X., and R. T. Pinker. 2012. "Revisiting Satellite Radiative Flux Computations at the Top of the Atmosphere." *International Journal of Remote Sensing* 33: 1383–1399.
Njoku, E. G., and L. Li. 1999. "Retrieval of Land Surface Parameters Using Passive Microwave Measurements at 6-18 GHz." *IEEE Transactions on Geoscience and Remote Sensing* 37: 79–93.
North, G. R., R. F. Cahalan, and J. A. Coakley. 1981. "Energy-Balance Climate Models." *Reviews of Geophysics* 19: 91–121.
Ogawa, K., and T. Schmugge. 2004. "Mapping Surface Broadband Emissivity of the Sahara Desert Using ASTER and MODIS Data." *Earth Interactions* 8: 1–14.
O'Halloran, T. L., B. E. Law, M. L. Goulden, Z. S. Wang, J. G. Barr, C. Schaaf, M. Brown, et al. 2012. "Radiative Forcing of Natural Forest Disturbances." *Global Change Biology* 18: 555–565.
Ohring, G., B. Wielicki, R. Spencer, B. Emery, and R. Datla. 2005. "Satellite Instrument Calibration for Measuring Global Climate Change – Report of a Workshop." *Bulletin of the American Meteorological Society* 86: 1303–1314.
Oreopoulos, L., E. Mlawer, J. Delamere, T. Shippert, J. Cole, B. Fomin, M. Iacono, et al. 2012. "The Continual Intercomparison of Radiation Codes: Results from Phase I." *Journal of Geophysical Research: Atmospheres* 117: D06118. doi:10.1029/2011JD016821.
Ouyang, X. Y., D. M. Chen, and Y. H. Lei. 2018. "A Generalized Evaluation Scheme for Comparing Temperature Products from Satellite Observations, Numerical Weather Model, and Ground Measurements Over the Tibetan Plateau." *IEEE Transactions on Geoscience and Remote Sensing* 56: 3876–3894.
Oyler, J. W., S. Z. Dobrowski, Z. A. Holden, and S. W. Running. 2016. "Remotely Sensed Land Skin Temperature as a Spatial Predictor of Air Temperature Across the Conterminous United States." *Journal of Applied Meteorology and Climatology* 55: 1441–1457.
Palle, E., P. R. Goode, P. Montanes-Rodriguez, and S. E. Koonin. 2004. "Changes in Earth's Reflectance Over the Past Two Decades." *Science* 304: 1299–1301.
Palle, E., P. R. Goode, P. Montanes-Rodriguez, A. Shumko, B. Gonzalez-Merino, C. M. Lombilla, F. Jimenez-Ibarra, et al. 2016. "Earth's Albedo Variations 1998-2014 as Measured from Ground-Based Earthshine Observations." *Geophysical Research Letters* 43: 4531–4538.
Palmer, M. D., and D. J. McNeall. 2014. "Internal Variability of Earth's Energy Budget Simulated by CMIP5 Climate Models." *Environmental Research Letters* 9: 034016.
Park, M. S., C. H. Ho, H. Cho, and Y. S. Choi. 2015. "Retrieval of Outgoing Longwave Radiation from COMS Narrowband Infrared Imagery." *Advances in Atmospheric Sciences* 32: 375–388.
Peng, J., A. Loew, X. L. Chen, Y. M. Ma, and Z. B. Su. 2016. "Comparison of Satellite-Based Evapotranspiration Estimates Over the Tibetan Plateau." *Hydrology and Earth System Sciences* 20: 3167–3182.
Perovich, D. K., and C. Polashenski. 2012. "Albedo Evolution of Seasonal Arctic Sea Ice." *Geophysical Research Letters* 39: L08501. doi:10.1029/2012GL051432.
Pinker, R. T., and L. Corio. 1984. "Surface Radiation Budget from Satellites." *Monthly Weather Review* 112: 209–215.
Pinker, R. T., J. A. Ewing, and J. D. Tarpley. 1985. "The Relationship Between the Planetary and Surface Net-Radiation." *Journal of Climate and Applied Meteorology* 24: 1262–1268.
Pinker, R. T., R. Frouin, and Z. Li. 1995. "A Review of Satellite Methods to Derive Surface Shortwave Irradiance." *Remote Sensing of Environment* 51: 108–124.
Pinker, R. T., X. Li, W. Meng, and E. A. Yegorova. 2007. "Toward Improved Satellite Estimates of Short-Wave Radiative Fluxes – Focus on Cloud Detection Over Snow: 2 Results." *Journal of Geophysical Research* 112: D07208. doi:10.1029/2005JD006698.
Pinker, R. T., and J. D. Tarpley. 1988. "The Relationship Between the Planetary and Surface Net-Radiation – An Update." *Journal of Applied Meteorology* 27: 957–964.
Pinker, R. T., J. D. Tarpley, I. Laszlo, K. E. Mitchell, P. R. Houser, E. F. Wood, J. C. Schaake, et al. 2003. "Surface Radiation Budgets in Support of the GEWEX Continental-Scale International Project (GCIP) and the GEWEX Americas Prediction Project (GAPP), Including the North American Land Data Assimilation System (NLDAS) Project." *Journal of Geophysical Research* 108: 8844. doi:10.1029/2002JD003301.
Pipunic, R. C., J. P. Walker, and A. Western. 2008. "Assimilation of Remotely Sensed Data for Improved Latent and Sensible Heat Flux Prediction: A Comparative Synthetic Study." *Remote Sensing of Environment* 112: 1295–1305.
Pistone, K., I. Eisenman, and V. Ramanathan. 2014. "Observational Determination of Albedo Decrease Caused by Vanishing Arctic Sea Ice." *Proceedings of the National Academy of Sciences* 111: 3322–3326.
Prigent, C., C. Jimenez, and F. Aires. 2016. "Toward "All Weather," Long Record, and Real-Time Land Surface Temperature Retrievals from Microwave Satellite Observations." *Journal of Geophysical Research: Atmospheres* 121: 5699–5717.
Prihodko, L., and S. N. Goward. 1997. "Estimation of Air Temperature from Remotely Sensed Surface Observations." *Remote Sensing of Environment* 60: 335–346.
Qin, J., Z. Chen, K. Yang, S. Liang, and W. Tang. 2011. "Estimation of Monthly-Mean Daily Global Solar Radiation Based on MODIS and TRMM Products." *Applied Energy* 88: 2480–2489.
Qin, J., S. Liang, R. Liu, H. Zhang, and B. Hu. 2007. "A Weak-Constraint Based Data Assimilation Scheme for Estimating Surface Turbulent Fluxes." *IEEE Geoscience and Remote Sensing Letters* 4: 649–653.

Qin, J., W. J. Tang, K. Yang, N. Lu, X. L. Niu, and S. Liang. 2015. "An Efficient Physically Based Parameterization to Derive Surface Solar Irradiance Based on Satellite Atmospheric Products." *Journal of Geophysical Research: Atmospheres* 120: 4975–4988.

Qin, W. M., L. C. Wang, A. W. Lin, M. Zhang, X. G. Xia, B. Hu, and Z. G. Niu. 2018. "Comparison of Deterministic and Data-Driven Models for Solar Radiation Estimation in China." *Renewable and Sustainable Energy Reviews* 81: 579–594.

Qu, Y. 2017. "Sea Surface Albedo." In *Comprehensive Remote Sensing, Vol. 5 Earth's Energy Budget*, edited by S. Liang, 163–185. Oxford: Elsevier.

Qu, Y., S. Liang, Q. Liu, T. He, S. Liu, and X. Li. 2015. "Mapping Surface Broadband Albedo from Satellite Observations: A Review of Literatures on Algorithms and Products." *Remote Sensing* 7: 990–1020.

Qu, Y., S. Liang, Q. Liu, X. Li, Y. Feng, and S. Liu. 2016. "Estimating Arctic Sea-Ice Shortwave Albedo from MODIS Data." *Remote Sensing of Environment* 186: 32–46.

Qu, Y., Q. Liu, S. Liang, L. Wang, N. Liu, and S. Liu. 2014. "Direct-Estimation Algorithm for Mapping Daily Land-Surface Broadband Albedo from MODIS Data." *IEEE Transactions on Geoscience and Remote Sensing* 52: 907–919.

Ramanathan, V. 1986. "Scientific Use of Surface Radiation Budget Data for Climate Studies." *Surface Radiation Budget for Climate Application* 1169: 58–86.

Rao, Y., S. Liang, and Y. Yu. 2018. "Land Surface Air Temperature Data are Considerably Different Among BEST-LAND, CRU-TEM4v, NASA-GISS, and NOAA-NCEI." *Journal of Geophysical Research – Atmosphere* 123: 5,880–885,900.

Rao, Y., S. Liang, Y. Yu, and D. Wang. 2019. "Estimating Daily Surface Air Temperature Using Satellite Land Surface Temperature and Top-of-Atmosphere Radiation Products Over Tibetan Plateau." *Remote Sensing of Environment*, Revised.

Raschke, E., and W. R. Bandeen. 1970. "The Radiation Balance of the Planet Earth from Radiation Measurements of the Satellite Nimbus II." *Journal of Applied Meteorology* 9: 215–238.

Reeves, J., J. Chen, X. L. Wang, R. Lund, and Q. Q. Lu. 2007. "A Review and Comparison of Changepoint Detection Techniques for Climate Data." *Journal of Applied Meteorology and Climatology* 46: 900–915.

Resplandy, L., R. F. Keeling, Y. Eddebbar, M. K. Brooks, R. Wang, L. Bopp, M. C. Long, J. P. Dunne, W. Koeve, and A. Oschlies. 2018. "Quantification of Ocean Heat Uptake from Changes in Atmospheric O-2 and CO2 Composition." *Nature* 563: 105–108.

Reynolds, R. W., T. M. Smith, C. Liu, D. B. Chelton, K. S. Casey, and M. G. Schlax. 2007. "Daily High-Resolution-Blended Analyses for Sea Surface Temperature." *Journal of Climate* 20: 5473–5496.

Rhee, J., J. Im, and G. J. Carbone. 2010. "Monitoring Agricultural Drought for Arid and Humid Regions Using Multi-Sensor Remote Sensing Data." *Remote Sensing of Environment* 114: 2875–2887.

Riihelä, A., T. Manninen, and V. Laine. 2013. "Observed Changes in the Albedo of the Arctic Sea-Ice Zone for the Period 1982-2009." *Nature Climate Change* 3: 895–898.

Riihela, A., T. Manninen, V. Laine, K. Andersson, and F. Kaspar. 2013. "CLARA-SAL: A Global 28 yr Timeseries of Earth's Black-Sky Surface Albedo." *Atmospheric Chemistry and Physics* 13: 3743–3762.

Roca, R., H. Brogniez, P. Chambon, O. Chomette, S. Cloché, M. E. Gosset, J.-F. Mahfouf, P. Raberanto, and N. Viltard. 2015. "The Megha-Tropiques Mission: A Review After Three Years in Orbit." *Frontiers in Earth Science* 3: 17.

Romano, F., D. Cimini, A. Cersosimo, F. Di Paola, D. Gallucci, S. Gentile, E. Geraldi, et al. 2018. "Improvement in Surface Solar Irradiance Estimation Using HRV/MSG Data." *Remote Sensing* 10: 1288.

Roujean, J. L., M. Leroy, and P. Y. Deschamps. 1992. "A Bidirectional Reflectance Model of the Earth's Surface for the Correction of Remote Sensing Data." *Journal of Geophysical Research* 97: 20455–20468.

Roujean, J. L., D. Tanre, F. M. Breon, and J. L. Deuze. 1997. "Retrieval of Land Surface Parameters from Airborne POLDER Bidirectional Reflectance Distribution Function During HAPEX-Sahel." *Journal of Geophysical Research: Atmospheres* 102: 11201–11218.

Ryu, Y., C. Jiang, H. Kobayashi, and M. Detto. 2018. "MODIS-Derived Global Land Products of Shortwave Radiation and Diffuse and Total Photosynthetically Active Radiation at 5 km Resolution from 2000." *Remote Sensing of Environment* 204: 812–825.

Ryu, Y., S. Kang, S. K. Moon, and J. Kim. 2008. "Evaluation of Land Surface Radiation Balance Derived from Moderate Resolution Imaging Spectroradiometer (MODIS) Over Complex Terrain and Heterogeneous Landscape on Clear Sky Days." *Agricultural and Forest Meteorology* 148: 1538–1552.

Sabol, J. D. E., A. R. Gillespie, E. Abbott, and G. Yamada. 2009. "Field Validation of the ASTER Temperature–Emissivity Separation Algorithm." *Remote Sensing of Environment* 113: 2328–2344.

Sanchez-Lorenzo, A., A. Enriquez-Alonso, M. Wild, J. Trentmann, S. M. Vicente-Serrano, A. Sanchez-Romero, R. Posselt, and M. Z. Hakuba. 2017. "Trends in Downward Surface Solar Radiation from Satellites and Ground Observations Over Europe During 1983–2010." *Remote Sensing of Environment* 189: 108–117.

Sanchez-Lorenzo, A., M. Wild, and J. Trentmann. 2013. "Validation and Stability Assessment of the Monthly Mean CM SAF Surface Solar Radiation Dataset Over Europe Against a Homogenized Surface Dataset (1983–2005)." *Remote Sensing of Environment* 134: 355–366.

Satheesh, S., and V. Ramanathan. 2000. "Large Differences in Tropical Aerosol Forcing at the Top of the Atmosphere and Earth's Surface." *Nature* 405: 60–63.
Sathiyamoorthy, V., B. P. Shukla, R. Sikhakolli, S. Chaurasia, B. Simon, B. S. Gohil, and P. K. Pal. 2013. "Top of Atmosphere Flux from the Megha-Tropiques ScaRaB." *Current Science* 104: 1656–1661.
Schaaf, C., F. Gao, A. Strahler, W. Lucht, X. Li, T. Tsung, N. Strugll, et al. 2002. "First Operational BRDF, Albedo Nadir Reflectance Products from MODIS." *Remote Sensing of Environment* 83: 135–148.
Schmetz, J., and Q. H. Liu. 1988. "Outgoing Longwave Radiation and its Diurnal-Variation at Regional Scales Derived from METEOSAT." *Journal of Geophysical Research* 93: 11192–11204.
Schmetz, J., P. Pili, S. Tjemkes, D. Just, J. Kerkmann, S. Rota, and A. Ratier. 2002. "Supplement to An Introduction to Meteosat Second Generation (MSG)." *Bulletin of the American Meteorological Society* 83: 992–992.
Schulz, J., P. Albert, H. D. Behr, D. Caprion, H. Deneke, S. Dewitte, B. Durr, et al. 2009. "Operational Climate Monitoring from Space: The EUMETSAT Satellite Application Facility on Climate Monitoring (CM-SAF)." *Atmospheric Chemistry and Physics* 9: 1687–1709.
Schwarz, M., D. Folini, M. Hakuba, and M. Wild. 2018. "From Point to Area: Worldwide Assessment of the Representativeness of Monthly Surface Solar Radiation Records." *Journal of Geophysical Research: Atmospheres* 123: 13,857–13,874.
Shah, M., M. Khan, H. Ullah, and S. Ali. 2018. "Thermal Anomalies Prior to the 2015 Gorkha (Nepal) Earthquake from Modis Land Surface Temperature and Outgoing Longwave Radiations." *Geodynamics & Tectonophysics* 9: 123–138.
Shi, Q., and S. Liang. 2013. "Characterizing the Surface Radiation Budget Over the Tibetan Plateau With Ground-Measured, Reanalysis, and Remote Sensing Data Sets: 2. Spatiotemporal Analysis." *Journal of Geophysical Research: Atmospheres* 118: 8921–8934.
Shi, L., S. Liang, J. Cheng, and Q. Zhang. 2016. "Integrating ASTER and GLASS Broadband Emissivity Products Using a Multi-Resolution Kalman Filter." *International Journal of Digital Earth* 9: 1098–1116.
Shi, H., Z. Xiao, S. Liang, and H. Ma. 2017. "A Method for Consistent Estimation of Multiple Land Surface Parameters from MODIS Top-of-Atmosphere Time Series Data." *IEEE Transactions on Geoscience and Remote Sensing* 55: 5158–5173.
Shi, H., Z. Xiao, S. Liang, and X. Zhang. 2016. "Consistent Estimation of Multiple Parameters from MODIS Top of Atmosphere Reflectance Data Using a Coupled Soil-Canopy-Atmosphere Radiative Transfer Model." *Remote Sensing of Environment* 184: 40–57.
Shuttleworth, W. J. 2007. "Putting the "Vap" Into Evaporation." *Hydrology and Earth System Sciences* 11: 210–244.
Smith, D. M., R. P. Allan, A. C. Coward, R. Eade, P. Hyder, C. L. Liu, N. G. Loeb, M. D. Palmer, C. D. Roberts, and A. A. Scaife. 2015. "Earth's Energy Imbalance Since 1960 in Observations and CMIP5 Models." *Geophysical Research Letters* 42: 1205–1213.
Sobrino, J. A., and Y. Julien. 2013. "Trend Analysis of Global MODIS-Terra Vegetation Indices and Land Surface Temperature Between 2000 and 2011." *IEEE Journal of Selected Topics in Applied Earth Observations and Remote Sensing* 6: 2139–2145.
Soliman, A., C. Duguay, W. Saunders, and S. Hachem. 2012. "Pan-Arctic Land Surface Temperature from MODIS and AATSR: Product Development and Intercomparison." *Remote Sensing* 4: 3833–3856.
Song, Z., S. Liang, D. Wang, Y. Zhou, and Y. Yu. 2018. "Long-Term Record of Top-of-Atmosphere Albedo Generated from AVHRR Data." *Remote Sensing of Environment* 211: 71–88.
Stackhouse, P. W., S. K. Gupta, S. J. Cox, J. C. Mikovitz, T. Zhang, and L. M. Hinkelman. 2011. "The NASA/GEWEX Surface Radiation Budget Release 3.0: 24.5-Year Dataset." *GEWEX News* 21: 10–12.
Stephens, G. L., J. Li, M. Wild, C. A. Clayson, N. Loeb, S. Kato, T. L'Ecuyer, P. W. Stackhouse, M. Lebsock, and T. Andrews. 2012. "An Update on Earth's Energy Balance in Light of the Latest Global Observations." *Nature Geoscience* 5: 691–696.
Stephens, G. L., D. O'Brien, P. J. Webster, P. Pilewski, S. Kato, and J. L. Li. 2015. "The Albedo of Earth." *Reviews of Geophysics* 53: 141–163.
Stroeve, J., T. Markus, L. Boisvert, J. Miller, and A. Barrett. 2014. "Changes in Arctic Melt Season and Implications for Sea Ice Loss." *Geophysical Research Letters* 41: 1216–1225.
Su, W. Y., N. G. Loeb, L. S. Liang, N. N. Liu, and C. T. Liu. 2017. "The El Nino-Southern Oscillation Effect on Tropical Outgoing Longwave Radiation: A Daytime Versus Nighttime Perspective." *Journal of Geophysical Research: Atmospheres* 122: 7820–7833.
Sun, F., M. D. Goldberg, X. Liu, and J. J. Bates. 2010. "Estimation of Outgoing Longwave Radiation from Atmospheric Infrared Sounder Radiance Measurements." *Journal of Geophysical Research: Atmospheres* 115: D09103. doi:10.1029/2009JD012799.
Sundström, A.-M., A. Arola, P. Kolmonen, Y. Xue, G. de Leeuw, and M. Kulmala. 2015. "On the Use of a Satellite Remote-Sensing-Based Approach for Determining Aerosol Direct Radiative Effect Over Land: A Case Study Over China." *Atmospheric Chemistry and Physics* 15: 505–518.
Susskind, J., G. Molnar, L. Iredell, and N. G. Loeb. 2012. "Interannual Variability of Outgoing Longwave Radiation as Observed by AIRS and CERES." *Journal of Geophysical Research: Atmospheres* 117: 18.

Tang, B., Z. L. Li, and R. H. Zhang. 2006. "A Direct Method for Estimating Net Surface Shortwave Radiation from MODIS Data." *Remote Sensing of Environment* 103: 115–126.
Tang, W. J., J. Qin, K. Yang, S. M. Liu, N. Lu, and X. L. Niu. 2016. "Retrieving High-Resolution Surface Solar Radiation With Cloud Parameters Derived by Combining MODIS and MTSAT Data." *Atmospheric Chemistry and Physics* 16: 2543–2557.
Tang, W., J. Qin, K. Yang, X. Niu, M. Min, and S. Liang. 2017. "An Efficient Algorithm for Calculating Photosynthetically Active Radiation With MODIS Products." *Remote Sensing of Environment* 194: 146–154.
Tang, B.-H., H. Wu, C. Li, and Z.-L. Li. 2011. "Estimation of Broadband Surface Emissivity from Narrowband Emissivities." *Optics Express* 19: 185–192.
Tarpley, J. D. 1979. "Estimating Incident Solar Radiation at the Surface from Geostationary Satellite Data." *Journal of Applied Meteorology* 18: 1172–1181.
Trenberth, K., and J. Fasullo. 2009. "Changes in the Flow of Energy Through the Earth's Climate System." *Meteorologische Zeitschrift* 18: 369–377.
Trenberth, K. E., and J. T. Fasullo. 2017. "Atlantic Meridional Heat Transports Computed from Balancing Earth's Energy Locally." *Geophysical Research Letters* 44: 1919–1927.
Trenberth, K. E., J. T. Fasullo, and M. A. Balmaseda. 2014. "Earth's Energy Imbalance." *Journal of Climate* 27: 3129–3144.
Trenberth, K. E., J. T. Fasullo, and J. Kiehl. 2009. "Earth's Global Energy Budget." *Bulletin of the American Meteorological Society* 90: 311–324.
Trenberth, K. E., J. T. Fasullo, K. V. Schuckmann, and L. Cheng. 2016. "Insights Into Earth's Energy Imbalance from Multiple Sources." *Journal of Climate* 29: 7495–7505.
Trenberth, K. E., Y. Zhang, J. T. Fasullo, and S. Taguchi. 2015. "Climate Variability and Relationships Between Top-of-Atmosphere Radiation and Temperatures on Earth." *Journal of Geophysical Research: Atmospheres* 120: 3642–3659.
Urbain, M., N. Clerbaux, A. Ipe, F. Tornow, R. Hollmann, E. Baudrez, A. V. Blazquez, and J. Moreels. 2017. "The CM SAF TOA Radiation Data Record Using MVIRI and SEVIRI." *Remote Sensing* 9: 466.
Verma, M., J. B. Fisher, K. Mallick, Y. Ryu, H. Kobayashi, A. Guillaume, G. Moore, et al. 2016. "Global Surface Net-Radiation at 5 km from MODIS Terra." *Remote Sensing* 8 (9): 739. doi:10.3390/rs8090739.
Vermote, E. F., N. Z. El Saleous, and C. O. Justice. 2002. "Atmospheric Correction of MODIS Data in the Visible to Middle Infrared: First Results." *Remote Sensing of Environment* 83: 97–111.
Vinukollu, R. K., E. F. Wood, C. R. Ferguson, and J. B. Fisher. 2011. "Global Estimates of Evapotranspiration for Climate Studies Using Multi-Sensor Remote Sensing Data: Evaluation of Three Process-Based Approaches." *Remote Sensing of Environment* 115: 801–823.
Viterbo, P., and A. K. Betts. 1999. "Impact on ECMWF Forecasts of Changes to the Albedo of the Boreal Forests in the Presence of Snow." *Journal of Geophysical Research: Atmospheres* 104: 27803–27810.
von Schuckmann, K., M. D. Palmer, K. E. Trenberth, A. Cazenave, D. Chambers, N. Champollion, J. Hansen, et al. 2016. "An Imperative to Monitor Earth's Energy Imbalance." *Nature Climate Change* 6: 138–144.
Wagner, S. C., Y. M. Govaerts, and A. Lattanzio. 2010. "Joint Retrieval of Surface Reflectance and Aerosol Optical Depth from MSG/SEVIRI Observations with an Optimal Estimation Approach: 2. Implementation and Evaluation." *Journal of Geophysical Research-Atmospheres* 115: 17.
Walton, C. C. 2016. "A Review of Differential Absorption Algorithms Utilized at NOAA for Measuring Sea Surface Temperature With Satellite Radiometers." *Remote Sensing of Environment* 187: 434–446.
Wan, Z. M. 2008. "New Refinements and Validation of the MODIS Land-Surface Temperature/Emissivity Products." *Remote Sensing of Environment* 112: 59–74.
Wan, Z., and Z. L. Li. 1997. "A Physics-Based Algorithm for Retrieving Land-Surface Emissivity and Temperature from EOS/MODIS Data." *IEEE Transactions on Geoscience and Remote Sensing* 35: 980–996.
Wang, K. C. 2014. "Measurement Biases Explain Discrepancies Between the Observed and Simulated Decadal Variability of Surface Incident Solar Radiation." *Scientific Reports* 4: 7.
Wang, K., and R. E. Dickinson. 2012. "A Review of Global Terrestrial Evapotranspiration: Observation, Modeling, Climatology, and Climatic Variability." *Reviews of Geophysics* 50: RG2005. doi:2010.1029/2011RG000373.
Wang, K., and R. E. Dickinson. 2013. "Global Atmospheric Downward Longwave Radiation at the Surface from Ground-Based Observations, Satellite Retrievals, and Reanalyses." *Reviews of Geophysics* 51: 150–185.
Wang, K. C., R. E. Dickinson, Q. Ma, J. A. Augustine, and M. Wild. 2013. "Measurement Methods Affect the Observed Global Dimming and Brightening." *Journal of Climate* 26: 4112–4120.
Wang, K. C., R. E. Dickinson, M. Wild, and S. Liang. 2012. "Atmospheric Impacts on Climatic Variability of Surface Incident Solar Radiation." *Atmospheric Chemistry and Physics* 12: 9581–9592.
Wang, X., and J. R. Key. 2005a. "Arctic Surface, Cloud, and Radiation Properties Based on the AVHRR Polar Pathfinder Dataset. Part II: Recent Trends." *Journal of Climate* 18: 2575–2593.
Wang, X. J., and J. R. Key. 2005b. "Arctic Surface, Cloud, and Radiation Properties Based on the AVHRR Polar Pathfinder Dataset. Part I: Spatial and Temporal Characteristics." *Journal of Climate* 18: 2558–2574.
Wang, K., and S. Liang. 2009a. "Estimation of Daytime Net Radiation from Shortwave Radiation Measurements and Meteorological Observations." *Journal of Applied Meteorology and Climatology* 48: 634–643.

Wang, K., and S. Liang. 2009b. "Evaluation of ASTER and MODIS Land Surface Temperature and Emissivity Products Using Surface Longwave Radiation Observations at SURFRAD Sites." *Remote Sensing of Environment* 113: 1156–1165.
Wang, W., and S. Liang. 2009c. "Estimation of High-Spatial Resolution Clear-Sky Longwave Downward and Net Radiation Over Land Surfaces from MODIS Data." *Remote Sensing of Environment* 113: 745–754.
Wang, W., and S. Liang. 2010. "A Method for Estimating Clear-Sky Instantaneous Land Surface Longwave Radiation from GOES Sounder and GOES-R ABI Data." *IEEE Geoscience and Remote Sensing Letters* 7: 708–712.
Wang, D., and S. Liang. 2016. "Estimating High-Resolution Top of Atmosphere Albedo from Moderate Resolution Imaging Spectroradiometer Data." *Remote Sensing of Environment* 178: 93–103.
Wang, D., and S. Liang. 2017. "Estimating Top-of-Atmosphere Daily Reflected Shortwave Radiation Flux Over Land from MODIS Data." *IEEE Transactions on Geoscience and Remote Sensing* 55: 4022–4031.
Wang, W., S. Liang, and J. A. Augustine. 2009. "Estimating Clear-Sky Land Surface Longwave Upwelling Radiation from MODIS Data." *IEEE Transactions on Geoscience and Remote Sensing* 47: 1555–1570.
Wang, D., S. Liang, T. He, Y. Cao, and B. Jiang. 2015. "Surface Shortwave Net Radiation Estimation from FengYun-3 MERSI Data." *Remote Sensing* 7: 6224–6239.
Wang, D., S. Liang, T. He, and Q. Shi. 2015. "Estimating Clear-Sky All-Wave Net Radiation from Combined Visible and Shortwave Infrared (VSWIR) and Thermal Infrared (TIR) Remote Sensing Data." *Remote Sensing of Environment* 167: 31–39.
Wang, D., S. Liang, T. He, and Q. Shi. 2015. "Estimation of Daily Surface Shortwave Net Radiation from the Combined MODIS Data." *IEEE Transactions on Geoscience and Remote Sensing* 53: 5519–5529.
Wang, D., S. Liang, T. He, and Y. Yu. 2013. "Direct Estimation of Land Surface Albedo from VIIRS Data: Algorithm Improvement and Preliminary Validation." *Journal of Geophysical Research* 118: 12577–12586.
Wang, D., S. Liang, R. Liu, and T. Zheng. 2010. "Estimation of Daily-Integrated PAR from Sparse Satellite Observations: Comparison of Temporal Scaling Methods." *International Journal of Remote Sensing* 31: 1661–1677.
Wang, W., S. Liang, and T. Meyer. 2008. "Validating MODIS Land Surface Temperature Products Using Long-Term Nighttime Ground Measurements." *Remote Sensing of Environment* 112: 623–635.
Wang, D., S. Liang, and H. Tao. 2014. "Mapping High-Resolution Surface Shortwave Net Radiation from Landsat Data." *IEEE Geoscience and Remote Sensing Letters* 11: 459–463.
Wang, H., and R. T. Pinker. 2009. "Shortwave Radiative Fluxes from MODIS: Model Development and Implementation." *Journal of Geophysical Research-Atmospheres* 114: 17.
Wang, T. X., J. C. Shi, Y. C. Yu, L. Husi, B. Gao, W. Zhou, D. B. Ji, T. J. Zhao, C. Xiong, and L. Chen. 2018. "Cloudy-Sky Land Surface Longwave Downward Radiation (LWDR) Estimation by Integrating MODIS and AIRS/AMSU Measurements." *Remote Sensing of Environment* 205: 100–111.
Wang, H. R., Y. P. Wang, X. Ye, D. J. Yang, K. Wang, H. D. Li, and W. Fang. 2017. "Instrument Description: The Total Solar Irradiance Monitor on the FY-3C Satellite, an Instrument With a Pointing System." *Solar Physics* 292: 12.
Wang, T. X., G. J. Yan, and L. Chen. 2012. "Consistent Retrieval Methods to Estimate Land Surface Shortwave and Longwave Radiative Flux Components Under Clear-Sky Conditions." *Remote Sensing of Environment* 124: 61–71.
Wang, T. X., G. J. Yan, X. H. Mu, Z. H. Jiao, L. Chen, and Q. Chu. 2018. "Toward Operational Shortwave Radiation Modeling and Retrieval Over Rugged Terrain." *Remote Sensing of Environment* 205: 419–433.
Wanner, W., X. Li, and A. Strahler. 1995. "On the Derivation of Kernels for Kernel-Driven Models of Bidirectional Reflectance." *Journal of Geophysical Research* 100: 21077–21089.
Wanner, W., A. H. Strahler, B. Hu, P. Lewis, J. P. Muller, X. Li, C. L. Barker Schaaf, and M. Barnsley. 1997. "Global Retrieval of Bidirectional Reflectance and Albedo Over Land from EOS MODIS and MISR Data: Theory and Algorithm." *Journal of Geophysical Research: Atmospheres* 102: 17143–17161.
Wen, J., Q. Liu, Q. Xiao, Q. Liu, D. You, D. Hao, S. Wu, and X. Lin. 2018. "Characterizing Land Surface Anisotropic Reflectance Over Rugged Terrain: A Review of Concepts and Recent Developments." *Remote Sensing* 10: 370.
Wentz, F. J., C. Gentemann, D. Smith, and D. Chelton. 2000. "Satellite Measurements of Sea Surface Temperature Through Clouds." *Science* 288: 847–850.
Wielicki, B. A., B. R. Barkstrom, B. A. Baum, T. P. Charlock, R. N. Green, D. P. Kratz, R. B. I. Lee, et al. 1998. "Clouds and the Earth's Radiant Energy System (CERES): Algorithm Overview." *IEEE Transactions on Geoscience and Remote Sensing* 36: 1127–1141.
Wielicki, B. A., T. M. Wong, N. Loeb, P. Minnis, K. Priestley, and R. Kandel. 2005. "Changes in Earth's Albedo Measured by Satellite." *Science* 308: 825–825.
Wielicki, B. A., D. F. Young, M. G. Mlynczak, K. J. Thome, S. Leroy, J. Corliss, J. G. Anderson, et al. 2013. "Achieving Climate Change Absolute Accuracy in Orbit." *Bulletin of the American Meteorological Society* 94: 1519–1539.
Wild, M. 2009. "Global Dimming and Brightening: A Review." *Journal of Geophysical Research-Atmospheres* 114: 31.
Wild, M. 2012. "Enlightening Global Dimming and Brightening." *Bulletin of the American Meteorological Society* 93: 27–37.
Wild, M. 2016. "Decadal Changes in Radiative Fluxes at Land and Ocean Surfaces and Their Relevance for Global Warming." *Wiley Interdisciplinary Reviews: Climate Change* 7: 91–107.

Wild, M., D. Folini, M. Z. Hakuba, C. Schar, S. I. Seneviratne, S. Kato, D. Rutan, C. Ammann, E. F. Wood, and G. Konig-Langlo. 2015. "The Energy Balance Over Land and Oceans: An Assessment Based on Direct Observations and CMIP5 Climate Models." *Climate Dynamics* 44: 3393–3429.

Wild, M., A. Ohmura, C. Schar, G. Muller, D. Folini, M. Schwarz, M. Z. Hakuba, and A. Sanchez-Lorenzo. 2017. "The Global Energy Balance Archive (GEBA) Version 2017: A Database for Worldwide Measured Surface Energy Fluxes." *Earth System Science Data* 9: 601–613.

Wu, X., and W. L. Smith. 1997. "Emissivity of Rough Sea Surface for 8–13 μm: Modeling and Verification." *Applied Optics* 36: 2609–2619.

Wu, S. B., J. G. Wen, D. Q. You, H. L. Zhang, Q. Xiao, and Q. H. Liu. 2018. "Algorithms for Calculating Topographic Parameters and Their Uncertainties in Downward Surface Solar Radiation (DSSR) Estimation." *IEEE Geoscience and Remote Sensing Letters* 15: 1149–1153.

Wu, H., X. Zhang, S. Liang, H. Yang, and G. Zhou. 2012. "Estimation of Clear-Sky Land Surface Longwave Radiation from MODIS Data Products by Merging Multiple Models." *Journal of Geophysical Research* 117: D22107. doi:10.1029/2012JD017567.

Wulder, M. A., T. Hilker, J. C. White, N. C. Coops, J. G. Masek, D. Pflugmacher, and Y. Crevier. 2015. "Virtual Constellations for Global Terrestrial Monitoring." *Remote Sensing of Environment* 170: 62–76.

Xiao, Z. Q., S. Liang, J. D. Wang, D. H. Xie, J. L. Song, and R. Fensholt. 2015. "A Framework for Consistent Estimation of Leaf Area Index, Fraction of Absorbed Photosynthetically Active Radiation, and Surface Albedo from MODIS Time-Series Data." *IEEE Transactions on Geoscience and Remote Sensing* 53: 3178–3197.

Xu, Y. M., A. Knudby, and H. C. Ho. 2014. "Estimating Daily Maximum Air Temperature from MODIS in British Columbia, Canada." *International Journal of Remote Sensing* 35: 8108–8121.

Xu, Y. M., A. Knudby, Y. Shen, and Y. H. Liu. 2018. "Mapping Monthly Air Temperature in the Tibetan Plateau From MODIS Data Based on Machine Learning Methods." *IEEE Journal of Selected Topics in Applied Earth Observations and Remote Sensing* 11: 345–354.

Xu, T., S. Liang, and S. Liu. 2011. "Estimating Turbulent Fluxes Through Assimilation of Geostationary Operational Environmental Satellites Data Using Ensemble Kalman Filter." *Journal of Geophysical Research* 116. doi:10.1029/2010JD015150.

Xu, T., S. Liu, S. Liang, and J. Qin. 2011. "Improving Predictions of Water and Heat Fluxes by Assimilating MODIS Land Surface Temperature Products Into the Common Land Model." *Journal of Hydrometeorology* 12: 227–244.

Yang, K., J. He, W. Tang, J. Qin, and C. C. K. Cheng. 2010. "On Downward Shortwave and Longwave Radiations Over High Altitude Regions: Observation and Modeling in the Tibetan Plateau." *Agricultural and Forest Meteorology* 150: 38–46.

Yang, K., T. Koike, and B. Ye. 2006. "Improving Estimation of Hourly, Daily, and Monthly Solar Radiation by Importing Global Data Sets." *Agricultural and Forest Meteorology* 137: 43–55.

Yang, S., X. L. L. Wang, and M. Wild. 2018. "Homogenization and Trend Analysis of the 1958-2016 In Situ Surface Solar Radiation Records in China." *Journal of Climate* 31: 4529–4541.

Yang, L., X. Zhang, S. Liang, Y. Yao, K. Jia, and A. Jia. 2018. "Estimating Surface Downward Shortwave Radiation Over China Based on the Gradient Boosting Decision Tree Method." *Remote Sensing* 10: 185.

Yao, Y. J., S. Liang, J. Cheng, S. M. Liu, J. B. Fisher, X. D. Zhang, K. Jia, et al. 2013. "MODIS-Driven Estimation of Terrestrial Latent Heat Flux in China Based on a Modified Priestley-Taylor Algorithm." *Agricultural and Forest Meteorology* 171-172: 187–202.

Yao, Y., S. Liang, X. Li, J. Chen, S. Liu, K. Jia, X. Zhang, Z. Xiao, J. B. Fisher, and Q. Mu. 2017. "Improving Global Terrestrial Evapotranspiration Estimation Using Support Vector Machine by Integrating Three Process-Based Algorithms." *Agricultural and Forest Meteorology* 242: 55–74.

Yao, Y., S. Liang, X. Li, Y. Hong, J. B. Fisher, N. Zhang, J. Chen, et al. 2014. "Bayesian Multimodel Estimation of Global Terrestrial Latent Heat Flux from Eddy Covariance, Meteorological, and Satellite Observations." *Journal of Geophysical Research: Atmospheres* 119: 2013JD020864.

Yao, Y. J., S. Liang, X. L. Li, S. M. Liu, J. Q. Chen, X. T. Zhang, K. Jia, et al. 2016. "Assessment and Simulation of Global Terrestrial Latent Heat Flux by Synthesis of CMIP5 Climate Models and Surface Eddy Covariance Observations." *Agricultural and Forest Meteorology* 223: 151–167.

Yao, Y., S. Liang, X. Li, Y. Zhang, J. Chen, K. Jia, X. Zhang, et al. 2017. "Estimation of High-Resolution Terrestrial Evapotranspiration from Landsat Data Using a Simple Taylor Skill Fusion Method." *Journal of Hydrology* 553: 508–526.

Yao, Y., S. Liang, J. Yu, S. Zhao, Y. Lin, K. Jia, X. Zhang, et al. 2017. "Differences in Estimating Terrestrial Water Flux from Three Satellite-Based Priestley-Taylor Algorithms." *International Journal of Applied Earth Observation and Geoinformation* 56: 1–12.

Yu, Y., Y. Liu, and P. Yu. 2017. "Land Surface Temperature Product Development for JPSS and GOES-R Missions." In *Comprehensive Remote Sensing, Vol. 5 Earth's Energy Budget*, edited by S. Liang, 284–303. Oxoford: Elsevier.

Yu, Y. Y., J. L. Privette, and A. C. Pinheiro. 2005. "Analysis of the NPOESS VIIRS Land Surface Temperature Algorithm Using MODIS Data." *IEEE Transactions on Geoscience and Remote Sensing* 43: 2340–2350.

Yu, S. S., X. Z. Xin, Q. H. Liu, H. L. Zhang, and L. Li. 2018. "Comparison of Cloudy-Sky Downward Longwave Radiation Algorithms Using Synthetic Data, Ground-Based Data, and Satellite Data." *Journal of Geophysical Research: Atmospheres* 123: 5397–5415.

Zakšek, K., and M. Schroedter-Homscheidt. 2009. "Parameterization of Air Temperature in High Temporal and Spatial Resolution from a Combination of the SEVIRI and MODIS Instruments." *ISPRS Journal of Photogrammetry and Remote Sensing* 64: 414–421.

Zeng, Z. Z., S. L. Piao, L. Z. X. Li, T. Wang, P. Ciais, X. Lian, Y. T. Yang, J. F. Mao, X. Y. Shi, and R. B. Myneni. 2018. "Impact of Earth Greening on the Terrestrial Water Cycle." *Journal of Climate* 31: 2633–2650.

Zhang, Y., T. He, S. Liang, D. Wang, and Y. Yu. 2018. "Estimation of All-Sky Instantaneous Surface Incident Shortwave Radiation from Moderate Resolution Imaging Spectroradiometer Data Using Optimization Method." *Remote Sensing of Environment* 209: 468–479.

Zhang, X. Y., and L. L. Li. 2016. "Estimating Net Surface Shortwave Radiation from Chinese Geostationary Meteorological Satellite FengYun-2D (FY-2D) Data Under Clear Sky." *Optics Express* 24: A476–A487.

Zhang, F. W., H. Q. Li, W. Y. Wang, Y. K. Li, L. Lin, X. W. Guo, Y. G. Du, et al. 2018. "Net Radiation Rather Than Surface Moisture Limits Evapotranspiration Over a Humid Alpine Meadow on the Northeastern Qinghai-Tibetan Plateau." *Ecohydrology* 11: 11.

Zhang, Y., and S. Liang. 2014. "Surface Radiative Forcing of Forest Disturbances Over Northeastern China." *Environmental Research Letters* 9: 024002. doi:024010.021088/021748-029326/024009/024002/024002.

Zhang, X., S. Liang, and G. Wang. 2017. "Surface Incident Shortwave Radiation." In *Comprehensive Remote Sensing Vol. 5 Earth's Energy Budget*, edited by S. Liang, 114–139. Oxford: Elsevier.

Zhang, X., S. Liang, G. Wang, Y. Yao, B. Jiang, and J. Cheng. 2016. "Evaluation of the Reanalysis Surface Incident Shortwave Radiation Products from NCEP, ECMWF, GSFC, and JMA Using Satellite and Surface Observations." *Remote Sensing* 8: 225.

Zhang, X. T., S. Liang, M. Wild, and B. Jiang. 2015. "Analysis of Surface Incident Shortwave Radiation from Four Satellite Products." *Remote Sensing of Environment* 165: 186–202.

Zhang, X., S. Liang, G. Zhou, H. Wu, and X. Zhao. 2014. "Generating Global LAnd Surface Satellite Incident Shortwave Radiation and Photosynthetically Active Radiation Products from Multiple Satellite Data." *Remote Sensing of Environment* 152: 318–332.

Zhang, Y. Q., J. L. Pena-Arancibia, T. R. McVicar, F. H. S. Chiew, J. Vaze, C. M. Liu, X. J. Lu, et al. 2016. "Multi-Decadal Trends in Global Terrestrial Evapotranspiration and Its Components." *Scientific Reports* 6: 12.

Zhang, Y. C., W. B. Rossow, A. A. Lacis, V. Oinas, and M. I. Mishchenko. 2004. "Calculation of Radiative Fluxes from the Surface to Top of Atmosphere Based on ISCCP and Other Global Data Sets: Refinements of the Radiative Transfer Model and the Input Data." *Journal of Geophysical Research: Solid Earth* 109: D19105. doi:10.1029/2003JD004457.

Zhang, Y. C., W. B. Rossow, and P. W. Stackhouse. 2007. "Comparison of Different Global Information Sources Used in Surface Radiative Flux Calculation: Radiative Properties of the Surface." *Journal of Geophysical Research-Atmospheres* 112: 20.

Zheng, T., S. Liang, and K. C. Wang. 2008. "Estimation of Incident Photosynthetically Active Radiation From GOES Visible Imagery." *Journal of Applied Meteorology and Climatology* 47: 853–868.

Zhou, Y., and R. D. Cess. 2001. "Algorithm Development Strategies for Retrieving the Downwelling Longwave Flux at the Earth's Surface." *Journal of Geophysical Research: Atmospheres* 106: 12477–12488.

Zhou, L., H. Chen, W. Hua, Y. Dai, and N. Wei. 2016. "Mechanisms for Stronger Warming Over Drier Ecoregions Observed Since 1979." *Climate Dynamics* 47: 12955–2974.

Zhou, Y., S. Liang, D. Wang, T. He, and Y. Yu. 2019. "Estimating High Spatial Resolution Outgoing Longwave Radiation at the Top of Atmosphere from MODIS Data." *Journal of Geophysical Research*, Submitted.

Zhou, Y., S. Liang, D. Wang, Z. Song, and Y. Yu. 2019. "Evaluation of Six Outgoing Longwave Radiation Satellite Products." *Journal of Geophysical Research*, Submitted.

Zhou, Y., S. Liang, D. Wang, and Y. Yu. 2019. "Generating 35-Year High-Resolution Outgoing Longwave Radiation Record from AVHRR Data." *Remote Sensing of Environment*, Submitted.

Zhou, C. L., and K. C. Wang. 2016. "Land Surface Temperature Over Global Deserts: Means, Variability, and Trends." *Journal of Geophysical Research: Atmospheres* 121: 14,344–14,357.

Zhou, Y., D. Wang, S. Liang, Y. Yu, and T. He. 2016. "Assessment of the Suomi NPP VIIRS Land Surface Albedo Data Using Station Measurements and High-Resolution Albedo Maps." *Remote Sensing* 8: 137.

Zhu, X. F., S. Liang, Y. Z. Pan, and X. T. Zhang. 2011. "Agricultural Irrigation Impacts on Land Surface Characteristics Detected From Satellite Data Products in Jilin Province, China." *IEEE Journal of Selected Topics in Applied Earth Observations and Remote Sensing* 4: 721–729.

Zhu, Z., S. Piao, R. B. Myneni, M. Huang, Z. Zeng, J. G. Canadell, P. Ciais, et al. 2016. "Greening of the Earth and its Drivers." *Nature Climate Change* 6: 791–795.

Zhu, P., M. van Ruymbeke, O. Karatekin, J. P. Noel, G. Thuillier, S. Dewitte, A. Chevalier, et al. 2015. "A High Dynamic Radiation Measurement Instrument: The Bolometric Oscillation Sensor (BOS)." *Geoscientific Instrumentation, Methods and Data Systems* 4: 89–98.